BENEMÉRITA UNIVERSIDAD AUTÓNOMA DE PUEBLA
FACULTAD DE CIENCIAS FÍSICO MATEMÁTICAS

Time resolution of particle detectors based on scintillation photons

Thesis submitted in partial fulfillment of the requirements for the degree of
Master of Science in Applied Physics

Presented by

Engr. Yael Antonio Vásquez Beltrán

Supervised by

Ph. D. Mario Rodríguez Cahuantzi

Co-supervised by

Ph. D. Ildefonso León Monzón

Puebla, Mexico

January 2023

Thesis title: Time resolution of particle detectors based on scintillation photons.

Student: Yael Antonio Vásquez Beltrán

COMMITTEE

Ph. D. Cristian Heber Zepeda Fernández

President

Ph. D. Eduardo Moreno Barbosa

Secretary

Ph. D. Guillermo Tejeda Muñoz

Member

Ph. D. Lucio Fidel Rebolledo Herrera

Substitute

Ph. D. Mario Rodríguez Cahuantzi

Supervisor

Ph. D. Ildefonso León Monzón

Co-supervisor

Abstract

In recent years, the design of particle detectors has evolved alongside emerging technologies related to the detection of photons. At the same time, the complexity of collider experiments requires particle detectors whose time resolution is in the order of picoseconds.

In this work, a study of the time resolution of particle detectors based on scintillating plastic and silicon photosensors (SiPM) is presented. The results are compared with the time resolution of similar detectors from CERN's ALICE-LHC experiment.

Acknowledgements

I would like to express my deepest gratitude to CONACYT for the financial support provided during these two years.

I would like to thank the support obtained by the CONACYT project A1-S-13525.

I would like to thank CONCYTEP for the support given to carry out this project.

I would like to express my deepest appreciation to my advisors Ph.D. Mario Rodríguez Cahuantzi and Ph.D. Ildefonso León Monzón for the support and guidance provided during the course of my thesis project.

I would like to thank my committee Ph. D. Cristian Heber Zepeda Fernández, Ph. D. Eduardo Moreno Barbosa, Ph. D. Guillermo Tejeda Muñoz, and Ph. D. Lucio Fidel Rebolledo Herrera for helping me finish the project.

I am infinitely grateful to my parents and my brother for their unconditional support.

I want to especially thank my girlfriend for accompanying me and motivating me throughout this journey.

I thank all my close friends for their friendship and the moments we shared together.

To my parents,
for letting me fly.

Contents

List of Tables

List of Figures

Chapter 1

Introduction

Particle detectors are devices used to detect, track, and/or identify ionizing particles. Detectors can be used to measure the energy of charged particles and other observables such as momentum, spin, charge, and particle identification, in addition to merely registering the presence of the particle.

Particle detectors are mainly used in collider and cosmic ray experiments that seek to study the fundamental properties of matter. Specifically, solid-state particle detectors based on plastic scintillators are optimized for the design of minimum bias trigger systems in colliders such as the VZERO [1] from the ALICE experiment [2] of the LHC at CERN.

One of the main characteristics of this class of detectors is their time resolution, whose value is of critical importance and must be optimized since it describes the minimum time unit in which the detector can distinguish between two consecutive physical events of interest. The time resolution depends on the geometry of the detector and the technique used for data acquisition, which is closely related to the instruments used [3, 4].

This work aims to quantify the time resolution of a compact particle detector created with BC404 scintillator plastic. In this detector, the light is collected using photomultipliers (tubes or silicon) and the data is acquired with instruments of the CAEN brand.

Subsequently, an analysis of data acquired using the trigger detectors VZERO and AD [5], which are part of the ALICE-LHC experiment at CERN, is done. The analysis retrieves an estimation of the time resolutions of both sensors, which are then compared to the time resolution of the detector proposed in this project.

The contents of this thesis are described below. The introduction to this work is presented in Chapter 1. In the Chapter 2, the interaction processes of radiation with matter are explained, as well as the operation of silicon photomultiplier sensors (SiPM) and the characteristics of the plastic scintillators used in this project. Chapter 3 shows an overview of each one of the detectors that make up the ALICE experiment, and also mentions the importance of time resolution within this experiment. Chapter 4 discusses the data acquisition processes and the characteristics of the data analysis for the data obtained in the characterization tests of the different detectors proposed in this work. Throughout Chapter 5, the results of time resolution, efficiency, and deposited charge of each one of the detectors characterized in this project are presented. Finally, Chapter 6 presents the conclusions of the results obtained in this thesis work.

In addition, in the Appendix A, some supplementary tests that were carried out are presented, among them one for the characterization of a SiPM detector with a LED, another for the characterization of a Resistive Plate Chambers (RPC) detector, and the last one for the characterization of a SiPM detector using a base designed to separate the triggers detectors from the SiPM detector.

Chapter 2

Particle detectors

2.1 Interaction processes of radiation with matter

Radiation is understood in terms of charged particles moving, which have enough energy to ionize the material they are passing through. Radiation sources can be classified in natural and artificial. Examples of natural radiation are cosmic radiation and environmental radioactivity (40K, 222Rn). Examples of artificial sources are particle accelerators, accelerators for medical applications, and nuclear reactors. These particles can interact with electrons and atomic nuclei through elastic collisions (changing the trajectory but maintaining kinetic energy) and inelastic collisions (changing the trajectory slightly and losing kinetic energy), which will cause a loss of energy transformed into excitation and ionization; and absorption or attenuation in the material.

2.1.1 Heavy charged particles (protons, ions)

Charged particles can interact with the medium in different ways:

- They can lose kinetic energy when they collide with the electrons in the material, which will produce braking radiation, which in turn will cause the electrons to feel the Coulomb field causing them to move up the layer (excitation) or leave the atom (ionization).
- By Cherenkov radiation, a process that occurs when the charged particle passes

through a dielectric medium reaching speeds greater than that of light in that medium.

- If the charged particle is subjected to magnetic fields and changes its trajectory, then it will lose energy by synchrotron radiation.

The stopping power S for charged particles in a given absorbent material is defined as the differential energy loss for that particle within the material divided by the corresponding differential path length:

$$S = -\frac{dE}{dX}. \tag{2.1}$$

According to equation (2.1), the stopping power S of a particle increases as the velocity of the particle decreases. As presented in [6], this can be better understood by the Bethe-Bloch equation (2.2), which describes the amount of energy loss,

$$-\frac{dE}{dX} = \frac{4\pi e^4 z^2}{m_0 v^2} NZ \left[\ln\left(\frac{2m_0 v^2}{I}\right) - \ln\left(1 - \frac{v^2}{c^2}\right) - \frac{v^2}{c^2} \right]. \tag{2.2}$$

This equation is valid when the velocity of the heavy particle is much greater than the velocities of the electrons in the orbits of the atoms of the material.

2.1.2 Light charged particles (electrons, positrons)

When the incident particles are of this type or any with similar mass, the electrons of the material will interact with the incident particles by Coulomb forces. The interaction will affect the path that the particles follow. An additional loss of energy will be caused by the collisions that occur between the electrons and the incident particles. The energy exchange of the collisions will be greater than in the case of incident heavy charged particles due to the fact that the masses of both parts are similar. This loss of energy can be expressed by equation (2.3), which following from [7] is denominated as collision stopping power,

$$-\left(\frac{dE}{dX}\right)_c = \frac{2\pi e^4 z^2}{m_0 v^2} NZ \left[\ln\left(\frac{m_0 v^2 E}{2I^2(1-\beta^2)}\right) - \ln(2)\left(2\sqrt{1-\beta^2} - 1 + \beta^2\right)\right] + \frac{2\pi e^4 z^2}{m_0 v^2} NZ \left[1 - \beta^2 + \frac{1}{8}\left(1 - \sqrt{1-\beta^2}\right)^2\right]. \tag{2.3}$$

Light charged particles can also lose energy by braking radiation, and the stopping power by radioactive processes is defined by equation (2.4),

$$-\left(\frac{dE}{dX}\right)_r = \frac{NEZ(Z+1)e^4}{137 m_0^2 c^4}\left[4\ln\left(\frac{2E}{m_0 c^2}\right) - \frac{4}{3}\right]. \tag{2.4}$$

For electrons with average energy, the energy of the photons produced by braking radiation is low, since most of the released energy is absorbed by the photons' production. The total stopping power for light particles is the sum of equation (2.3) and equation (2.4), which is expressed in equation (2.5),

$$\left(\frac{dE}{dX}\right) = \left(\frac{dE}{dX}\right)_c + \left(\frac{dE}{dX}\right)_r. \tag{2.5}$$

2.1.3 Neutral particles (neutrons, photons)

Given their physical properties, neutrons have the possibility of penetrating more matter without being detected by conventional detectors. Neutrons are more penetrating than alpha and beta radiation, and even in certain cases, they can become more penetrating than gamma radiation itself, as shown in Figure 2.1.

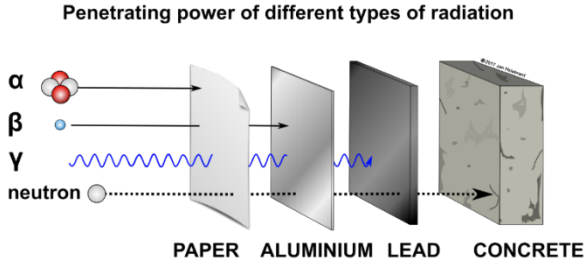

Figure 2.1: Penetrating power of different types of radiation.

2.2 Silicon photomultiplier (SiPM)

Silicon photomultipliers (SiPM) are relatively new photon detection devices, whose development began in 1993. They consist of a detection area divided into cells that are composed of multiple avalanche diodes (APDs). The length of a cell side is called cell pitch, and currently, there are SiPMs with cell pitch in the range of 25 μm to 100 μm. The cells work in Geiger mode, which means that each APD counts photons without any information about the energy or the number of simultaneous events [8].

SiPMs are semiconductors and have a valence band and a conduction band separated by a small energy gap. Therefore, when a photon interacts with the material, electrons from the valence band could be easily excited to the conduction band, and by applying an appropriate voltage, these electrons can be collected to form a measurable current, after being amplified.

From an electronic point of view, a SiPM is composed of an array of inversely polarized photodiodes (APDs), connected in parallel between them, as shown in Figure 2.2. Furthermore, like diodes, SiPMs have an intrinsic characteristic called breakdown voltage (V_{bd}), which is defined as the voltage at which the reverse-biased diode begins to conduct. A polarization voltage (V_b) is applied to the SiPM, necessarily greater than V_{bd} so that there is conduction. After applying a V_b higher than V_{bd} on the SiPM, an electric field appears that accelerates the free charge carriers.

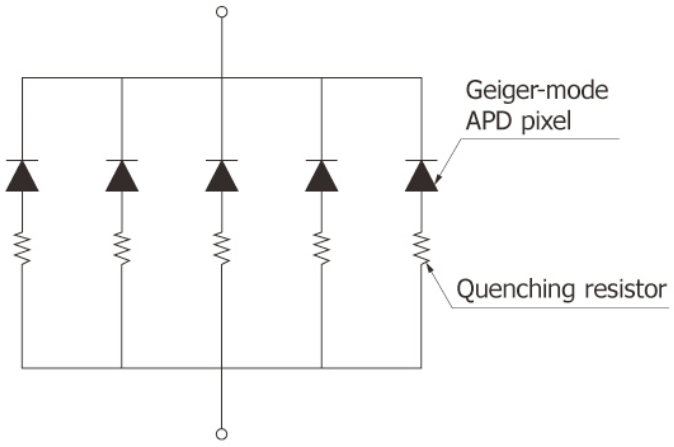

Figure 2.2: The cells of a SiPM are photodiodes polarized in reverse and connected in parallel with each other.

As shown in Figure 2.2, a resistance through which current flows when there is a cascade of electrons produced by the arrival of a photon is usually placed in series with the SiPM. This resistance produces a voltage drop over the SiPM, which decreases below the breakdown voltage and stops conducting.

In Figure 2.3, some of the mentioned characteristics can be observed, and among them, the great variation in the current occurs with a small variation in voltage once the V_{bd} has been exceeded. Unlike common diodes, SiPMs are optimized to work in this range of voltages that involve large variations in currents.

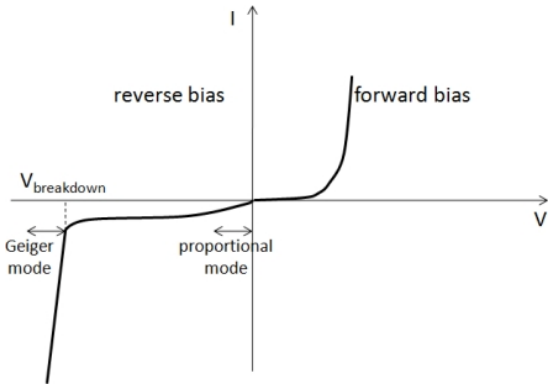

Figure 2.3: When reverse-biased, it is possible to reach a voltage range near V_{bd} in which a small variation produces a large change in current.

A notable characteristic of SiPMs compared to PMTs is the photon detection efficiency (PDE) which is the percentage of detected photons out of the total that reaches the detector. Efficiency is higher in the case of SiPMs, reaching in some cases 50% [9, 10] (in the UV range), while efficiency in PMTs is typically between 5% and 25% (with the maximum in the green, 530 nm).

In addition, the typical voltages to which a PMT must be subjected for its correct operation are of the order of kV, while with a SiPM it is possible to work with operating voltages of the order of 30 V, which in general becomes much simpler than PMTs. Due to its different operating principle, it has been possible to reduce the size of SiPMs to the order of mm^2, presenting a significant advantage over PMTs in terms of experiments that must be easily transferable. On the other hand, SiPMs have a disadvantage in case they need to cover a large detection area due to their small dimensions.

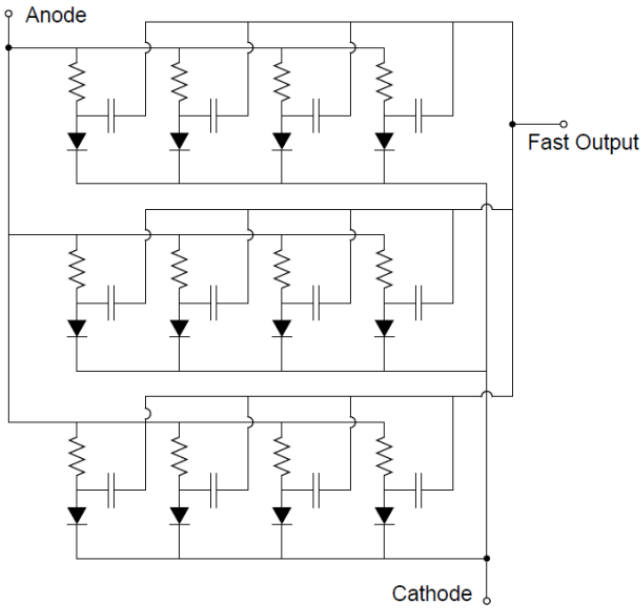

Figure 2.4: Silicon photomultiplier structure [8].

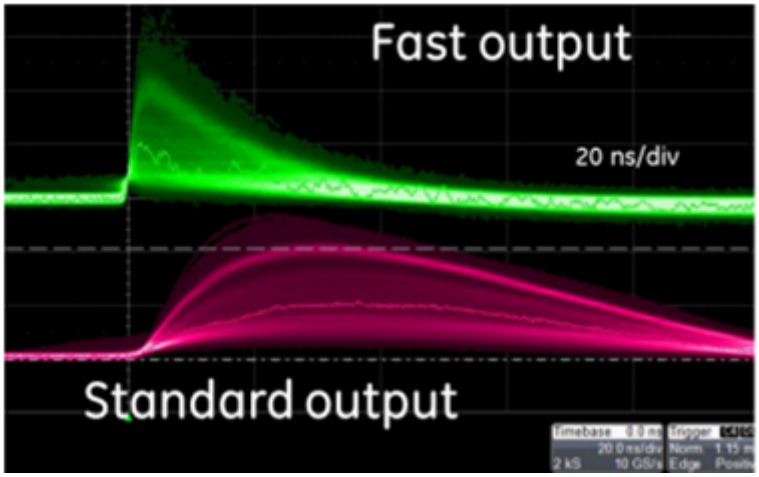

Figure 2.5: Standard and fast outputs from SensL SiPM [8].

The electronic diagram of a SiPM is shown in Figure 2.4. SiPMs have two output signals, the standard output and the fast output, whose characteristics can be seen in the example in Figure 2.5. The fast signal usually has a pulse width of 10 to 40 ns, while the standard signal can last more than 200 ns. The pulse width of the standard and fast pulses depends on the size and series of the SiPM.

The SiPM offers an attractive alternative that combines the low light sensing capabilities of the PMT while offering all the benefits of a solid-state sensor. The SiPM features low-voltage operation, insensitivity to magnetic fields, mechanical robustness,

and excellent response uniformity. Due to these traits, the SensL SiPM has rapidly gained proven performance in the fields of medical imaging, hazard and threat detection, biophotonics, high physical energy, and LiDAR [8].
Some problems associated with SiPM:

- Thermal noise: it is the dominant one in long measurement times, it appears due to the random promotion of charge carriers.

- Optical crosstalk: sometimes electrons and holes in a cascade of a cell can recombine forming a photon that activates a contiguous cell, generating a false detection. This phenomenon can be reduced by improving the isolation between the different cells.

- Afterpulsing: when there are impurities in the crystalline silicon, it may happen that some charge carrier remains trapped for a time, generating a cascade when it is released.

2.2.1 Silicon photomultiplier performance parameters

Users of SiPM sensors will typically need to have an understanding of the following parameters: breakdown voltage and overvoltage, gain, fill factor, photon detection efficiency (PDE), dark count rate (DCR), optical crosstalk, afterpulsing, and temperature dependency.

- Breakdown voltage and overvoltage

The breakdown voltage (V_{bd}) is the bias point at which the electric field strength generated in the depletion region is sufficient to create a Geiger discharge. The V_{bd} point is clearly identified on a current versus voltage plot by a sudden increase of electric current, as shown in Figure 2.6. The precise value of the V_{bd} is determined as the value of the voltage intercept of a straight line fit to a plot of $\sqrt{I} vs V$, where I is the dark current and V is the voltage, as shown in Figure 2.7 [11].

SiPM sensors are operated at a bias point that is typically 10% - 25% higher than the V_{bd}. The difference between the V_{bd} and the bias point is referred overvoltage (ΔV). Both the V_{bd} and the recommended ΔV range are given in the SiPM product datasheets [18]. These values allow the user to calculate the V bias to apply.

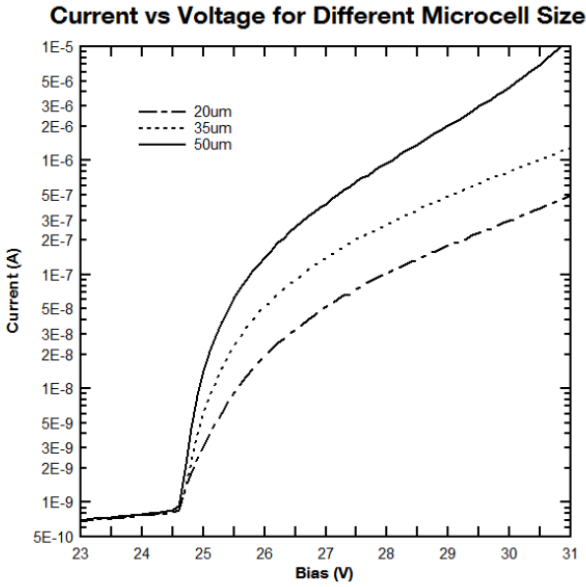

Figure 2.6: Dark current vs Voltage plots for 3 mm sensors with 20 μm, 35 μm, and 50 μm microcells [18].

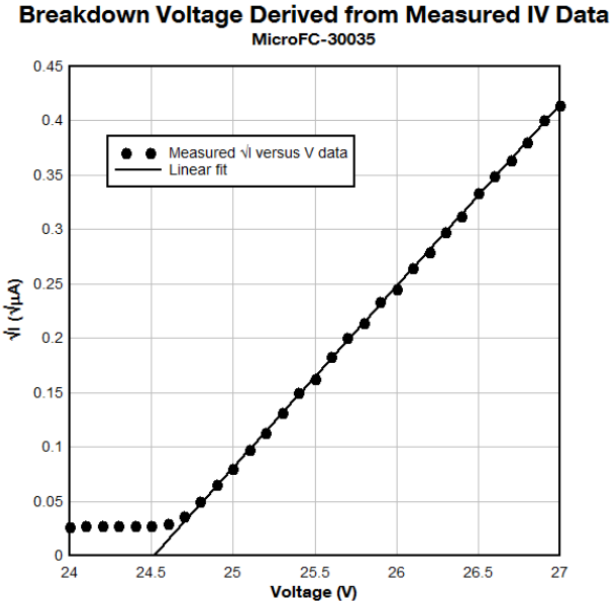

Figure 2.7: Breakdown voltage [18].

- Gain

The gain of a SiPM sensor is defined as the amount of charge created for each detected photon and is a function of the overvoltage and microcell size. Each microcell in the SiPM generates a highly uniform and quantized amount of charge every time an avalanche is generated by an absorbed photon in the active volume. The gain of a microcell (and hence the sensor) is then defined as the ratio of the charge from an activated microcell to the charge on an electron. Using the overvoltage ΔV, the microcell capacitance C, and the electron charge q, the gain G can be calculated by

$$G = \frac{C \times \Delta V}{q}. \tag{2.6}$$

- Fill Factor

The fill factor refers to the percentage of the SiPM sensor surface area that is sensitive to light. Due to the structure of the SiPM, each microcell needs to be separated from its neighbor for optical and electrical isolation purposes. In addition, some surface area is required for the quench resistor and signal tracks. All of these considerations result in a "dead space" around the microcell. The separation between microcells and the space required for the quench resistor and tracking is more or less constant, regardless of the microcell size. Therefore, larger microcells result in a higher percentage of active surface area (active area/total area).
A higher fill factor (larger microcells) results in higher PDE and gain, but also in higher capacitances, longer recovery times, and lower dynamic range. A lower fill factor (smaller microcells) results in lower PDE and gain, but also in lower capacitances, shorter recovery times, and higher dynamic range [18].

- Photon Detection Efficiency (PDE)

The photon detection efficiency (PDE) is a measure of the sensitivity of a SiPM and is a function of the wavelength of the incident light, the applied overvoltage, and the microcell fill factor. The PDE is the statistical probability that an incident photon interacts with a microcell to produce an avalanche, and is defined as:

$$PDE(\lambda, V) = \eta(\lambda) \times \varepsilon(V) \times F \tag{2.7}$$

where $\eta(\lambda)$ is the quantum efficiency of silicon, $\varepsilon(V)$ is the avalanche initiation probability and F is the fill factor of the device. A typical PDE versus wavelength plot is shown in Figure 2.8. The PDE plot is used to define the peak wavelength (λ_p) and the wavelength range.

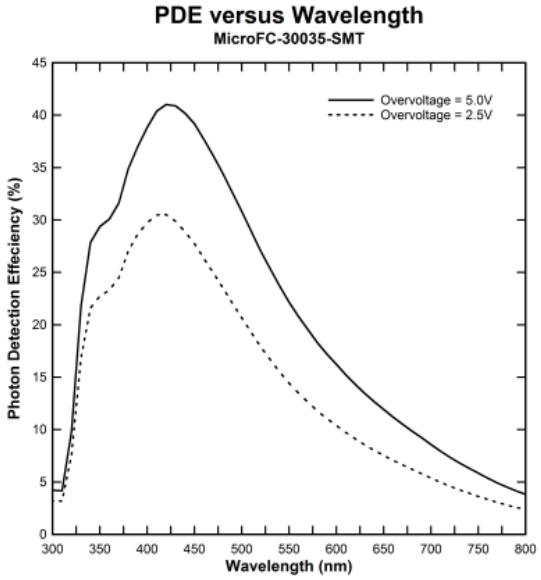

Figure 2.8: Photon Detection Efficiency (PDE) [18].

- Dark Count Rate (DCR)

The main source of noise in a SiPM is the dark count rate (DCR), which is primarily due to thermal electrons generated in the active volume. The DCR is a function of the active area, the overvoltage, and the temperature.

Each dark count is a result of a thermally generated electron that initiates an avalanche in the high-field region. The signals resulting from the breakdown of the microcell, due to either photon-generated or thermally-generated electrons, are identical. Therefore, thermally generated electrons form a source of noise at the single photon level. If a threshold can be set above the single photon level then false triggers from the noise can be significantly reduced. However, the dark counts will contribute to the measured signal.

Since the dark count is comprised of a series of pulses, its magnitude is quoted as a pulse rate (kHz), or pulse rate per unit area (kHz/mm^2). For continuous or current integration measurements, it is sometimes more convenient to consider the contribution as a "dark current" which is also quoted on the SensL datasheets [18].

The DCR can be measured with a simple counting system, setting a threshold set at the half-photon level. The DCR increases with increasing bias as shown in Figure 2.9, creating an inherent trade-off between increasing PDE and DCR.

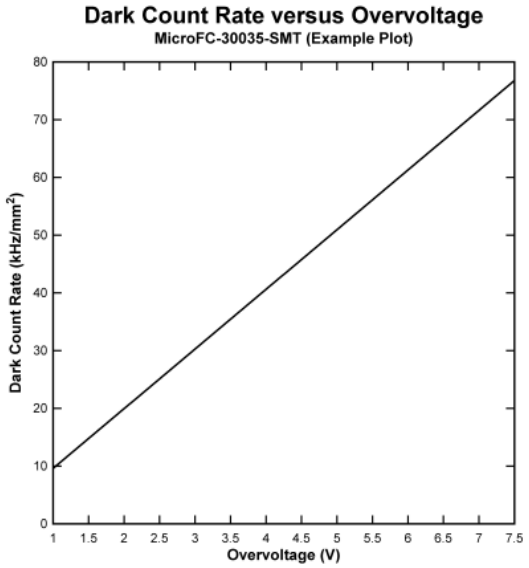

Figure 2.9: Dark Count Rate (DCR) as a function of overvoltage for a 3 mm, 35 μm Microcell SiPM [18].

- Optical Crosstalk

An additional component of SiPM noise is that of optical crosstalk between microcells. Optical crosstalk is a function of overvoltage and is also affected by the fill factor of a sensor. During an avalanche, accelerated carriers in the high-field region will emit photons that can initiate a secondary avalanche in a neighboring microcell. The crosstalk is defined as the probability that an avalanching microcell will cause an avalanche in a second microcell. The process happens instantaneously and as a consequence, single incident photons may occasionally generate signals equivalent to 2 or 3 photons, or even higher.

Figure 2.10 shows the crosstalk increasing with overvoltage, which is due to the increased number of carriers crossing the junction due to higher gain. There is an inherent trade-off between PDE (maximized using a high overvoltage) and crosstalk (minimized using a lower overvoltage). Therefore, plots of the type in Figure 2.11 can be useful.

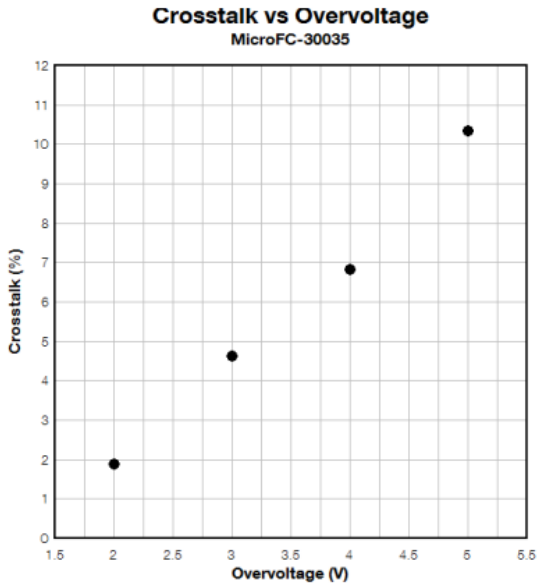

Figure 2.10: Crosstalk vs Overvoltage for 3 mm SiPM with 35 μm Microcells [18].

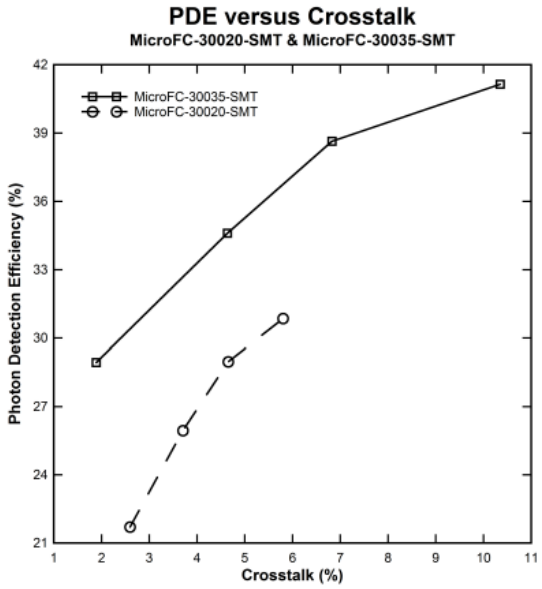

Figure 2.11: PDE vs Crosstalk for 3 mm SiPM with 20 μm and 35 μm Microcells [18].

- Afterpulsing

During breakdown, carriers can become trapped in defects in the silicon. After a delay of up to several ns, the trapped carriers are released, potentially initiating an avalanche and creating an afterpulse in the same microcell. Afterpulses with short delay that occur during the recovery time of the microcell tend to have a negligible impact as the microcell is not fully charged. However, longer delay afterpulses can impact measurements with the SiPM if the rate is high. The afterpulse probability is determined by measuring the statistical distribution of consecutive pairs of dark counts when triggered at one-half of the single photoelectron amplitude. Afterpulse probability increases with overvoltage (due to increased avalanche initiation probability).

- Temperature Dependency

The primary effects of temperature change on the SiPM are a change in the breakdown voltage and the dark count rate. The breakdown voltage changes linearly as a function of temperature, as shown in Figure 2.12. For stable operation in the presence of significant temperature fluctuations, either bias compensation or thermal regulation should be considered. An increase in temperature will increase the dark count rate, therefore actively cooling a SiPM will significantly reduce the DCR.

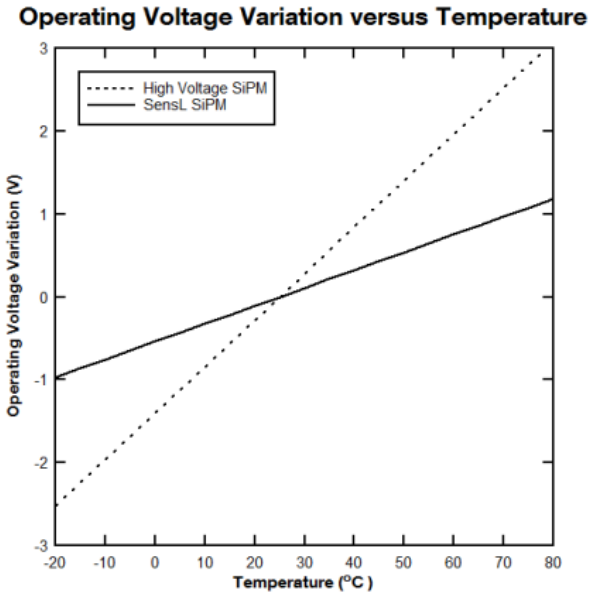

Figure 2.12: Impact of temperature change on the operating voltage [18].

2.3 Plastic scintillators

The scintillation emission of a typical plastic scintillator has a maximum of around 425 nm. Plastic scintillators are characterized by a relatively large light output, typically 25-30% of NaI(Tl), and a short decay time of around 2 ns. This makes the material suited for fast-timing measurements. The exact emission wavelength and decay time depend on the type of organic activator and on the host material. A large number of different plastic scintillators are available, each for a specific application. In Figure 2.13 examples of different plastic scintillators are shown.

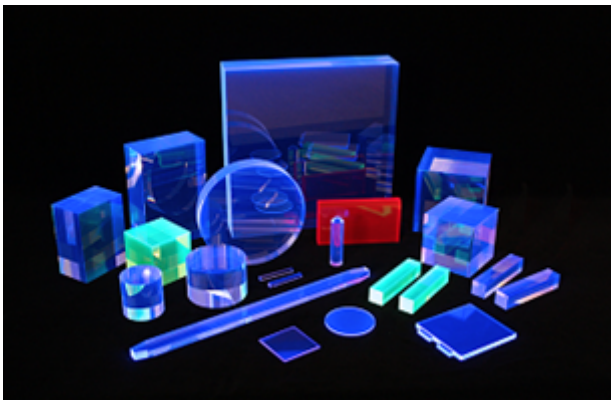

Figure 2.13: Examples of plastic scintillators.

Plastic sheets cast from the monomer ensure the highest light yield and best internal light transmission. All raw materials undergo extensive purification prior to polymerization and the finished sheets exhibit highly uniform scintillation and optical properties. Scintillators are machined to final dimensions using diamond tooling to provide optimum quality surfaces for total internal reflection [9].

2.3.1 BC-404 General Characteristics

BC-404 plastic scintillators are largely used as thin sheets for alpha and beta detection. BC-404 can also be used in fast-counting applications. In Table 2.1 the characteristics of the BC-404 plastic scintillator are shown, and in Figure 2.14, the graph of its emission spectra is observed [12].

Table 2.1: BC-404 general characteristics

BC-404 Characteristics	
Application	Fast Counting
Scintillation Properties	
Light Output, % Anthracene	68
Rise Time, ns	0.7
Decay Time, ns	1.8
Pulse Width, Fwhm, ns	2.2
Wavelengh Of Max. Emission, ns	408
Ligth: Attenuation Length, cm	140
Bulk Light Attenuation Length	160

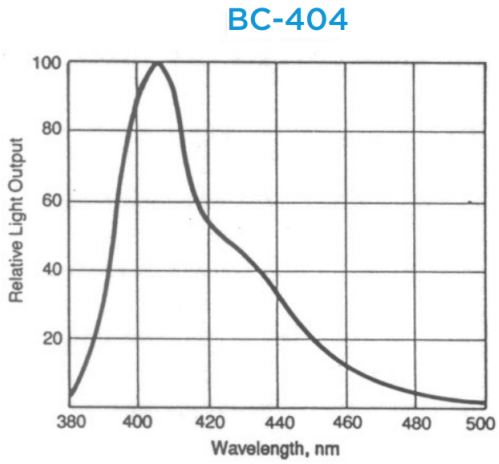

Figure 2.14: BC-404 emission spectra [12].

2.3.2 BC-422Q General Characteristics

BC-422Q plastic scintillator is intended for use in ultra-fast timing and ultra-fast counting applications. It is quenched with various weight percentages of benzophenone (specified at time of order) to improve timing properties. However, the faster timing comes at the expense of total light output. In Table 2.2, the characteristics of the BC-422Q plastic scintillator are shown, and in Figure 2.15, the graph of its emission spectra is observed [10].

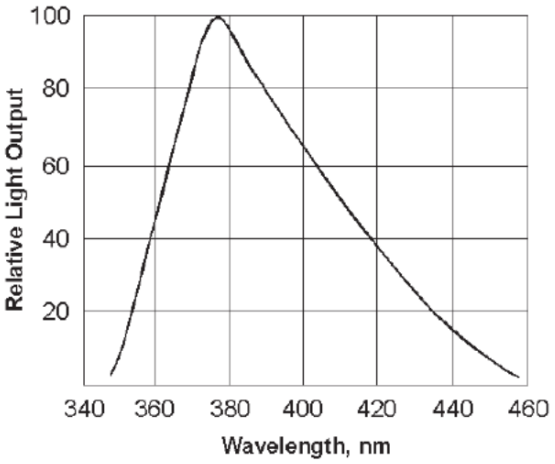

Figure 2.15: BC-422Q emission spectra [10].

Table 2.2: BC-422Q general characteristics

BC-422Q Characteristics	
Application	Ultra-Fast Counting
Scintillation Properties	
Light Output, % Anthracene	55
Rise Time, ns	350
Decay Time, ns	1.6
Pulse Width, Fwhm, ns	1.3
Base	Polyvinyltoluene
Density, g/cc	1.032
Expansion Coefficient (per°C,¡67°C)	7.8×10^{-5}
Refractive index	1.58
Softening Point	70 °C

Chapter 3

ALICE Experiment

3.1 ALICE

The ALICE Collaboration has built a detector optimized to study the collisions of nuclei at the ultra-relativistic energies provided by the LHC. The aim is to study the physics of strongly interacting matter at the highest energy densities reached so far in the laboratory. In such conditions, an extreme phase of matter (called the quark-gluon plasma) is formed. ALICE is also studying proton-proton and proton-nucleus collisions both as a comparison with nucleus-nucleus collisions.

The ALICE collaboration uses the 10,000-tonne ALICE detector, 26 m long, 16 m high, and 16 m wide, to study quark-gluon plasma. The detector sits in a vast cavern 56 m below ground close to the village of St Genis-Pouilly in France, receiving beams from the LHC. The detector consists of two main components: the central part composed of detectors dedicated to the study of hadronic signals and electrons, and the forward muon spectrometer dedicated to the study of quarkonia behavior in dense matter. The central part is embedded in a large solenoid magnet with a weak field (full current of 6000 A and magnetic field of 670 $millitesla$). The innermost part of the detector is the tracking system, which consists of the inner tracking system (ITS) and the outer tracking system.

The principal component of the outer tracking system is the time projection chamber (TPC). The TPC is a cylindrical device filled with gas and incorporating uniform

electric and magnetic fields, ideal for separating, tracking, and identifying thousands of charged particles in a dense environment, such as the thousands of particles produced in an energetic heavy-nuclei collision. It is the main detector in many high-energy physics experiments.

The overall dimensions of the ALICE experiment [2] span 16x16x26 m^3 with a total weight of approximately 10,000 *tons*. ALICE is made up of 18 detection systems, each with its own specific technology and design that is driven by both the physical requirements and the experimental conditions expected at the LHC. The different subsystems were optimized to provide the best resolution to reconstruct the high transverse moment, as well as excellent particle identification over a wide moment range.

3.2 ALICE detector structure

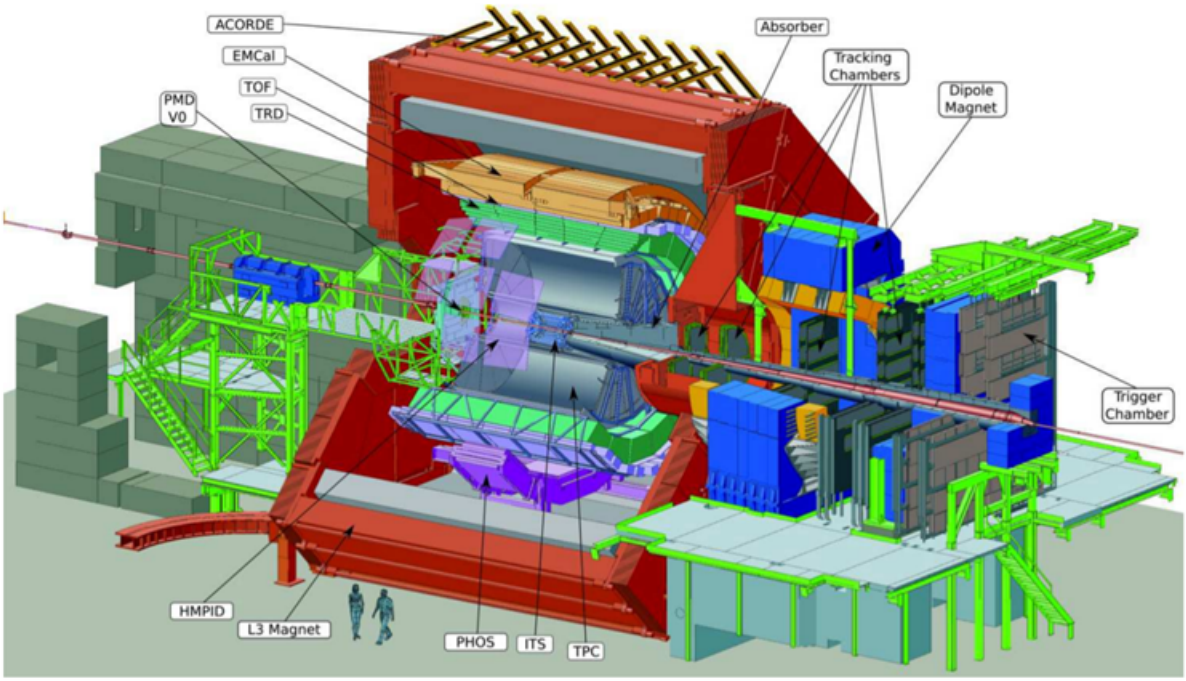

Figure 3.1: General diagram of the ALICE detector.

As shown in Figure 3.1, the central part consists of mostly concentric cylindrical detectors; such as the internal trajectory system (ITS), the time projection chamber (TPC), the system that measures the time of flight of charged particles (TOF), Cherenkov type detectors (HMPID), radiation detectors (TRD), and electromagnetic calorimeters

(PHOS and EMCAL). All these detectors except HMPID, EMCal, and PHOS fully cover the azimuth angle. There are also several detectors smaller than those mentioned above: a calorimeter at zero degrees with respect to the LHC beam (ZDC), a detector to measure the multiplicity of photons (PMD), one to measure the multiplicity of particles in the front region (FMD), the zero time level detector (T0), and the vertex detector (V0). These detectors are used as trigger systems for different types of setups and studies (they help to characterize global collision events) [2].

3.2.1 Time of flight (TOF) detector

The TOF detector [13], shown in Figure 3.2, is made up of 1638 MRPCs (Multi-gap Resistive Plate Chambers) and is divided into 18 sectors with respect to the azimuthal component. It covers a total area of 160 m^2. Its design is based on reaching a global resolution of time around 100 ps with the objective of identifying kaons and pions with energies greater than 2.5 GeV/c and protons with energies above 4 GeV/c in a pseudo-speed interval $\eta < |0.9|$. Using the information from the TPC and ITS, the mass of the particles can be calculated.

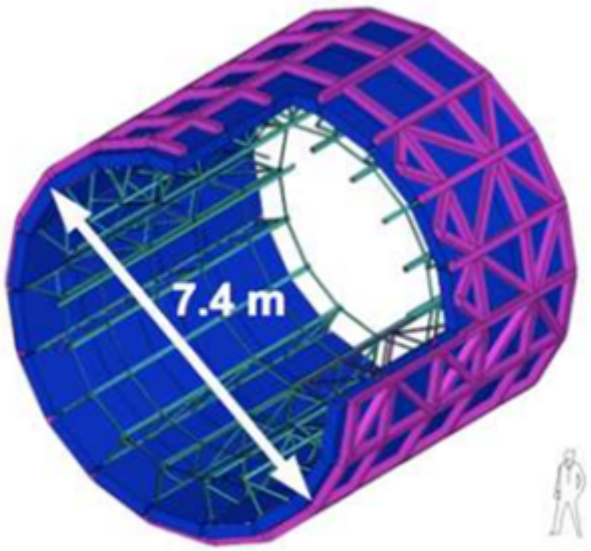

Figure 3.2: TOF detector.

3.2.2 Time measurement with TOF detector

The measurement technique that the TOF detector uses consists of the measurement of the factor β of a particle by means of independent measurements of the trajectory length. Since the information of the moment is available, it is possible to obtain an indirect measurement of the particle's mass. A particle with momentum p moving along a path of length L with a time of flight t has a mass of

$$m = p\sqrt{\frac{t^2}{L^2} - \frac{1}{c^2}}. \tag{3.1}$$

The error in the measurement of the mass is given by

$$\frac{\delta m}{m} = \frac{E^2}{m^2} \times \frac{\delta L}{L}. \tag{3.2}$$

If we consider two particles with masses m_1 and m_2, respectively, and both with the same moment p, then the time of flight difference is given by

$$\Delta t \approx \frac{L}{2c}\frac{m_1^2 - m_2^2}{p^2}, \tag{3.3}$$

where L is the length of the path and is valid as long as

$$\frac{m_1^2 - m_2^2}{p^2} \ll 1. \tag{3.4}$$

Furthermore, the standard deviation is given by

$$n_{L,m_{1,2}} = \frac{\Delta t}{\sigma} = \frac{L(m_1^2 - m_2^2)}{2p^2 c\sigma}. \tag{3.5}$$

3.2.3 Calorimeters

A calorimeter [14] measures the energy a particle loses as it passes through. It is usually designed to stop entirely or "absorb" most of the particles coming from a collision, forcing them to deposit all of their energy within the detector, thus measuring

their full energy. The calorimeters have to perform two different tasks at the same time, stopping particles and measuring energy loss, so they usually consist of layers of different materials: a "passive" or "absorbing" high-density material, for example, lead; interleaved with an "active" medium such as plastic scintillators or liquid argon. Electromagnetic calorimeters measure the energy of electrons and photons as they interact with the electrically charged particles in matter. Hadronic calorimeters sample the energy of hadrons (particles containing quarks, such as protons and neutrons) as they interact with atomic nuclei. Calorimeters can stop most known particles except muons and neutrinos.

3.2.4 Particle identification detectors

In addition to measuring a particle's momentum with tracking devices and its energy with calorimeters, physicists have further methods of narrowing down a particle's identity. All these methods rely on measuring the particle's velocity and calculating the particle's mass considering the momentum measured with tracking devices. In this form, the particle's identity can be determined.

The velocity can be measured using several methods. The simplest is to measure how much time it takes for a particle to travel a certain distance, using precise TOF detectors. Another method looks at how much a particle ionizes the matter that it passes through, as this is velocity-dependent and can be measured by tracking devices. Collecting all these clues from different parts of the detector, physicists build up a snapshot of what was in the detector at the moment of a collision. The next step is to scour the collisions for unusual particles, or for results that do not fit current theories [14].

3.2.5 Cherenkov radiation

Cherenkov radiation is a form of energy that we can perceive as a blue glow emitted when electrically charged particles composing atoms (i.e. electrons and protons) are moving at speeds faster than that of light in a specific medium. Devices sensitive to this

particular form of radiation, called Cherenkov detectors [15], have been used extensively to detect the presence of charged subatomic particles moving at high velocities.

3.3 Importance of time resolution

The time resolution defines how accurately can the time instant at which a particle crossed the detector be determined. It indicates the minimum unit of time in which the detector can distinguish two consecutive physical events of interest. Three examples of the importance of building detectors with very good time resolution are mentioned below.

- Trigger system with plastic scintillator detectors

If it is desired to use plastic scintillator detectors as a trigger in particle collisions where numerous particles are generated, it is necessary to have a good time resolution so that the trigger can identify each time a particle passes the detector. If two particles are approaching and the time resolution is not good enough, the detector would only identify one event and the second particle would go unnoticed.

- TOF detectors and identification of pions and kaons

In the characterization of ion collisions, it is important to be able to distinguish between pions and kaons. In a collision different types of particles will be generated. If two particles reach the detector and are very close together, as in the case of pions and kaons, one will hit just slightly before the other. When the particles hit the TOF detector, it will record the times and obtain two measurements of time. Therefore, since the TOF detectors calculate the mass of the particle as a function of the time of flight, a very good time resolution is critical to distinguish pions from kaons. This is why detectors with excellent time resolution are needed, such as Resistive Plate Chambers (RPC) gas detectors. These detectors have a very high potential difference and have multigap. In the case of ALICE, the time resolution of the TOF detector has been documented to be 56 ps [13].

- Positron emission tomography (PET)

A positron emission tomography scan is an effective way to identify a variety of conditions, including cancer, heart disease, and brain disorders. It is very important that an excellent time resolution can be obtained since, for example, the time resolution Δt will be directly proportional to the position Δx, and based on these data the image of the tissue that is emitting the gamma rays by the process of annihilation in the whole body is reconstructed, as shown in Figure 3.3 [16, 17].

In Figure 3.3, there is shown the concept of TOF positron emission tomography (TOF PET): (a) Illustration of a detector ring detecting pairs of gamma photons from the annihilation events with (green) and without (red) the TOF technique; (b) The probability distribution of the annihilation position along the line of response (LoR) in TOF PET; (c) The equal probability of the annihilation position along the LoR in non-TOF PET.

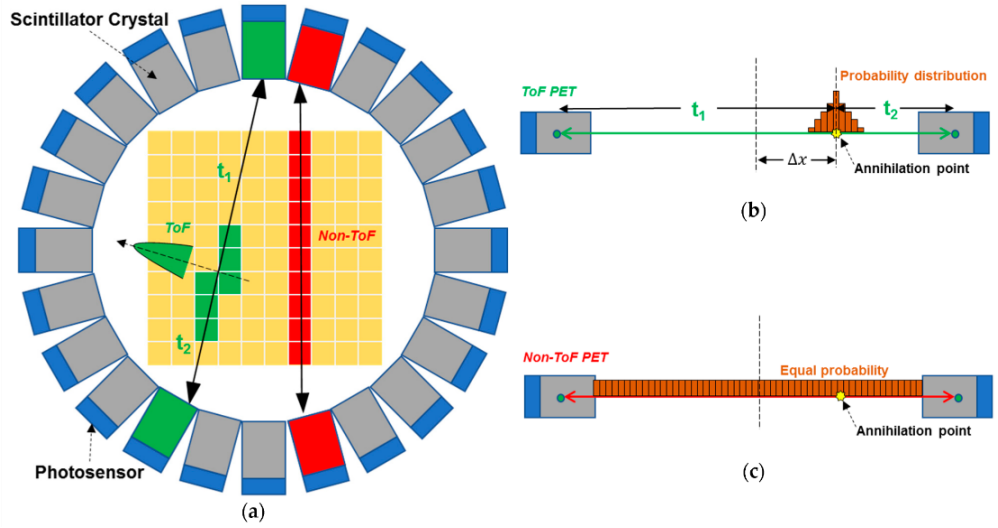

Figure 3.3: Concept of time-of-flight positron emission tomography (TOF PET) [16].

Chapter 4

Data Acquisition and Analysis

4.1 Detector configurations

The characterization of six different detectors was performed since the configurations of plastic scintillators and silicon photomultipliers (SiPM) were modified. The detectors configurations were as follows:

1. BC-404 hexagonal plastic scintillator (old) with 6x6 *mm* SiPM (old).
2. BC-404 hexagonal plastic scintillator (old) with 3x3 *mm* SiPM (new).
3. BC-404 hexagonal plastic scintillator (new) with 6x6 *mm* SiPM (old).
4. BC-404 hexagonal plastic scintillator (new) with 3x3 *mm* SiPM (new).
5. BC-404 hexagonal plastic scintillator (thick) with a 6x6 *mm* SiPM on each side (Two SiPMs).
6. BC-422Q square plastic scintillator with 6x6 *mm* SiPM (old).

The BC-404 hexagonal plastic scintillator (old) is a plastic that was manufactured a few years ago and has already been used several times so it has some scratches. On the other hand, the hexagonal plastic scintillator (new) is a plastic that was recently manufactured and had not been used before the development of this project.

In the case of SiPMs, the 6x6 *mm* SiPM (old) is a SiPM board that was manufactured a few years ago and has already been used several times, while the 3x3 *mm* SiPM (new) is a SiPM board that was recently manufactured and had not been used before the development of this project.

In Figure 4.1 there is the BC-404 hexagonal plastic scintillator (old), in Figure 4.2 the BC-404 hexagonal plastic scintillator (new) is shown, in Figure 4.3 the BC-422Q square plastic scintillator is shown, in Figure 4.4 there is the 6x6 *mm* SiPM (old) and in Figure 4.5 the 3x3 *mm* SiPM sensor (new) is located. Finally, in Figure 4.6 the BC-404 hexagonal plastic scintillator (thick) with a SiPM on each side (Two SiPMs) is shown.

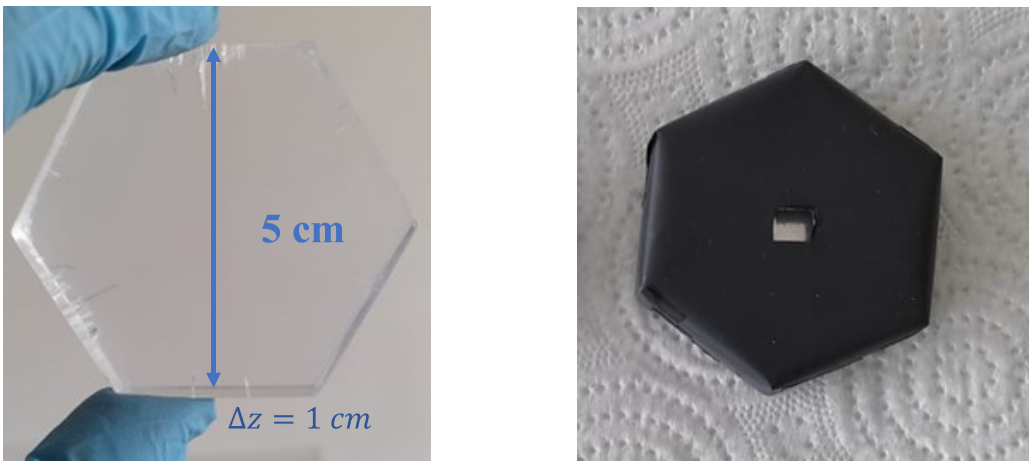

(a) Unlined (b) Lined

Figure 4.1: BC-404 Hexagonal Plastic Scintillator (Old).

(a) Unlined (b) Lined

Figure 4.2: BC-404 Hexagonal Plastic Scintillator (New).

(a) Unlined (b) Lined

Figure 4.3: BC-422Q Square Plastic Scintillator.

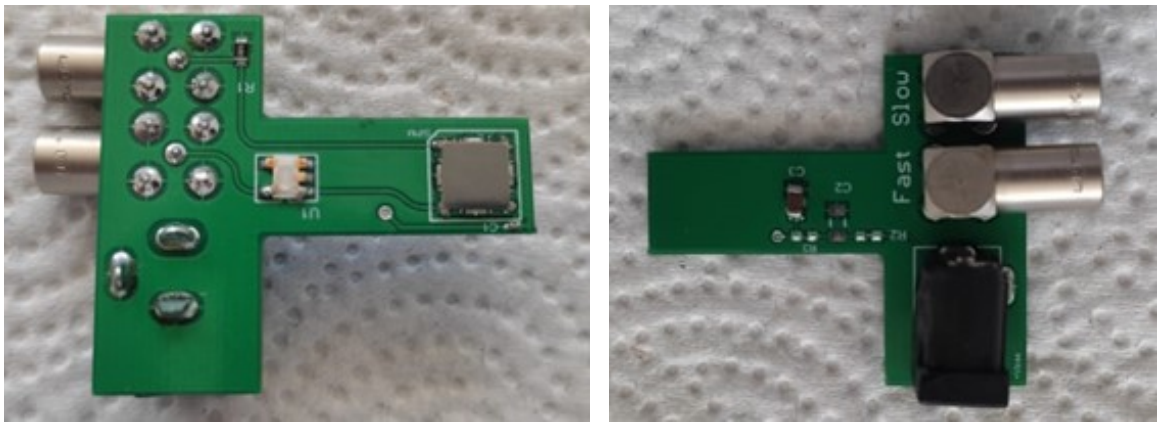

(a) Front (b) Back

Figure 4.4: 6x6 *mm* SiPM (Old).

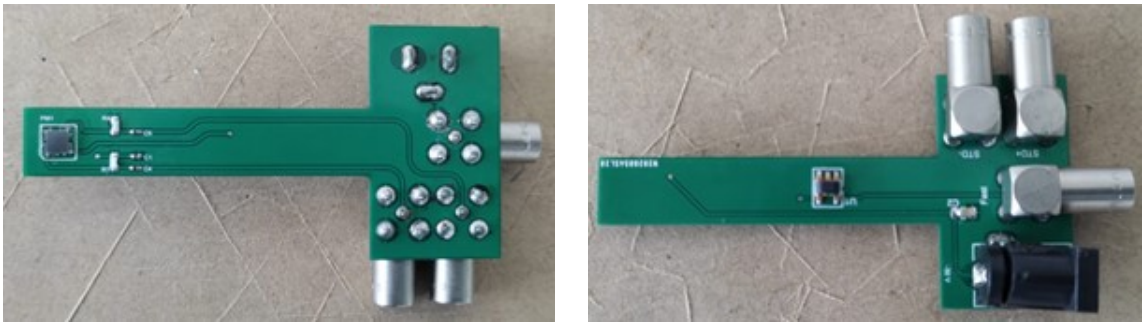

(a) Front (b) Back

Figure 4.5: 3x3 *mm* SiPM (New).

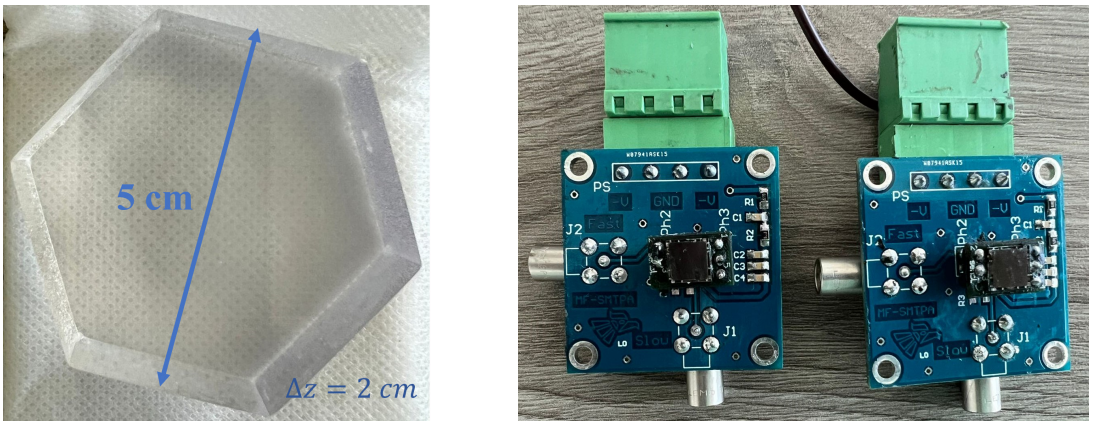

(a) Plastic Scintillator (Thick) (b) Two SiPMs Boards

Figure 4.6: BC-404 hexagonal plastic scintillator (thick) with 6x6 *mm* SiPM on each side (Two SiPMs).

The measurements of the plastic scintillators used are as follows:

- BC-404 hexagonal plastic scintillator (old): Apothem length of 2.5 *cm* and thickness of 1 *cm*.
- BC-404 hexagonal plastic scintillator (new): Apothem length of 2.5 *cm* and thickness of 1 *cm*.
- BC-404 hexagonal plastic scintillator (thick): Apothem length of 2.5 *cm* and thickness of 2 *cm*.
- BC-422Q square plastic scintillator: Side of 2 *cm* and thickness of 3 *mm*.

The characteristics of the 6 x 6 *mm* and 3 x 3 *mm* SiPM sensors used can be found in the datasheet [18].

During the manipulation of the plastic scintillator, the use of gloves was primordial to prevent contamination. The plastic scintillator was cleaned using gauze and methyl alcohol. Moreover, scratches and imperfections on its surface were removed by polishing. In Figure 4.7 the cleaned and polished hexagonal plastic scintillator can be seen.

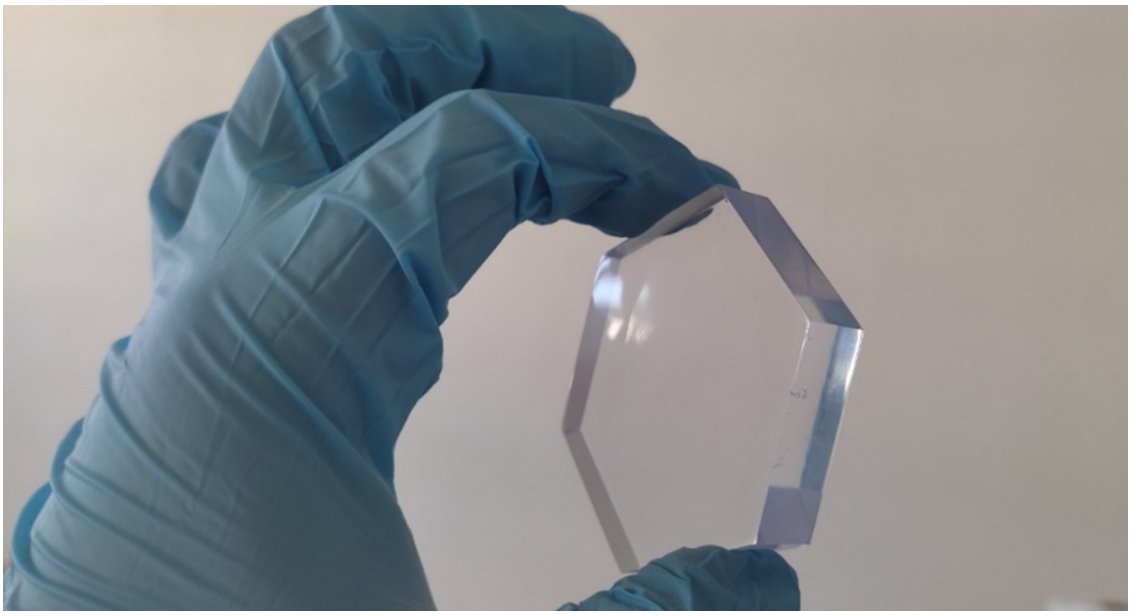

Figure 4.7: Clean hexagonal plastic scintillator.

The lining of the plastic scintillators consists of three layers. The first layer is with mylar film, while the next two are with tyvek paper. A small window must be cut to collocate one of the SiPM detector, either the 3x3 *mm* or the 6x6 *mm*. In Figure 4.8 the layers that cover the plastic scintillator are located.

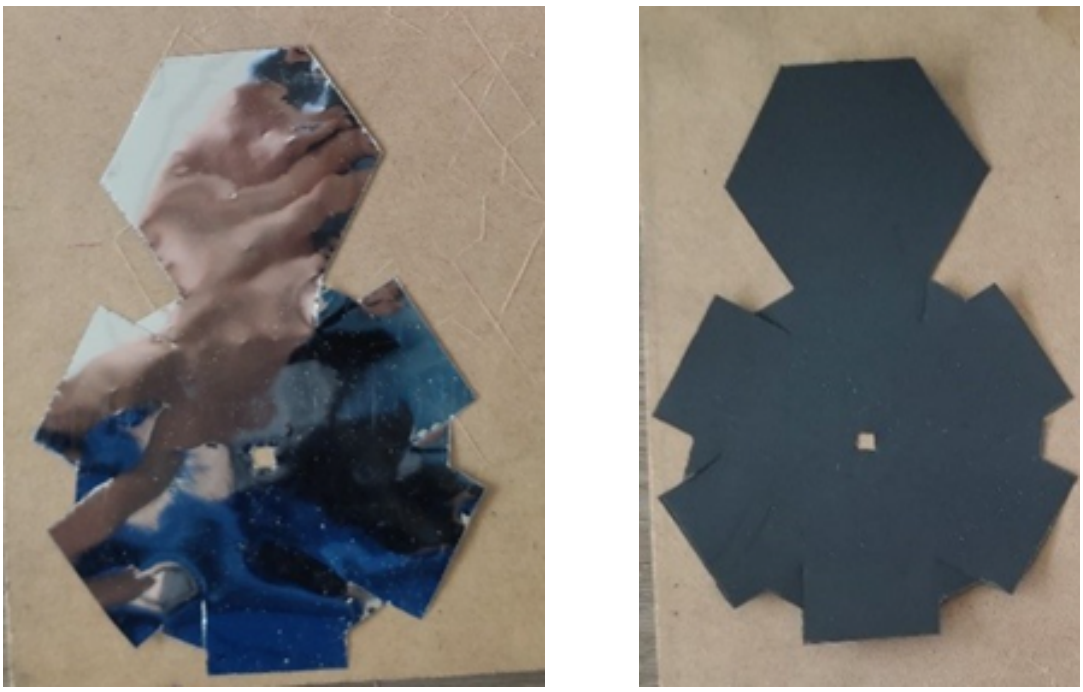

(a) Mylar film (b) Tyvek paper

Figure 4.8: Mylar film and Tyvek paper for the lining.

A drop of Rhodorsil paste 7 is placed in the window, which is an optical grease that facilitates the detection of photons between the SiPM and the plastic scintillator. This can be observed in Figure 4.9. Finally, the SiPM detectors are fixed with electrical tape so that the detectors fit into the window and remain directly on the plastic scintillator, as in Figure 4.10

Figure 4.9: Rhodorsil paste 7 optical grease.

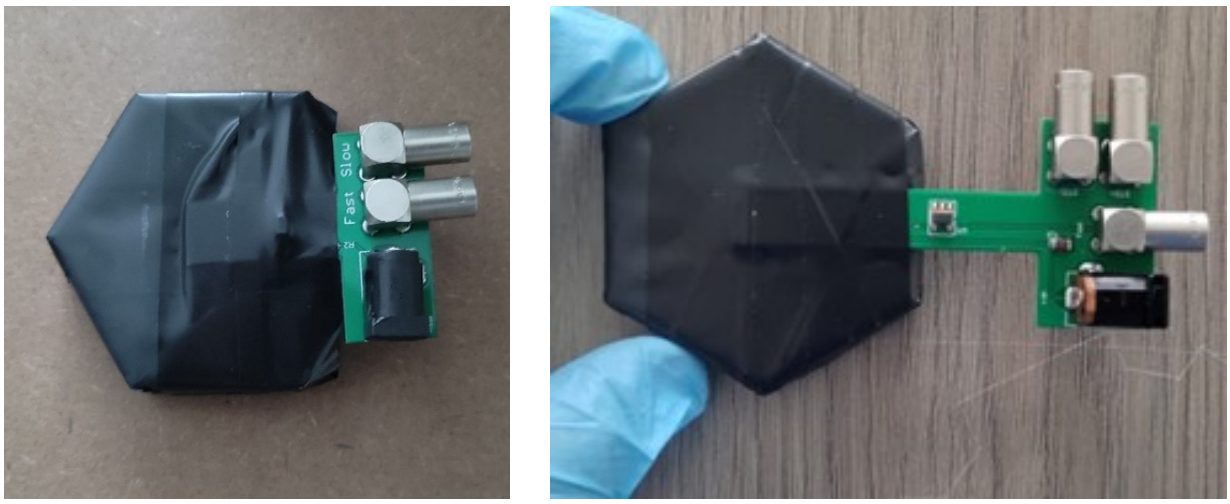

(a) Old SiPM detector (b) New SiPM detector

Figure 4.10: SiPM detectors (old and new) with hexagonal plastic scintillators.

Two PMT detectors were also characterized to find their optimal operating voltages since these detectors were used as a trigger for the characterization tests of the aforementioned SiPM detectors and these voltages were maintained for the other tests.

The characterization of the PMT detectors consisted of aligning both detectors so that the particles (atmospheric muons) crossed both PMTs perpendicularly, and an event counter was used, which counts each time a pulse is generated, to record the number of events of both PMT detectors. The supply voltages of the PMTs were modified until the event outcomes of the two PMTs were very similar. The optimal supply voltages for the PMT UP was - 970 V and for PMT DOWN was -985 V. These PMTs are shown in Figure 4.11.

Figure 4.11: PMTs used as trigger for the SiPM characterization tests.

4.2 Data acquisition

The characterization of the detectors was performed with two different sets of equipment to compare the results of the time resolution with each configuration. The first characterization was done with the CAEN DT5742B digitizer, while the second characterization was done using the modules CAEN V1290N TDC and CAEN V792N QDC.

For each case, the instrumentation detailed below was also used: CAEN DT1471ET high voltage power supply; BK Precision Model 9110 Power Supply; CAEN V925 FanIn-FanOut; CAEN V976 NIM translator; CAEN V974 and V975 amplifiers; CAEN V1718 VME Bridge; LeCROY's 62IL discriminator and LeCROY's 622C coincidences module.

The general experimental setup used can be seen in Figure 4.12, the connection diagram of the tests with the digitizer and the 6x6 *mm* SiPM (old) is shown in Figure 4.13, while the connection diagram of the tests with the digitizer and the 3x3 *mm* SiPM (new) is displayed in Figure 4.14. The difference is that the charge deposited on the 3x3 *mm* SiPM (new) is smaller, so the pulse size is also smaller, and a higher amplification was needed to be able to analyze the pulses of this SiPM properly.

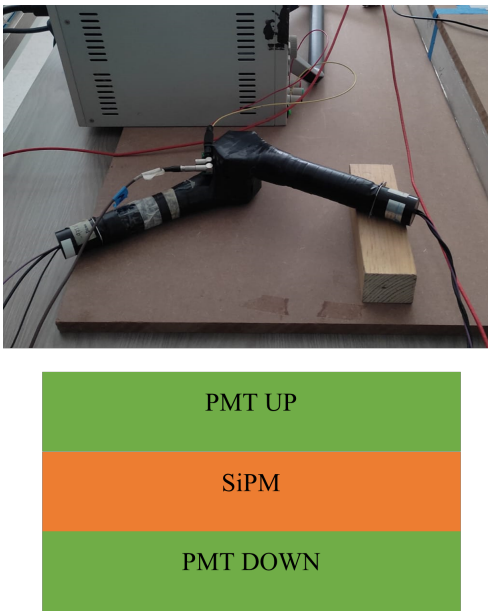

Figure 4.12: General experimental setup for the characterization of the SiPM detectors.

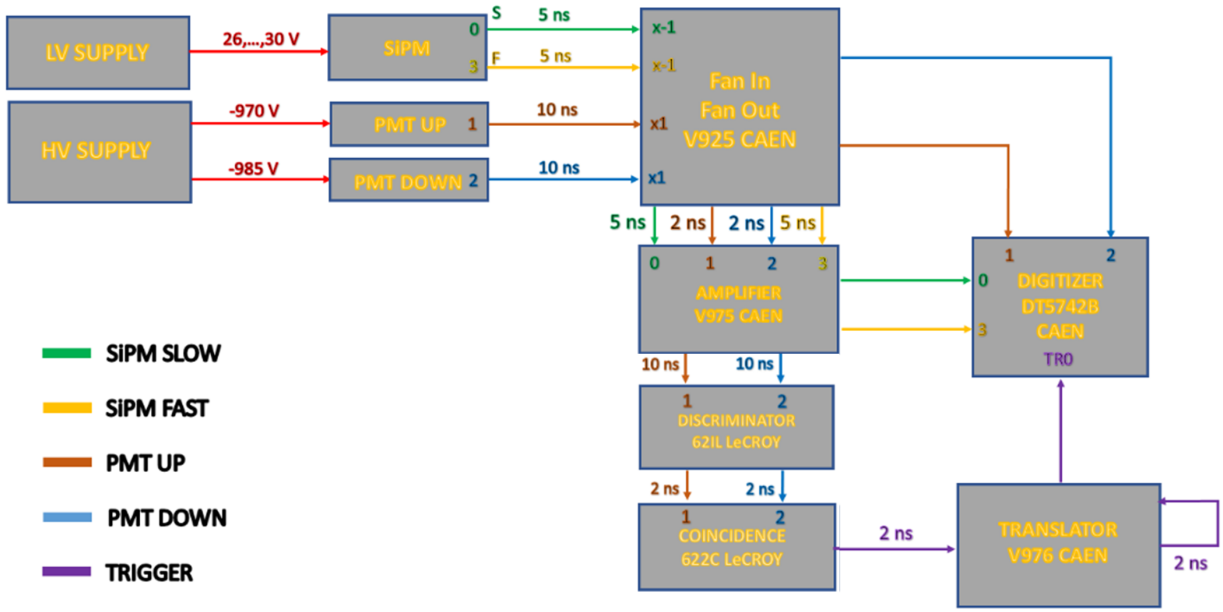

Figure 4.13: Connection diagram for the characterization with the digitizer of detectors with 6x6 *mm* SiPM (old).

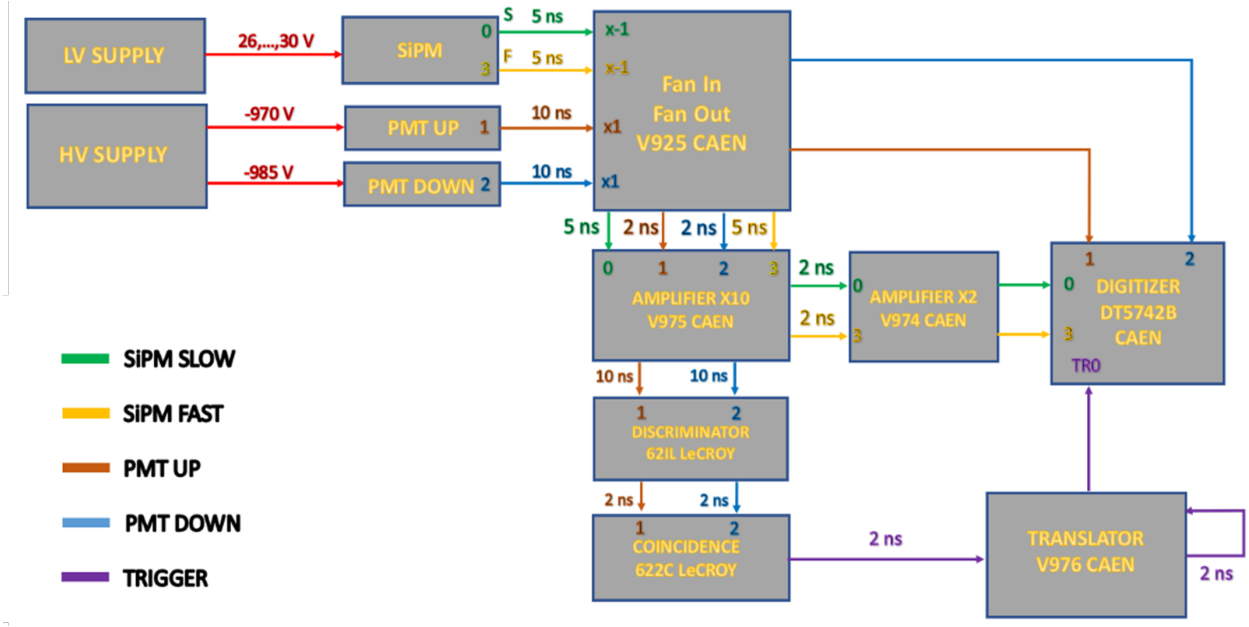

Figure 4.14: Connection diagram for the characterization with the digitizer of detectors with 6x6 *mm* SiPM (new).

The experimental setup for the detector configuration of BC-404 hexagonal plastic scintillator (thick) with a 6x6 *mm* SiPM on each side (Two SiPMs) is shown in Figure 4.14. The signals that were analyzed from this configuration were the SiPM 1 standard signal, the SiPM 2 standard signal, and the SiPM 1 fast signal.

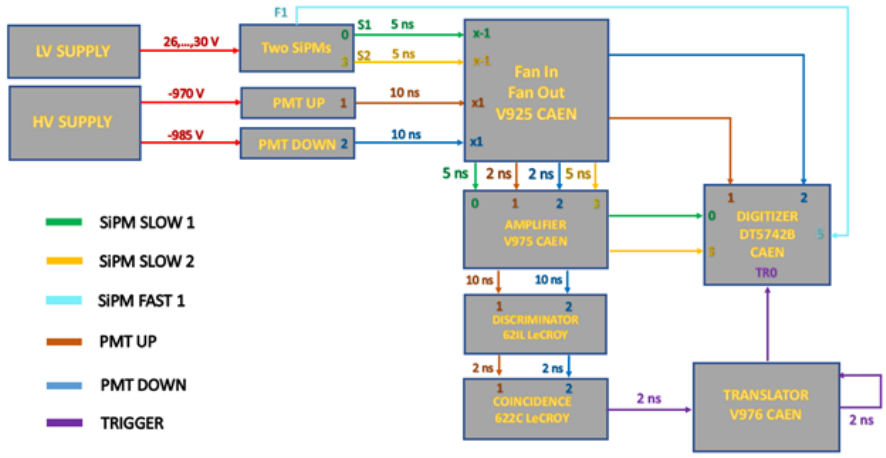

Figure 4.15: Connection diagram for the characterization with the digitizer of the BC-404 hexagonal plastic scintillator (thick) with a 6x6 mm SiPM on each side (Two SiPMs) detector.

On the other hand, the connection diagram of the tests with the TDC and QDC modules can be seen in Figure 4.16. The amplification of the SiPM pulses was also modified so that the QDC module could detect them for each value of the supply voltage analyzed. The data were collected by computer through the VME Bridge module. However, it was not possible to analyze the charge deposited on the pulse of the fast output signal because the QDC instrument was not capable of detecting this pulse. This is due to the small size of the fast signal and the low charge deposited. Therefore, the charge deposited analysis and efficiency analysis were performed only on the standard output signal.

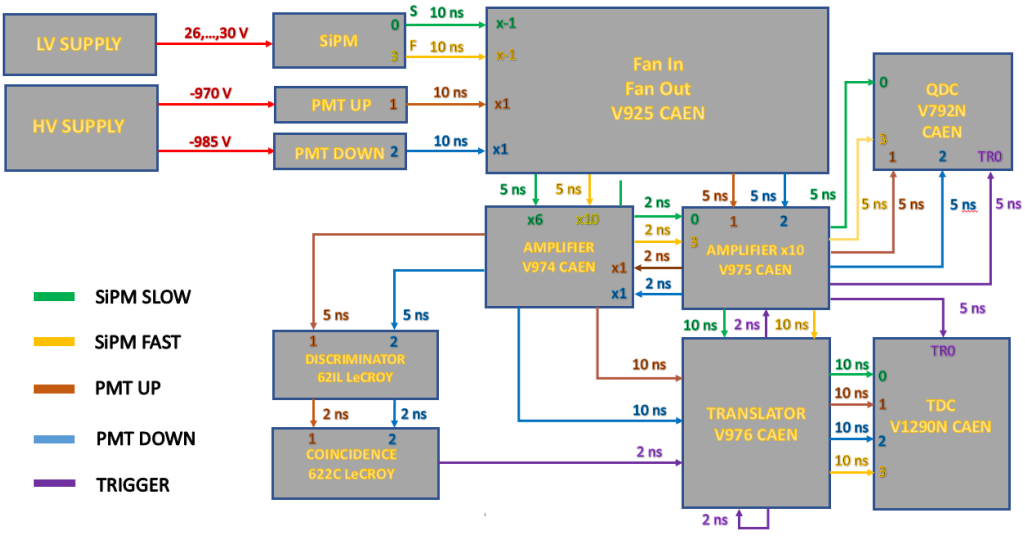

Figure 4.16: Connection diagram for the characterization of SiPM detectors using TDC and QDC modules.

In addition, the characterization of the systematic error introduced by all the instrumentation that is being used was performed, both in the case of the digitizer and in the case of the TDC module. The systematic error in the tests with the digitizer was obtained using the configuration of Figure 4.17. The generator creates a pulse signal similar to that obtained from PMT detectors and passes through the instrumentation used in the characterization tests. Cables of different lengths were used so that the delay value in *ns* that should exist between the pulses was known and Gaussian adjustments were made to the time differences. The systematic error obtained in this case was 242 *ps*. This value is considered within the error bars when calculating the time resolution of the detector characterization results using the digitizer.

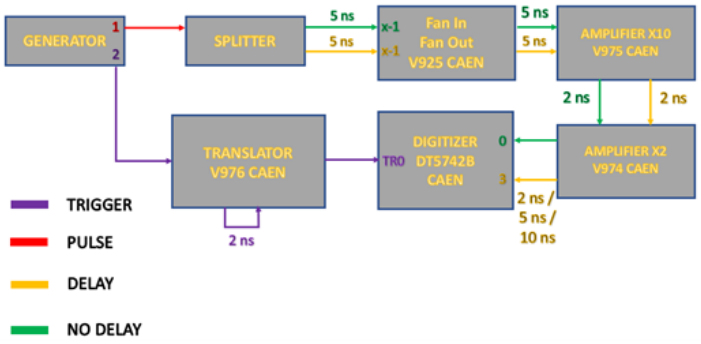

Figure 4.17: Connection diagram for the characterization of the instrumentation with the digitizer.

On the other hand, the systematic error in the tests with the TDC was obtained using the configuration of Figure 4.18. The systematic error value obtained for the tests with the TDC was 127 *ps*. This value is also considered within the error bars when calculating the time resolution of the detector characterization results using the TDC.

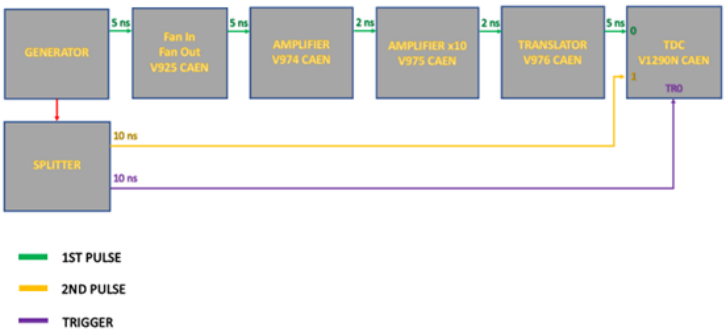

Figure 4.18: Connection diagram for the characterization of the instrumentation with the TDC module.

4.3 Data analysis

The data were analyzed with the root framework to obtain the results of time resolution and efficiency of each of the detector configurations for supply voltage values in the range 26 V to 30 V, using both SiPM output signals: the standard (or slow) output and the fast output.

Within the data collected there are events that can be generated by electronic noise from the instrumentation being used, from the facilities, and even from the characteristics of the environment at the time of testing. Therefore, it is necessary to adequate the event selection to obtain the results of time resolution and efficiency of the detectors that are being characterized.

Using the digitizer, it was possible to analyze the charge and time of each event in a way that they are related to each other. Nevertheless, during the tests with the TDC and QDC modules, it was not possible to relate the TDC events with the QDC events, so they had to be analyzed as separate events for each instrument used.

The particle charge of each event corresponds to the area of the pulse measured, and for practical purposes is expressed in ADC counts of the corresponding event. The computation of the ADC counts is performed using the integration trapezoidal method.

4.3.1 Selection criteria for the digitizer tests

The selection criteria of valid events for the digitizer are described by the four points below:

1. The SiPM sensor pulses start times must be less than the PMT Up and Down pulse start times. Applies to both the slow signal and the fast signal. In Figure 4.19, there is an example of the pulses obtained from the digitizer and the start times of each signal, where $t_3(s)$ is the start time of the SiPM standard signal, $t_3(f)$ is the start time of the SiPM fast signal, t_2 is the start time of the PMT Down signal and t_1 is the start time of the PMT Up signal.

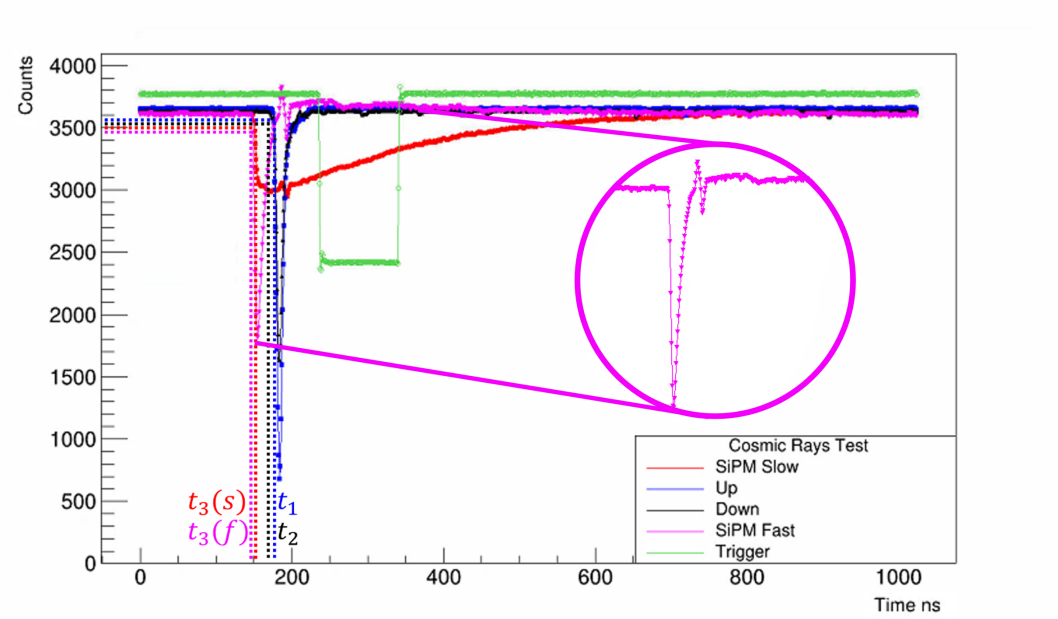

Figure 4.19: First selection criterion for the digitizer, where t3 must be less than t2 and t1, being the SiPM, PMT Down and PMT Up start times respectively.

2. The pulse width for the SiPM slow signal must be greater than 100 ns and less than 900 ns, while the pulse width for the SiPM fast signal must be greater than 10 ns and less than 40 ns. In Figure 4.20, there are the pulses of the slow and fast outputs of the SiPM in red and pink, respectively. Times t_3 and t_4 are the pulse start and end times, respectively, for each of the SiPM output signals.

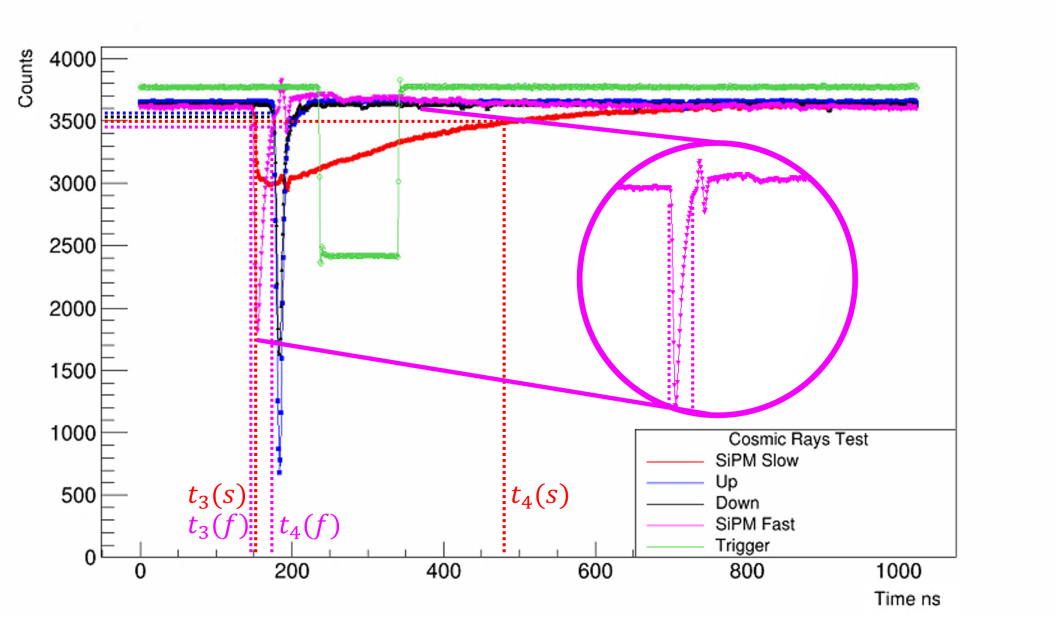

Figure 4.20: Second selection criterion for the digitizer, where the pulse width of the SiPM signals must be within a range to be considered valid.

3. The pulse area for the slow signal from the SiPM must be less than the maximum value on the digitizer display before it saturates. The value obtained was 900,000 ADC counts. For the SiPM fast signal, the SiPM pulse area must be greater than a value of 10000 ADC counts, since lower values are considered noise. In Figure 4.21, the pulses of the SiPM signals and the parts corresponding to the pulse area of the slow signal as area (s) and to the area of the fast signal pulse as area (f) can be seen.

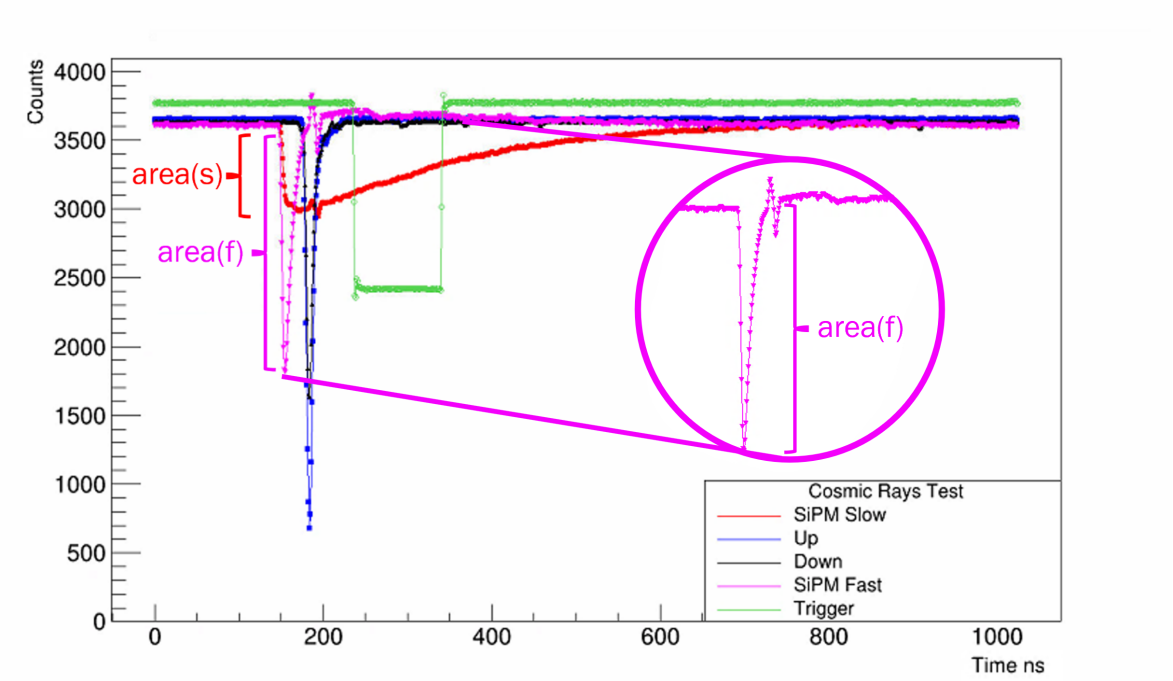

Figure 4.21: Third selection criterion for the digitizer, where the pulse area of the SiPM signals must be within a range to be considered valid.

4. The events of greatest interest are within the average of the PMT charges, giving a radius around the average of 10,000 ADC counts. In Figure 4.22, the graph of the PMT Up charge against the PMT Down charge can be seen and it is possible to visualize a pattern with a circle where the greatest number of events are found. Within the red circle, the events of interest will be considered for the analysis of the time resolution and the efficiency of the SiPM detectors.

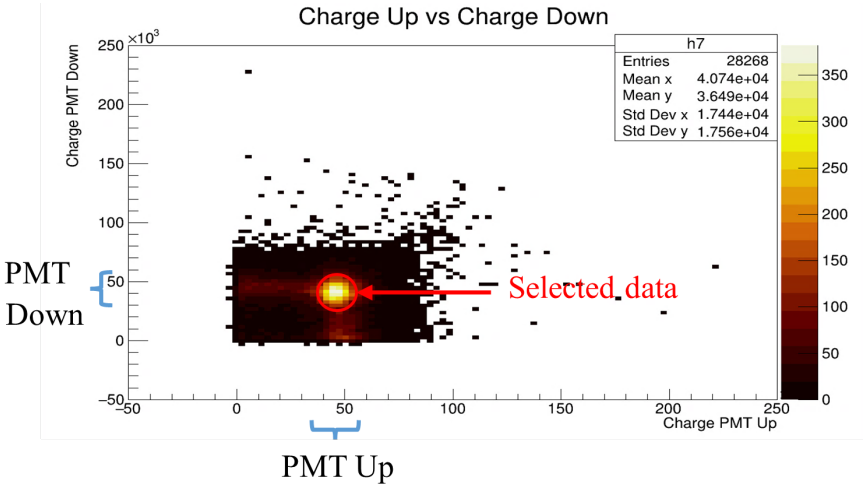

Figure 4.22: Fourth selection criterion for the digitizer, where the events of interest are those within a delimited radius given by the average of the PMTs charges.

4.3.2 Selection criteria for the TDC and QDC tests

The selection criteria of valid events for the TDC are described below:

1. The SiPM sensor pulse arrival time must be less than the PMT Up and PMT Down pulse arrival times. Applies to both the standard signal and the fast signal. Figure 4.23, shows an example of the differences between the arrival times of each PMT and SiPM signal, with the PMT-SiPM differences always being positive, that is, the SiPM signals have a shorter arrival time.

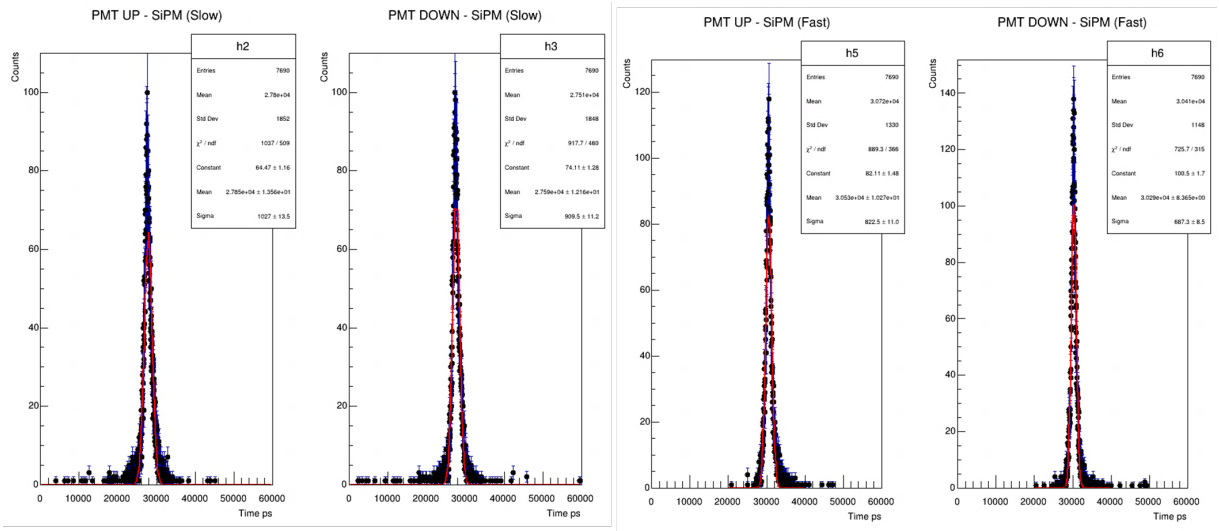

Figure 4.23: First selection criterion for the TDC, where the arrival times of the SiPM must be less than the arrival times of the PMT Up and the PMT Down.

2. The events of interest are within the average of the differences between the arrival times of the PMTs. Figure 4.24 shows an example of the difference between the arrival times of the PMT Up and the PMT Down. These events are constrained around the average, thus eliminating noise events that could occur in coincidences between PMTs.

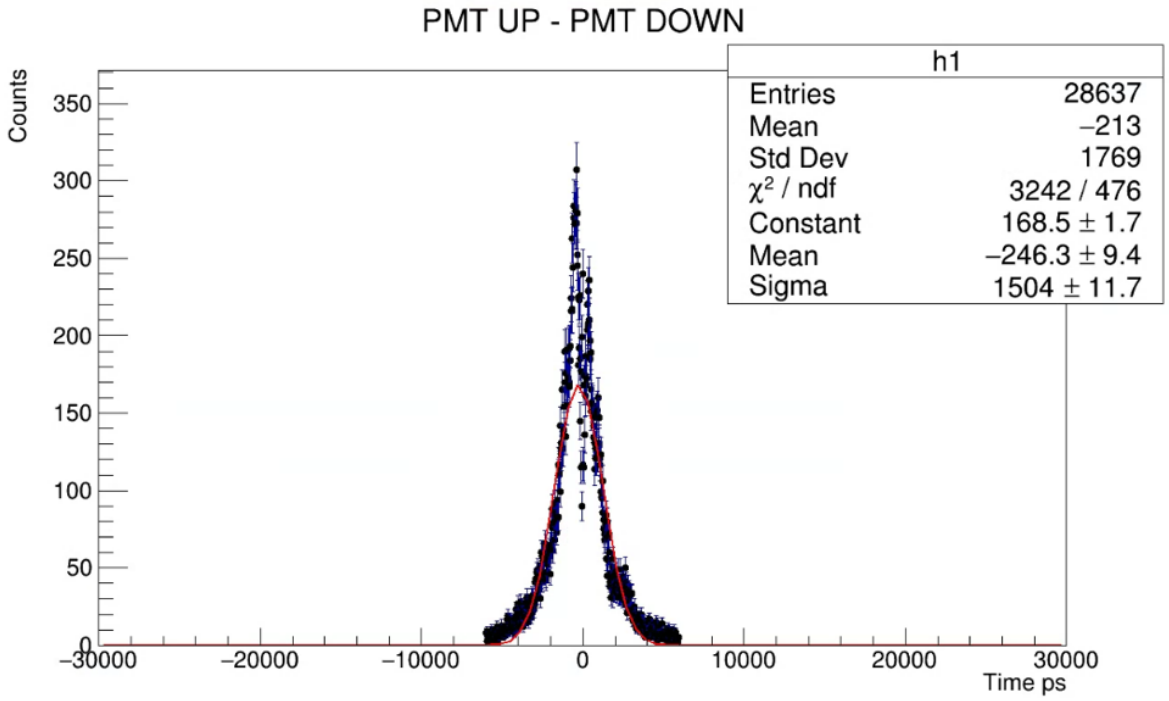

Figure 4.24: Second selection criterion for the TDC, where the events of interest are around the average of the differences between the arrival times of the PMT Up and PMT Down.

On the other hand, the selection criterion of valid events for the QDC was defined with respect to the following description:

- The events of greatest interest are within the average of the PMT charges, giving a radius around the average of 565 ADC counts. Figure 4.25 shows the graph of the PMT Up charge against the PMT Down charge. Within the red circle, the events of interest will be considered for the analysis of the time resolution and the efficiency of the SiPM detectors.

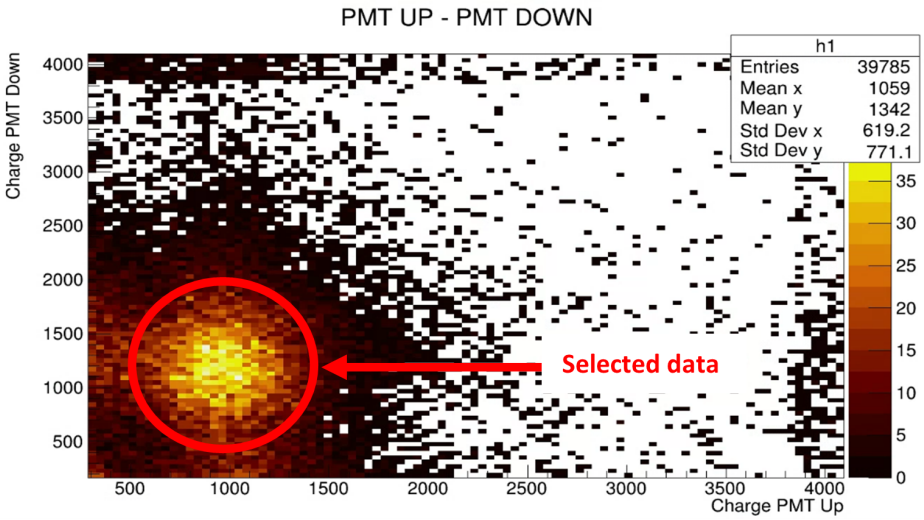

Figure 4.25: Selection criterion for the QDC, where the events of interest are those within a delimited radius given by the average of the PMTs charges.

4.3.3 Efficiency

The equation used to calculate the efficiency is

$$P(SiPM|PMTUp \wedge PMTDown) = \frac{N_{SiPM}}{N_{PMT}} = \frac{N(SiPM \wedge PMTUp \wedge PMTDown)}{N(PMTUp \wedge PMTDown)}, \tag{4.1}$$

where N_{SiPM} is the number of events that fulfilled the 3-fold coincidence condition, defined by the logic AND between PMT Up, PMT Down, and the SiPM detector, while N_{PMT} is the total number of events given by the 2-fold coincidence between the PMT Up and PMT Down.

For the square plastic scintillator an estimate was made with respect to the area, given by the following equation

$$P(SiPM|PMTUp \wedge PMTDown) = \frac{N_{SiPM}}{N_{PMT}} \times ScaleFactor, \tag{4.2}$$

where

$$ScaleFactor = \frac{SquareArea}{HexArea} = \frac{4cm^2}{21.65cm^2} = 5.4125. \tag{4.3}$$

4.3.4 Time resolution

In order to compute the time resolution, the sensors' parameters are referred as follows. The PMT Up time resolution is denoted by σ_1, the PMT Down time resolution is denoted by σ_2, the SiPM time resolution is denoted by σ_3, the variance of the difference between the starting time of the PMT Up and PMT Down events is denoted by σ_{12}, the variance of the difference between the starting time of the PMT Up and SiPM events is denoted by σ_{13}, and the variance of the difference between starting time of the PMT Down and SiPM events is denoted by σ_{23}.
The variance of correlated random variables is given by

$$\sigma_{12}^2 = \sigma_1^2 + \sigma_2^2 - 2\rho\sigma_1\sigma_2, \tag{4.4}$$

where ρ is the correlation. In this case, the correlation between the variables of each detector is zero, because there is no relationship between them. Therefore, the variance of correlated random variables is simplified to

$$\sigma_{12}^2 = \sigma_1^2 + \sigma_2^2. \tag{4.5}$$

Applying the same procedure to each pair of variables, the following relations are obtained

$$\sigma_{13}^2 = \sigma_1^2 + \sigma_3^2, \tag{4.6}$$

$$\sigma_{23}^2 = \sigma_2^2 + \sigma_3^2. \tag{4.7}$$

From the data, σ_{12}, σ_{13} and σ_{23} are already known, but it is necessary to know the SiPM detector time resolution σ_3. Solving both equations for σ_3 and adding the results, the following is obtained

$$2\sigma_3^2 = \sigma_{13}^2 + \sigma_{23}^2 - \sigma_1^2 - \sigma_2^2. \tag{4.8}$$

Substituting (4.5) into the previous equation and solving for σ_3, the SiPM time resolution is finally given by

$$\sigma_3^2 = \sqrt{\frac{\sigma_{13}^2 + \sigma_{23}^2 - \sigma_{12}^2}{2}}. \tag{4.9}$$

Moreover, the time resolution error E at each point is given by

$$E = \sigma_3 - \sqrt{\sigma_3^2 - (\sigma_{Sys}^2 + \sigma_{Sta}^2)}, \tag{4.10}$$

where σ_3 is the SiPM time resolution, σ_{Sys} is the Systematic error, and σ_{Sta} is the Stadistical error.

An example of the time differences between the SiPM and the PMTs is shown in Figure 4.26. The value of σ_{12} is the sigma from the first plot, the value of σ_{13} is the sigma from the second plot, and the value of σ_{23} is the sigma from the third plot.

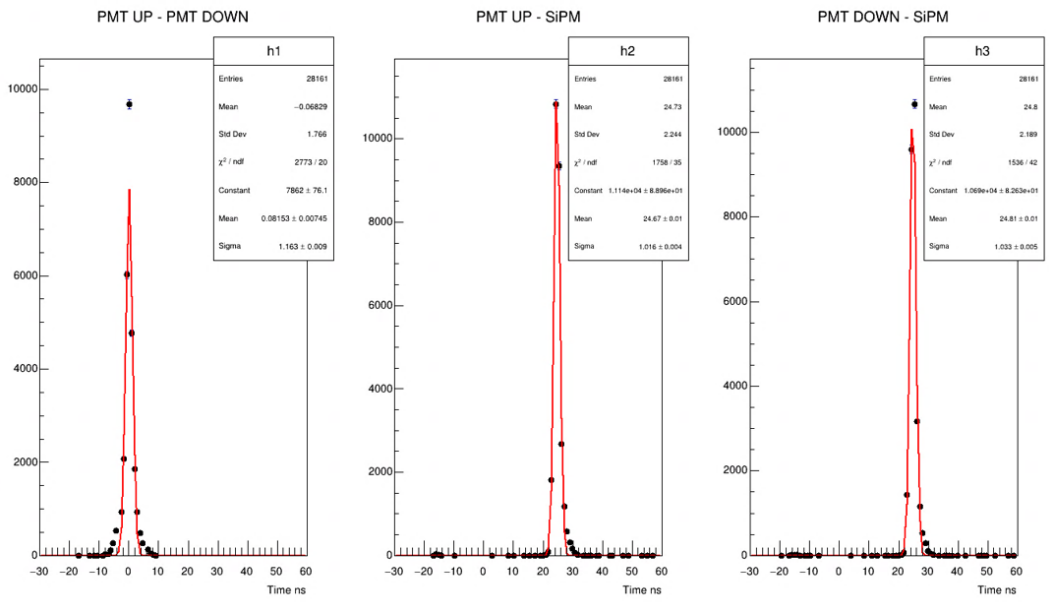

Figure 4.26: Example of how time resolution is obtained..

Chapter 5

Results

5.1 BC-404 plastic scintillator detectors results using the digitizer

Results of time resolution and efficiency for each configuration are shown below; Table 5.1 and Figure 5.1 show the values and their plot, respectively, for data obtained from the detector configuration of BC-404 hexagonal plastic scintillator (old) and the 6x6 *mm* SiPM (old); Table 5.2 and Figure 5.2 show the values and their plot, respectively, for data obtained from the detector configuration of BC-404 hexagonal plastic scintillator (old) and the 3x3 *mm* SiPM (new); Table 5.3 and Figure 5.3 show the values and their plot, respectively, for data obtained from the configuration of BC-404 hexagonal plastic scintillator (new) and the 6x6 *mm* SiPM (old); finally, Table 5.4 and Figure 5.4 show the values and their plot, respectively, for data obtained from the detector of BC-404 hexagonal plastic scintillator (new) and the 3x3 *mm* SiPM (new).

The gain tables and graphs are shown in the following order: Table 5.5 and Figure 5.5 show the values and their plot, respectively, for data obtained from the detector with BC-404 hexagonal scintillator plastic (old) and the 6x6 *mm* SiPM (old); Table 5.6 and Figure 5.6 show the values and their plot, respectively, for data obtained from the detector with hexagonal BC-404 plastic scintillator (old) and the 3x3 *mm* SiPM (new); Table 5.7 and Figure 5.7 show the values and their plot, respectively, for data obtained

from the detector with BC-404 hexagonal plastic scintillator (new) and the 6x6 *mm* SiPM (old); Table 5.8 and Figure 5.8 show the values and their plot, respectively, for data obtained from the detector with hexagonal plastic BC-404 scintillator (new) and the 3x3 *mm* SiPM (new).

Table 5.1: Results of the detector configuration of BC-404 hexagonal plastic scintillator (old) with 6x6 *mm* SiPM (old) using the digitizer.

BC-404 hexagonal plastic scintillator (old) with 6x6 *mm* SiPM (old)				
	Standard Signal		Fast Signal	
Voltage (V)	Efficiency (%)	Time Resolution (ps)	Efficiency (%)	Time Resolution (ps)
26	24.96	622 ± 48.9	72.27	719 ± 41.9
27	57.25	504 ± 61.9	89.80	507 ± 61.5
28	98.56	404 ± 80.5	95.92	416 ± 77.6
29	99.66	320 ± 110.6	99.43	387 ± 84.9
30	99.61	306 ± 118.7	99.58	366 ± 91.4

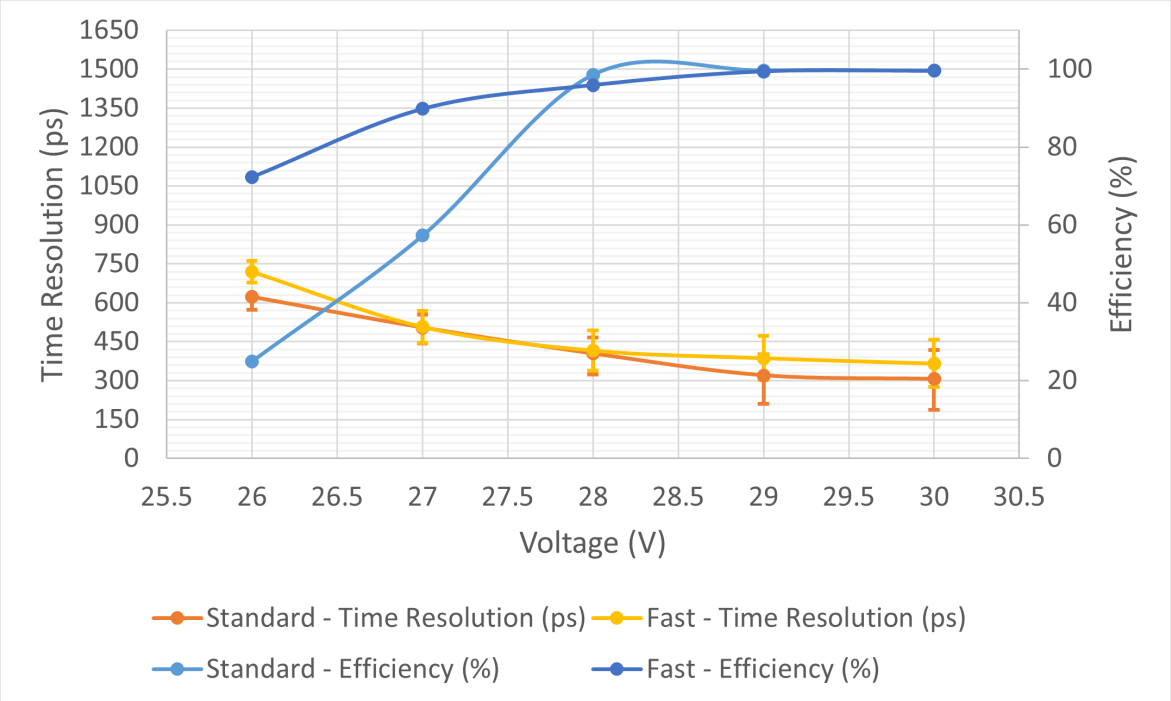

Figure 5.1: Results of the time resolution and efficiency of the detector configuration of BC-404 hexagonal plastic scintillator (old) with 6x6 *mm* SiPM (old) using the digitizer.

Table 5.2: Results of the detector configuration of BC-404 hexagonal plastic scintillator (old) with 3x3 *mm* SiPM (new) using the digitizer.

BC-404 hexagonal plastic scintillator (old) with 3x3 *mm* SiPM (new)				
	Standard Signal		Fast Signal	
Voltage (V)	Efficiency (%)	Time Resolution (ps)	Efficiency (%)	Time Resolution (ps)
26	24.71	996 ± 29.8	26.75	876 ± 34.0
27	49.57	812 ± 36.9	42.96	739 ± 40.7
28	67.46	635 ± 47.9	58.85	721 ± 41.8
29	76.87	626 ± 48.6	61.55	623 ± 48.9
30	85.96	607 ± 50.3	67.94	560 ± 55.0

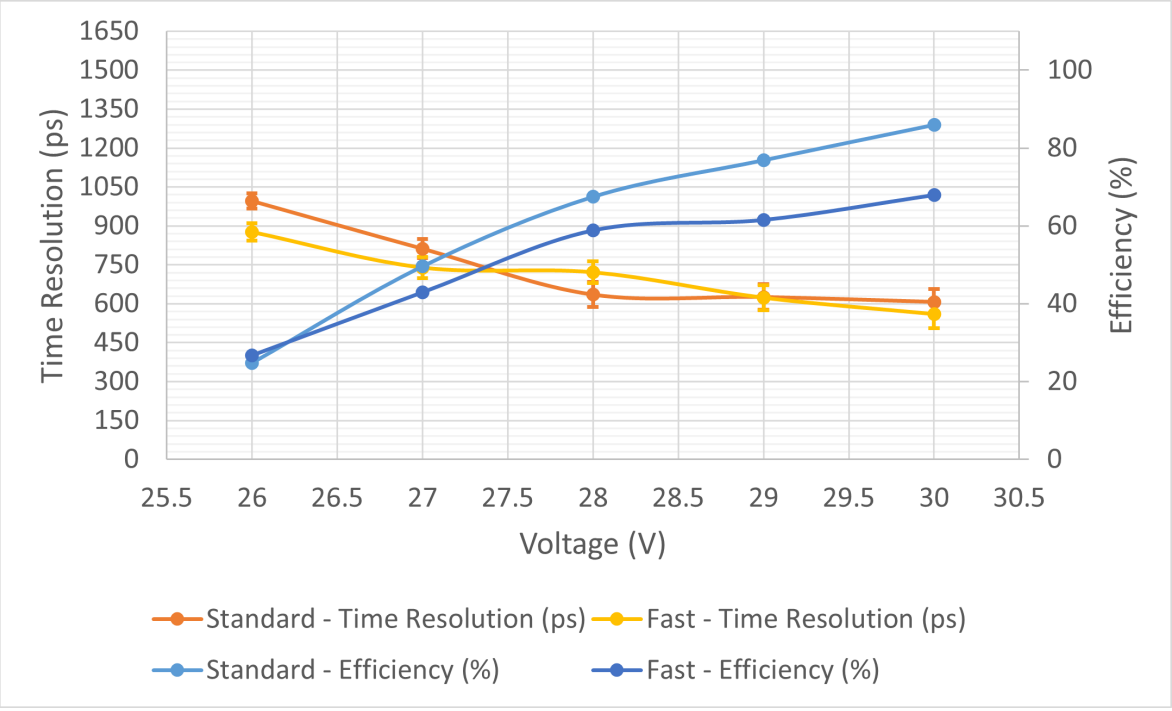

Figure 5.2: Results of the time resolution and efficiency of the detector configuration of BC-404 hexagonal plastic scintillator (old) with 3x3 *mm* SiPM (new) using the digitizer.

Table 5.3: Results of the detector configuration of BC-404 hexagonal plastic scintillator (new) with 6x6 *mm* SiPM (old) using the digitizer.

BC-404 hexagonal plastic scintillator (new) with 6x6 *mm* SiPM (old)				
	Standard Signal		Fast Signal	
Voltage (V)	Efficiency (%)	Time Resolution (ps)	Efficiency (%)	Time Resolution (ps)
26	43.65	942 ± 31.6	35.94	999 ± 29.7
27	85.33	542 ± 57.0	79.41	799 ± 37.5
28	96.39	508 ± 61.3	91.39	639 ± 47.6
29	99.99	482 ± 65.1	99.95	546 ± 56.5
30	99.99	505 ± 61.7	99.97	502 ± 62.2

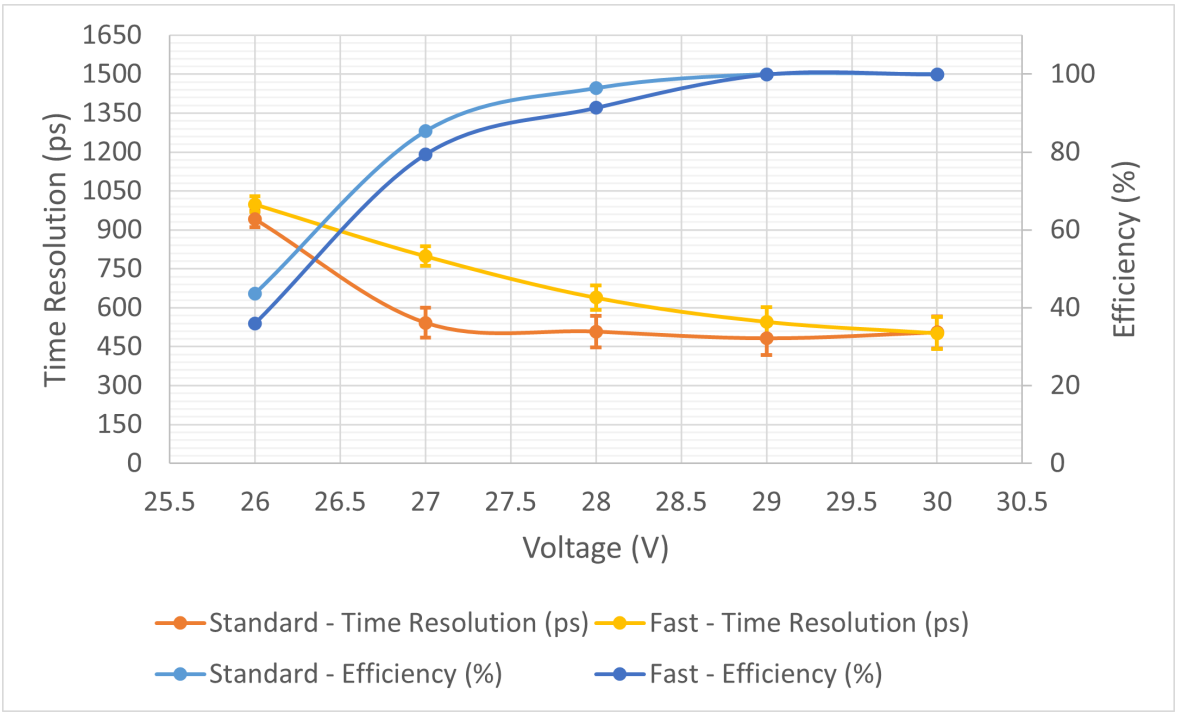

Figure 5.3: Results of the time resolution and efficiency of the detector configuration of BC-404 hexagonal plastic scintillator (new) with 6x6 *mm* SiPM (old) using the digitizer.

Table 5.4: Results of the detector configuration of BC-404 hexagonal plastic scintillator (new) with 3x3 *mm* SiPM (new) using the digitizer.

BC-404 hexagonal plastic scintillator (new) with 3x3 *mm* SiPM (new)				
	Standard Signal		Fast Signal	
Voltage (V)	Efficiency (%)	Time Resolution (ps)	Efficiency (%)	Time Resolution (ps)
26	53.28	1424 ± 20.7	41.88	1176 ± 25.2
27	81.60	887 ± 33.6	45.57	784 ± 38.3
28	93.13	582 ± 52.7	57.63	678 ± 44.6
29	99.59	557 ± 55.3	77.17	631 ± 45.0
30	99.64	485 ± 64.7	64.53	597 ± 51.2

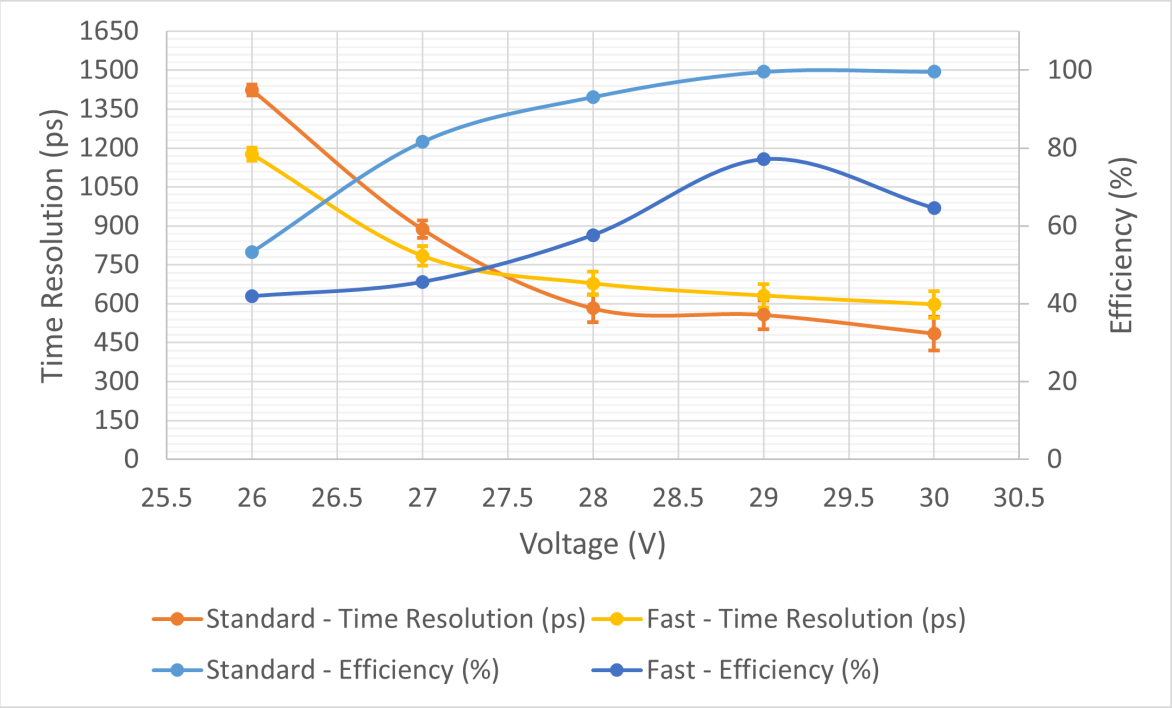

Figure 5.4: Results of the time resolution and efficiency of the detector configuration of BC-404 hexagonal plastic scintillator (new) with 3x3 *mm* SiPM (new) using the digitizer.

Table 5.5: Gain results of the detector configuration of BC-404 hexagonal plastic scintillator (old) with 6x6 *mm* SiPM (old) using the digitizer.

BC-404 hexagonal plastic scintillator (old) with 6x6 *mm* SiPM (old)		
	Standard Signal	Fast Signal
Voltage (V)	MPV (ADC Counts)	MPV (ADC Counts)
26	19550	693
27	32030	1794
28	63760	3314
29	108700	5190
30	157300	7596

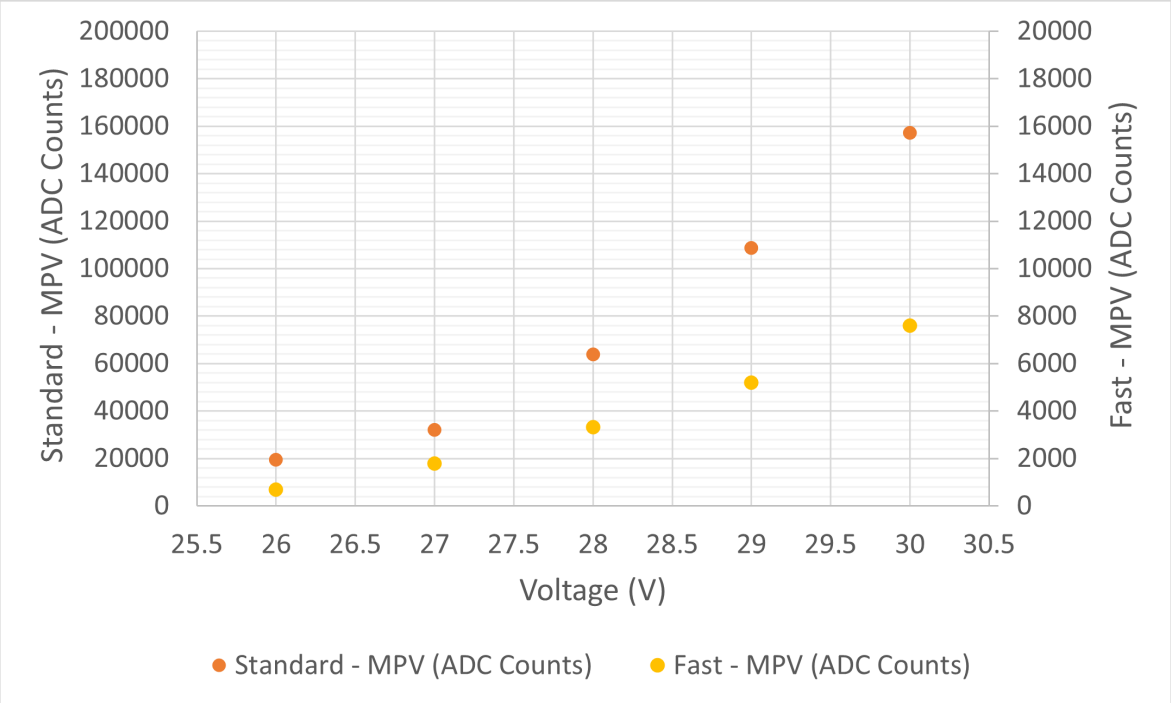

Figure 5.5: Gain results of the detector configuration of BC-404 hexagonal plastic scintillator (old) with 6x6 *mm* SiPM (old) using the digitizer.

Table 5.6: Gain results of the detector configuration of BC-404 hexagonal plastic scintillator (old) with 3x3 *mm* SiPM (new) using the digitizer.

BC-404 hexagonal plastic scintillator (old) with 3x3 *mm* SiPM (new)		
	Standard Signal	Fast Signal
Voltage (V)	MPV (ADC Counts)	MPV (ADC Counts)
26	6405	5
27	14650	15
28	47540	45
29	61250	57
30	76200	72

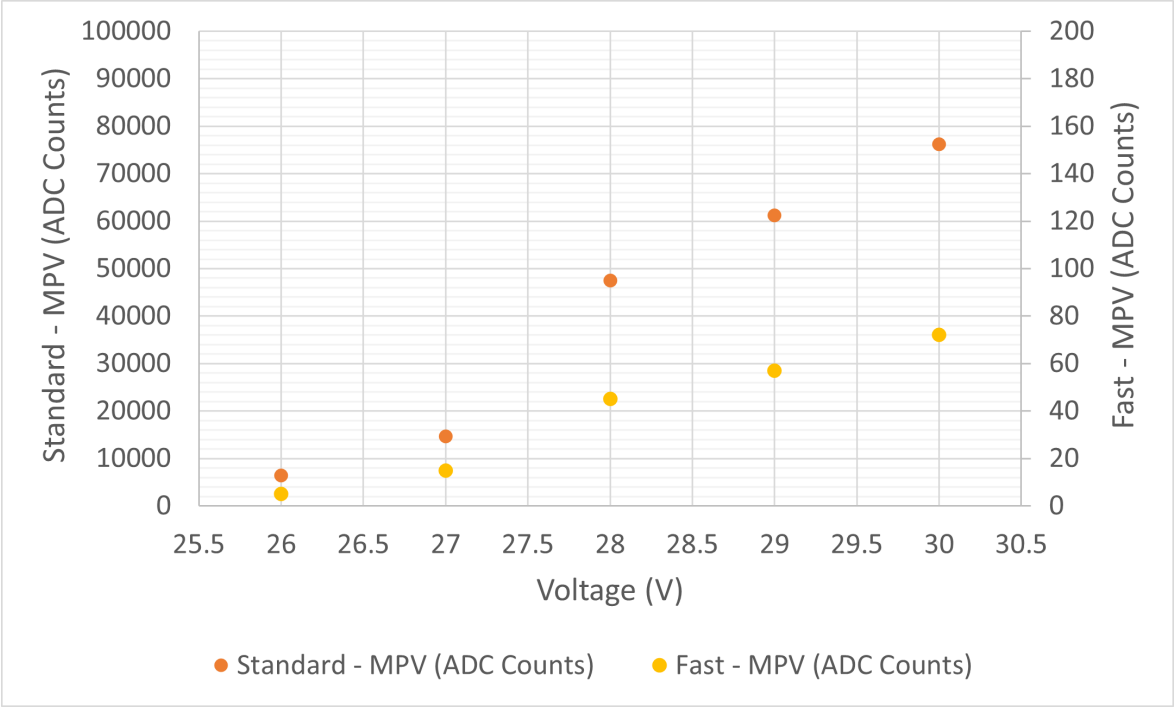

Figure 5.6: Gain results of the detector configuration of BC-404 hexagonal plastic scintillator (old) with 3x3 *mm* SiPM (new) using the digitizer.

Table 5.7: Gain results of the detector configuration of BC-404 hexagonal plastic scintillator (new) with 6x6 *mm* SiPM (old) using the digitizer.

BC-404 hexagonal plastic scintillator (new) with 6x6 *mm* SiPM (old)		
	Standard Signal	Fast Signal
Voltage (V)	MPV (ADC Counts)	MPV (ADC Counts)
26	19400	647
27	23040	796
28	35940	1313
29	53160	2161
30	70360	3378

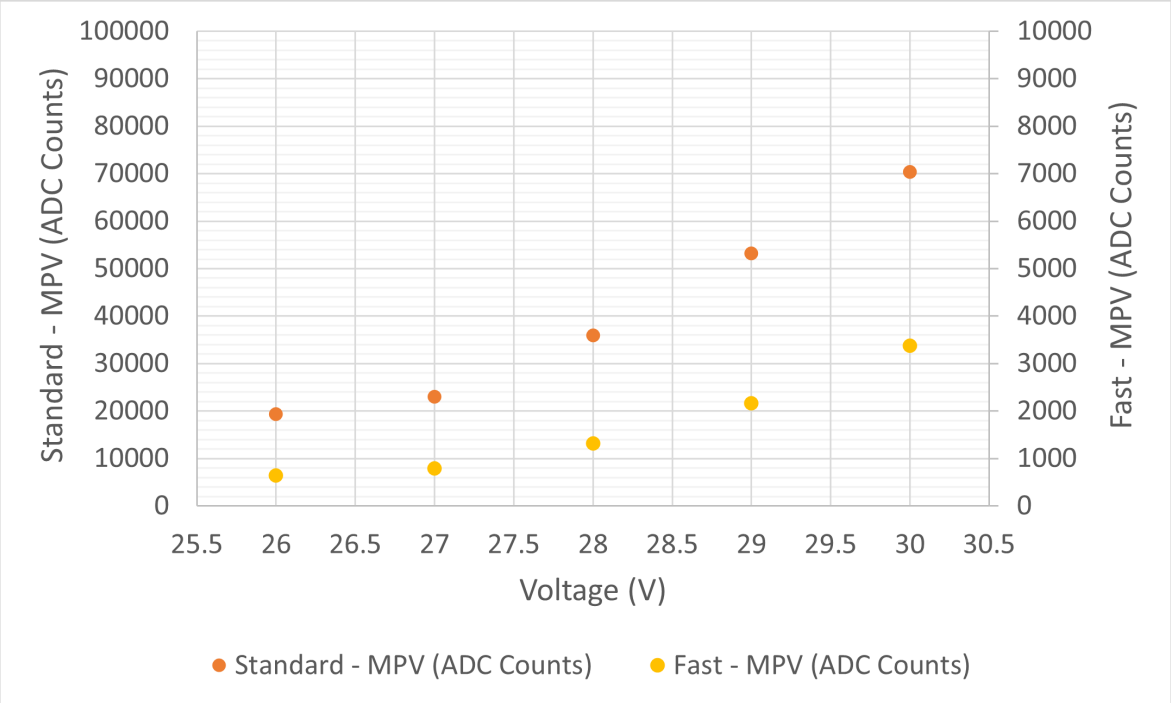

Figure 5.7: Gain results of the detector configuration of BC-404 hexagonal plastic scintillator (new) with 6x6 *mm* SiPM (old) using the digitizer.

Table 5.8: Gain results of the detector configuration of BC-404 hexagonal plastic scintillator (new) with 3x3 *mm* SiPM (new) using the digitizer.

BC-404 hexagonal plastic scintillator (new) with 3x3 *mm* SiPM (new)		
	Standard Signal	Fast Signal
Voltage (V)	MPV (ADC Counts)	MPV (ADC Counts)
26	23320	100
27	28750	133
28	43950	711
29	70560	756
30	89800	983

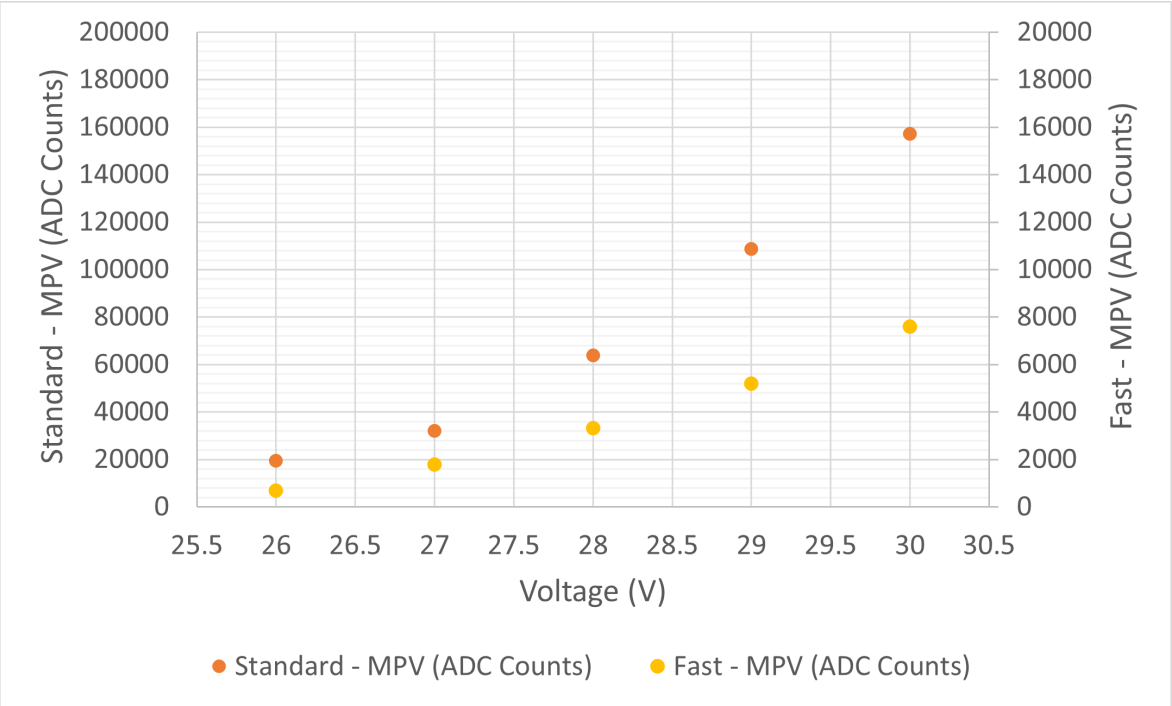

Figure 5.8: Gain results of the detector configuration of BC-404 hexagonal plastic scintillator (new) with 3x3 *mm* SiPM (new) using the digitizer.

From these results, it can be highlighted that the best time resolution and the best efficiency were obtained using the detector configuration of BC-404 hexagonal plastic scintillator (old) with the 6x6 *mm* SiPM sensor (old). The value of the best time resolution obtained is 306 ± 118.7 *ps* for the standard signal and 366 ± 91.4 *ps* for the fast signal. The measurements were taken applying a supply voltage of 30 V to this

SiPM detector. Additionally, good behavior of the detector gain is observed using the detector configuration of BC-404 hexagonal plastic scintillator (old) with the 6x6 *mm* SiPM sensor (old) in both cases.

Results with detector configurations using the 3x3 *mm* SiPM (new) have higher time resolution and non-exponential gain behavior. The board that was made for the 3x3 *mm* SiPM (new) had some manufacturing imperfections that greatly impaired the features expected from this device.

Furthermore, by analyzing these results, it is possible to observe that the BC-404 hexagonal plastic scintillator (new) is slightly slower than the BC-404 hexagonal plastic scintillator (old).

5.2 Two SiPMs detector results using the digitizer

Table 5.9 and Figure 5.9 show the time resolution and efficiency data and plot, respectively, of the tests performed with the BC-404 hexagonal plastic scintillator (thick) with a 6x6 *mm* SiPM on each side (Two SiPMs) detector. For this detector, the time resolutions obtained were also compared when calculating the time resolution with the minimum time value between the two SiPM detectors and the average between the two SiPM time values. These results are shown in Table 5.10 and Figure 5.10. Also, Table 5.11 and Figure 5.11 show the gain obtained with this detector.

Analyzing these results, it is possible to highlight that the best time resolution is obtained when calculating the time resolution with the average between the two SiPM standard signal time values. The value obtained is 308 ± 117.5 *ps* by applying a supply voltage of 30 V to these SiPM detectors. Also, good behavior of the detector gain is observed using the detector configuration of BC-404 hexagonal plastic scintillator (thick) with a 6x6 *mm* SiPM on each side (Two SiPMs) with both signals.

Table 5.9: Results of the detector configuration of BC-404 hexagonal plastic scintillator (thick) with a 6x6 *mm* SiPM on each side (TwoSiPMs) using the digitizer.

BC-404 hexagonal plastic scintillator (thick) with a 6x6 *mm* SiPM on each side (TwoSiPMs)						
	Standard Signal 1		Standard Signal 2		Fast Signal 1	
Voltage (V)	Efficiency (%)	Time Resolution (ps)	Efficiency (%)	Time Resolution (ps)	Efficiency (%)	Time Resolution (ps)
26	2.93	553 ± 55.8	2.93	723 ± 41.7	2.67	630 ± 48.3
27	62.86	510 ± 61.1	62.86	713 ± 42.3	58.29	492 ± 63.6
28	98.80	454 ± 69.9	98.80	514 ± 60.5	96.93	517 ± 60.1
29	99.47	420 ± 76.7	99.47	463 ± 68.3	99.15	509 ± 61.2
30	99.54	416 ± 77.6	99.54	428 ± 75.0	99.53	461 ± 68.6

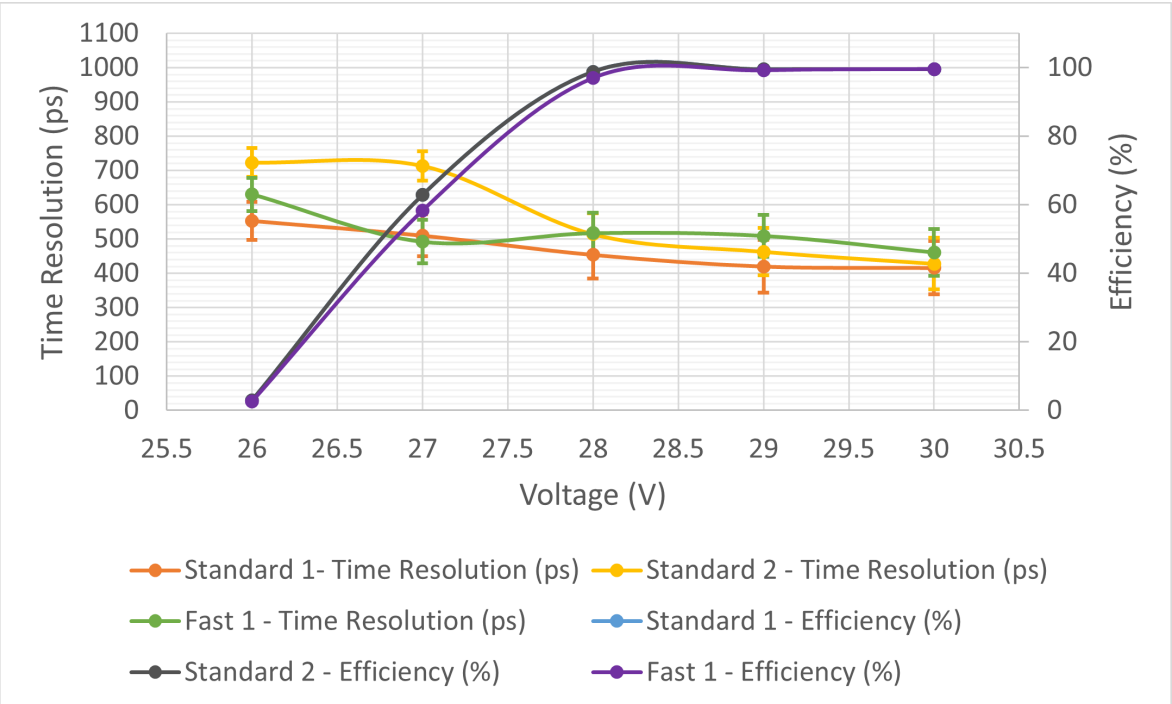

Figure 5.9: Results of the time resolution and efficiency of the detector configuration of BC-404 hexagonal plastic scintillator (thick) with a 6x6 *mm* SiPM on each side (TwoSiPMs) using the digitizer.

Table 5.10: Average and minimum time results of the detector of BC-404 hexagonal plastic scintillator (thick) with a 6x6 *mm* SiPM on each side (TwoSiPMs) using the digitizer.

BC-404 hexagonal plastic scintillator (thick) with a 6x6 *mm* SiPM on each side (TwoSiPMs)		
	Average Time	Minimum Time
Voltage (V)	Time Resolution (ps)	Time Resolution (ps)
26	476 ± 66.1	634 ± 48.0
27	473 ± 66.6	587 ± 52.2
28	376 ± 88.2	459 ± 69.0
29	330 ± 105.7	426 ± 75.4
30	308 ± 117.5	419 ± 77.0

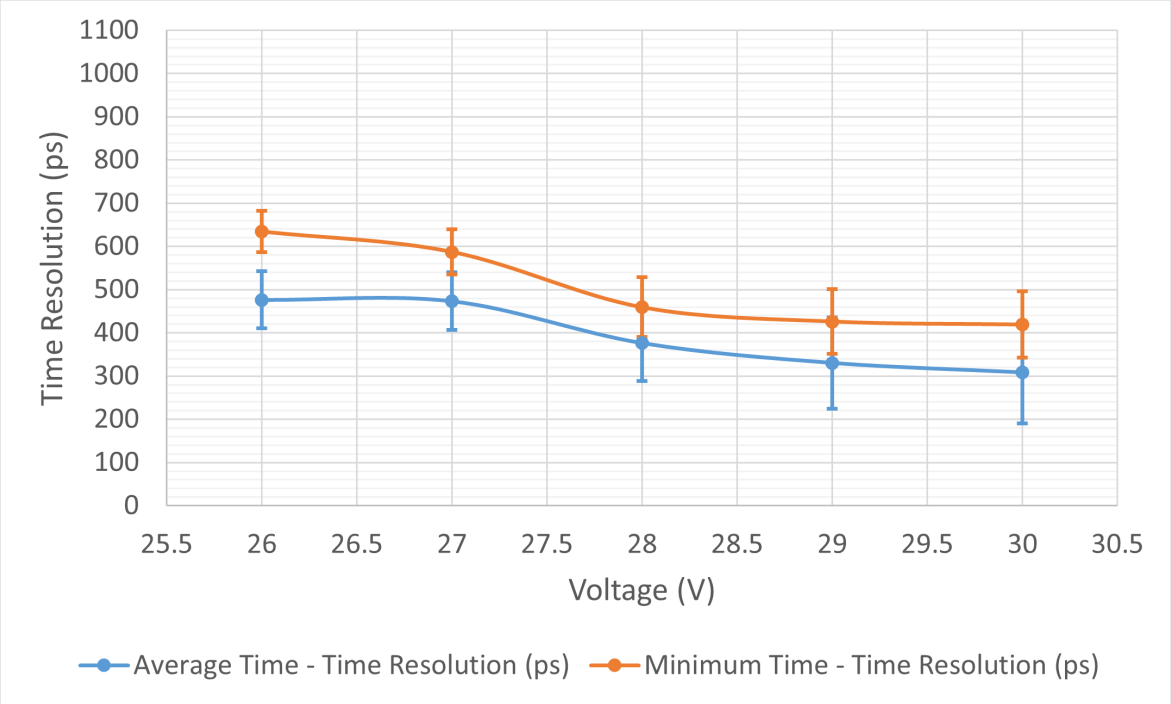

Figure 5.10: Results of the time resolution obtained using the minimum and average values of the detector configuration of BC-404 hexagonal plastic scintillator (thick) with a 6x6 *mm* SiPM on each side (TwoSiPMs) using the digitizer.

Table 5.11: Gain results of the detector configuration of BC-404 hexagonal plastic scintillator (thick) with a 6x6 *mm* SiPM on each side (TwoSiPMs) using the digitizer.

BC-404 hexagonal plastic scintillator (thick) with a 6x6 *mm* SiPM on each side (TwoSiPMs)			
	Standard Signal 1	Standard Signal 2	Fast Signal 1
Voltage (V)	MPV (ADC Counts)	MPV (ADC Counts)	MPV (ADC Counts)
26	71200	68420	13860
27	96910	82520	14440
28	155300	125700	15110
29	233300	189100	17930
30	398600	304100	22520

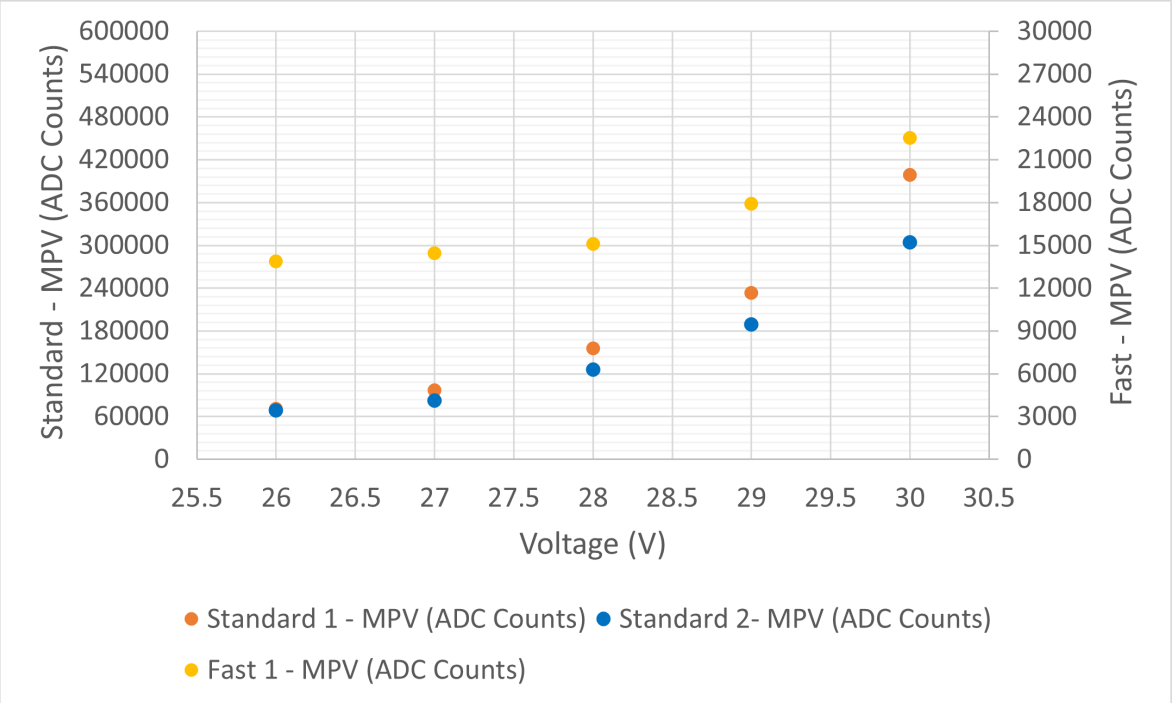

Figure 5.11: Gain results of the detector configuration of BC-404 hexagonal plastic scintillator (thick) with a 6x6 *mm* SiPM on each side (TwoSiPMs) using the digitizer.

5.3 BC-422Q plastic scintillator detector results using the digitizer

Results of time resolution and efficiency of the tests performed with the BC-422Q square plastic scintillator detector with the 6x6 *mm* SiPM (old) are shown in Table 5.12 and Figure 5.12. Additionally, Table 5.13 and Figure 5.13 show the gain obtained with this detector.

These results show that BC-422Q square plastic scintillator is slightly faster than BC-404 hexagonal plastic scintillators. The value of the best time resolution obtained is 304 ± 120 *ps* for the standard signal and 297 ± 124.8 *ps* for the fast signal by applying a supply voltage of 30 V to this SiPM detector. The gain behaves exponentially, indicating the good functioning of the detector.

Table 5.12: Results of the time resolution and efficiency of the detector configuration of BC-422Q square plastic scintillator with 6x6 *mm* SiPM (old) using the digitizer.

BC-422Q square plastic scintillator with 6x6 *mm* SiPM (old)				
	Standard Signal		Fast Signal	
Voltage (V)	Efficiency (%)	Time Resolution (*ps*)	Efficiency (%)	Time Resolution (*ps*)
26	42.12	711 ± 42.4	57.03	458 ± 69.1
27	84.43	466 ± 67.7	75.72	346 ± 98.7
28	91.21	314 ± 113.9	89.19	324 ± 108.5
29	88.52	331 ± 105.2	92.74	294 ± 127.0
30	92.57	304 ± 120.0	94.63	297 ± 124.8

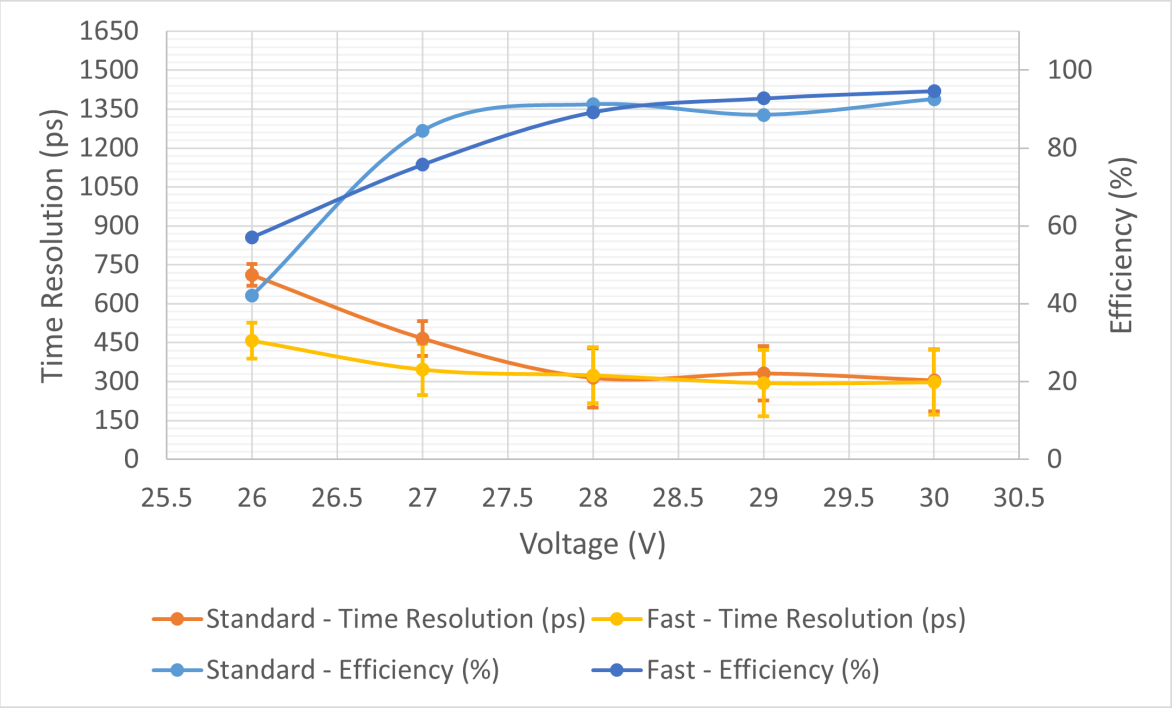

Figure 5.12: Gain results of the detector configuration of BC-422Q square plastic scintillator with 6x6 *mm* SiPM (old) using the digitizer.

Table 5.13: Gain results of the detector configuration of BC-422Q square plastic scintillator with 6x6 *mm* SiPM (old) using the digitizer.

BC-422Q square plastic scintillator with 6x6 *mm* SiPM (old)		
	Standard Signal	Fast Signal
Voltage (V)	MPV (ADC Counts)	MPV (ADC Counts)
26	44160	1848
27	93090	3671
28	169500	6323
29	297100	11720
30	579100	19010

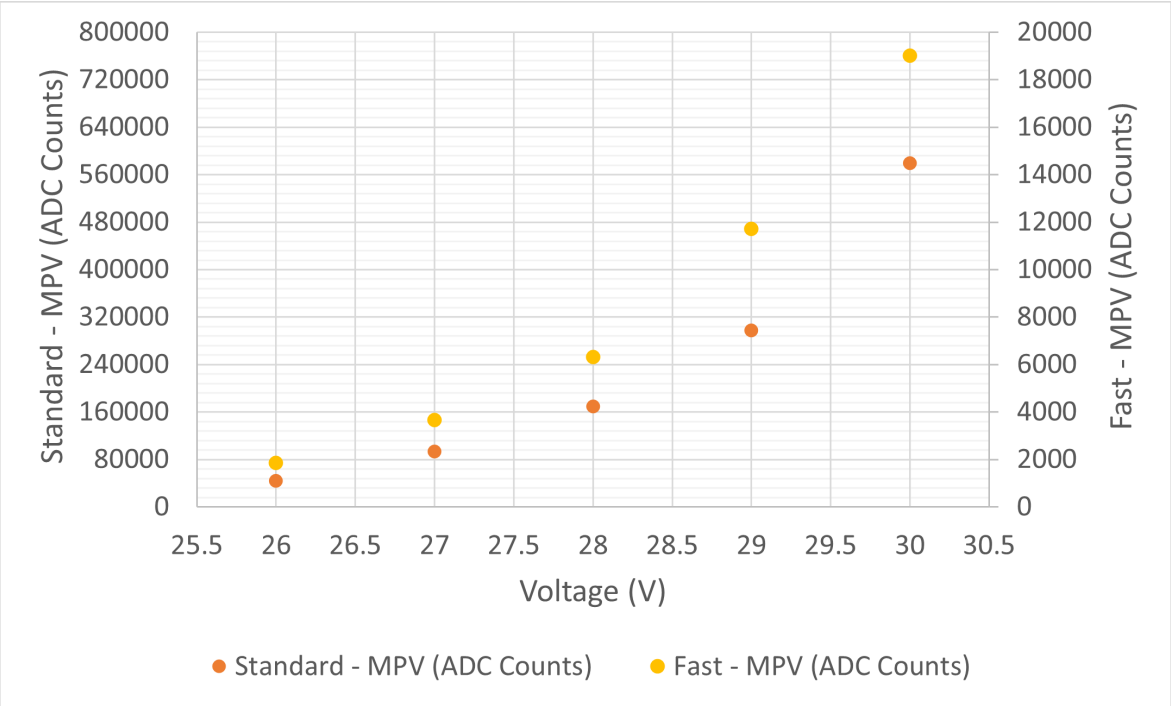

Figure 5.13: Gain results of the detector configuration of BC-422Q square plastic scintillator with 6x6 *mm* SiPM (old) using the digitizer.

5.4 BC-404 plastic scintillator detectors results using the TDC and QDC

Similarly, the results of time resolution and efficiency were obtained using the TDC and QDC instruments. The results for each of the configurations are shown below; Table 5.14 and Figure 5.14 show the data and plot, respectively, of the tests performed with the detector configuration of BC-404 hexagonal plastic scintillator (old) and the 6x6 *mm* SiPM (old); Table 5.15 and Figure 5.15 show the data and plot, respectively, of the tests performed with the detector configuration of BC-404 hexagonal plastic scintillator (old) and the 3x3 *mm* SiPM (new); Table 5.16 and Figure 5.16 show the data and plot, respectively, of the tests performed with the detector configuration of BC-404 hexagonal plastic scintillator (new) and the 6x6 *mm* SiPM (old); finally, Table 5.17 and Figure 5.17 show the data and plot, respectively, of the tests performed with the detector configuration of BC-404 hexagonal plastic scintillator (new) and the 3x3 *mm* SiPM (new).

In addition, the gain obtained with the QDC for the detectors was analyzed during the tests with supply voltages from 26 V to 30 V. The gain tables and graphs are shown in the following order: Table 5.18 and Figure 5.18 show the results obtained for the detector with BC-404 hexagonal scintillator plastic (old) and the 6x6 mm SiPM (old); Table 5.19 and Figure 5.19 show the results obtained for the detector with hexagonal BC-404 plastic scintillator (old) and the 3x3 mm SiPM (new); Table 5.20 and Figure 5.20 show the results obtained for the detector with BC-404 hexagonal plastic scintillator (new) and the 6x6 mm SiPM (old); Table 5.21 and Figure 5.21 show the results obtained for the detector with hexagonal plastic BC-404 scintillator (new) and the 3x3 mm SiPM (new).

In the measurements with the 3x3 mm SiPM (new) with supply voltages of 26 V and 27 V, the pulses could not be distinguished from the noise due to the very small size of the pulses. Therefore, the analysis of these values was discarded, and also those of the 26 V case with the 6x6 mm SiPM detector (old).

From these results, it can be highlighted that the best time resolution and the best efficiency were obtained using the detector configuration of BC-404 hexagonal plastic scintillator (old) with the 6x6 mm SiPM sensor (old). The value of the best time resolution obtained is 611 $\pm$ 13.3 ps for the standard signal and 159 $\pm$ 63.3 ps for the fast signal by applying a supply voltage of 30 V to this SiPM detector. Additionally, good behavior of the detector gain is observed using the detector configuration of BC-404 hexagonal plastic scintillator (old) with the 6x6 mm SiPM sensor (old) in both cases.

Table 5.14: Results of the detector configuration of BC-404 hexagonal plastic scintillator (old) with 6x6 *mm* SiPM (old) using the TDC and QDC.

BC-404 hexagonal plastic scintillator (old) with 6x6 *mm* SiPM (old)			
	Standard Signal		Fast Signal
Voltage (V)	Efficiency (%)	Time Resolution (ps)	Time Resolution (ps)
26	51.53	1978 ± 4.1	1568 ± 5.1
27	79.92	1769 ± 4.6	961 ± 8.4
28	98.40	1275 ± 6.3	759 ± 10.7
29	99.51	892 ± 9.1	397 ± 20.8
30	99.24	611 ± 13.3	159 ± 63.3

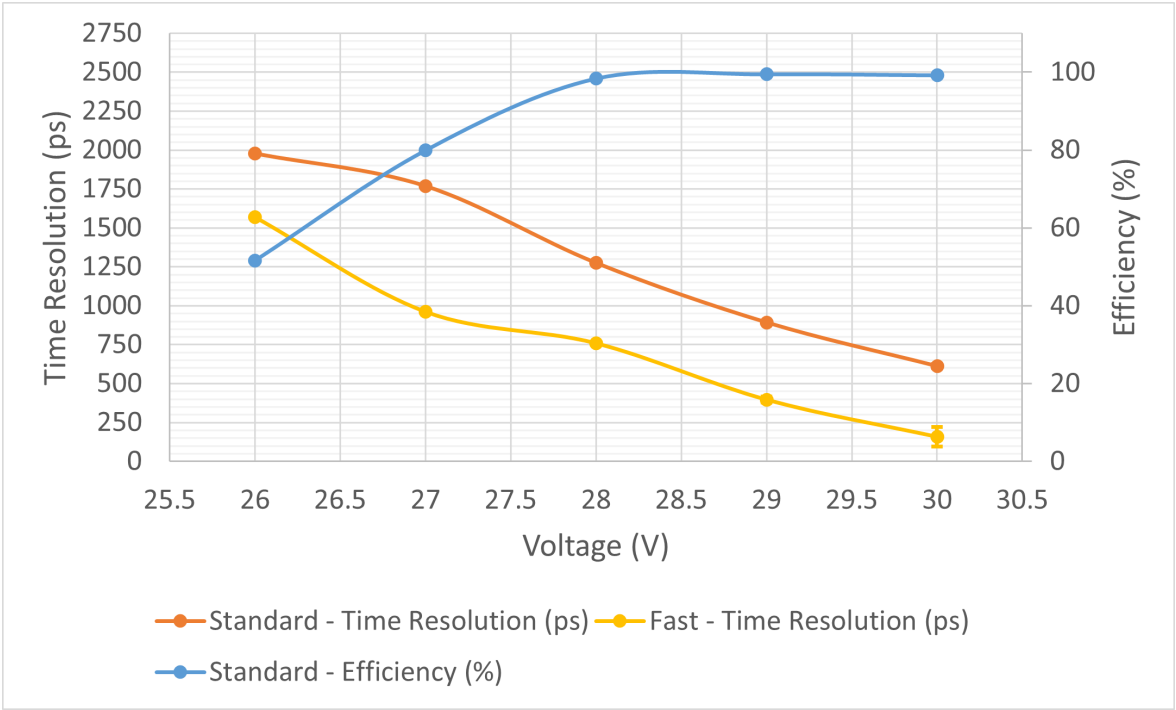

Figure 5.14: Results of the time resolution and efficiency of the detector configuration of BC-404 hexagonal plastic scintillator (old) with 6x6 *mm* SiPM (old) using the TDC and QDC.

Table 5.15: Results of the detector configuration of BC-404 hexagonal plastic scintillator (old) with 3x3 mm SiPM (new) using the TDC and QDC.

BC-404 hexagonal plastic scintillator (old) with 3x3 mm SiPM (new)			
	Standard Signal		Fast Signal
Voltage (V)	Efficiency (%)	Time Resolution (ps)	Time Resolution (ps)
26	-	-	-
27	32.83	917 ± 8.8	1470 ± 5.5
28	98.12	647 ± 12.6	1146 ± 7.1
29	98.25	631 ± 12.9	1009 ± 8.0
30	99.64	466 ± 17.6	917 ± 8.8

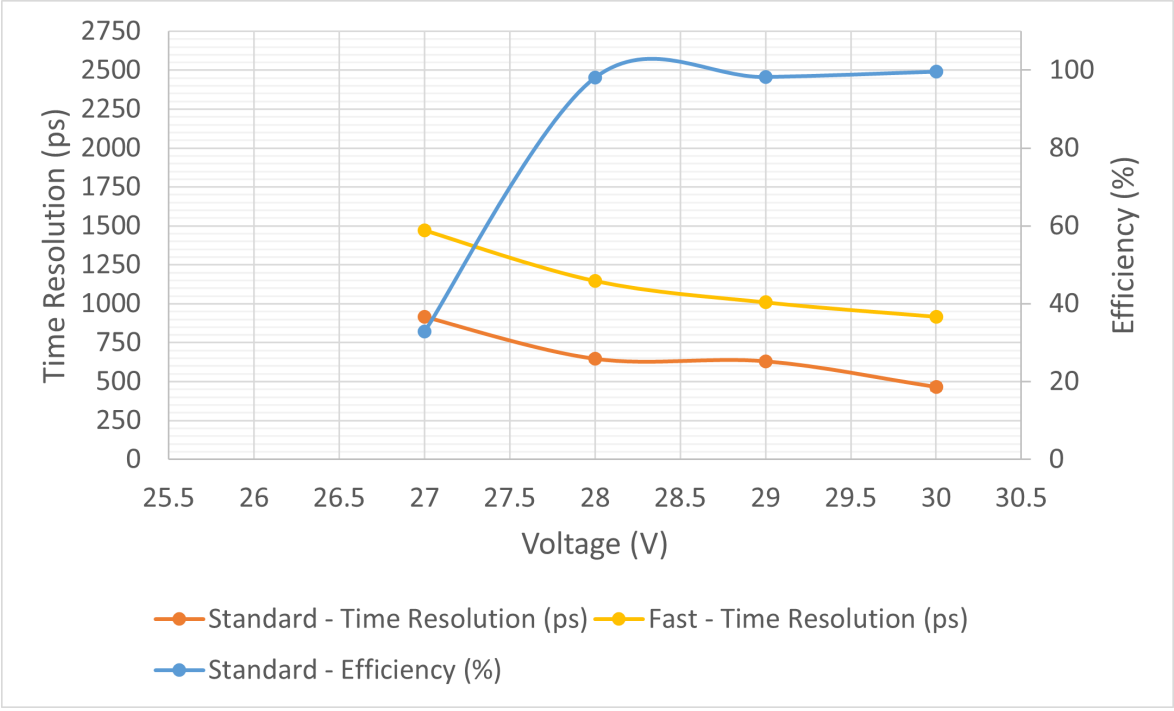

Figure 5.15: Results of the time resolution and efficiency of the detector configuration of BC-404 hexagonal plastic scintillator (old) with 3x3 mm SiPM (new) using the TDC and QDC.

Table 5.16: Results of the detector configuration of BC-404 hexagonal plastic scintillator (new) with 6x6 *mm* SiPM (old) using the TDC and QDC.

BC-404 hexagonal plastic scintillator (new) with 6x6 *mm* SiPM (old)			
	Standard Signal		Fast Signal
Voltage (V)	Efficiency (%)	Time Resolution (ps)	Time Resolution (ps)
26	49.55	1999 ± 4.0	1584 ± 5.1
27	78.47	1669 ± 4.8	1350 ± 6.0
28	98.59	1373 ± 5.9	825 ± 9.8
29	98.95	949 ± 8.5	424 ± 19.4
30	99.31	597 ± 13.7	199 ± 45.8

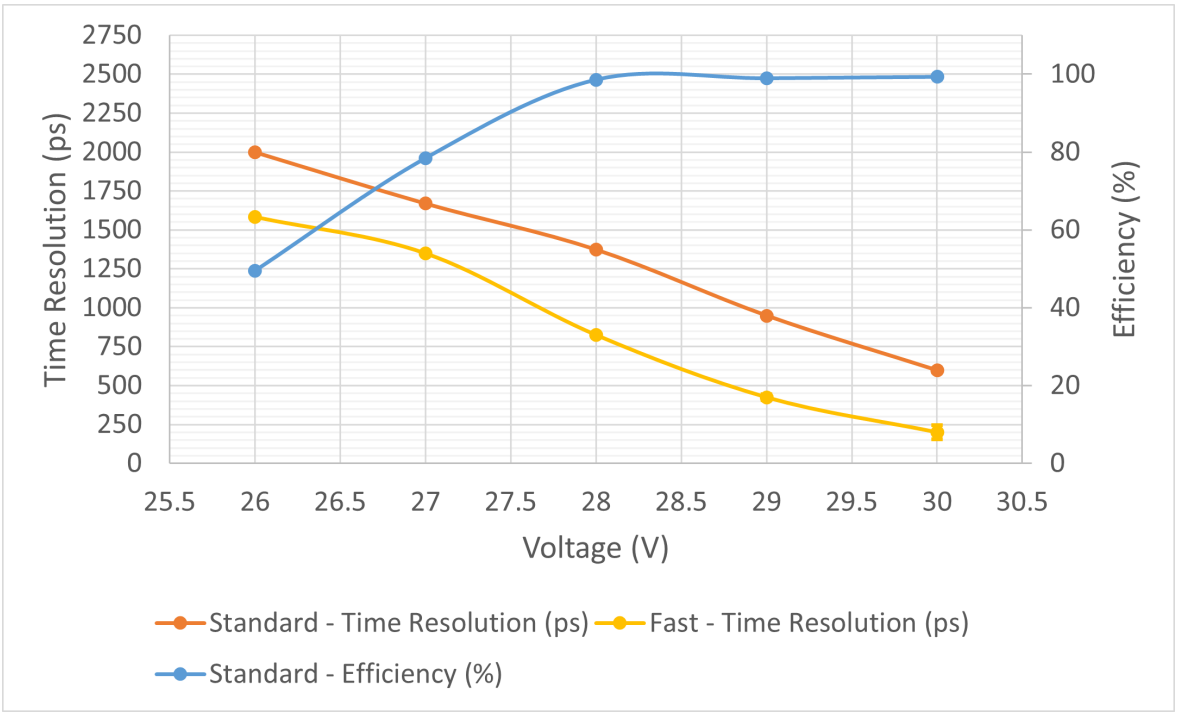

Figure 5.16: Results of the time resolution and efficiency of the detector configuration of BC-404 hexagonal plastic scintillator (new) with 6x6 *mm* SiPM (old) using the TDC and QDC.

Table 5.17: Results of the detector configuration of BC-404 hexagonal plastic scintillator (new) with 3x3 mm SiPM (new) using the TDC and QDC.

BC-404 hexagonal plastic scintillator (new) with 3x3 mm SiPM (new)			
	Standard Signal		Fast Signal
Voltage (V)	Efficiency (%)	Time Resolution (ps)	Time Resolution (ps)
26	-	-	-
27	-	-	-
28	96.53	2888 ± 2.8	1419 ± 5.7
29	97.55	2009 ± 4.0	1451 ± 5.6
30	99.30	1521 ± 5.3	1367 ± 5.9

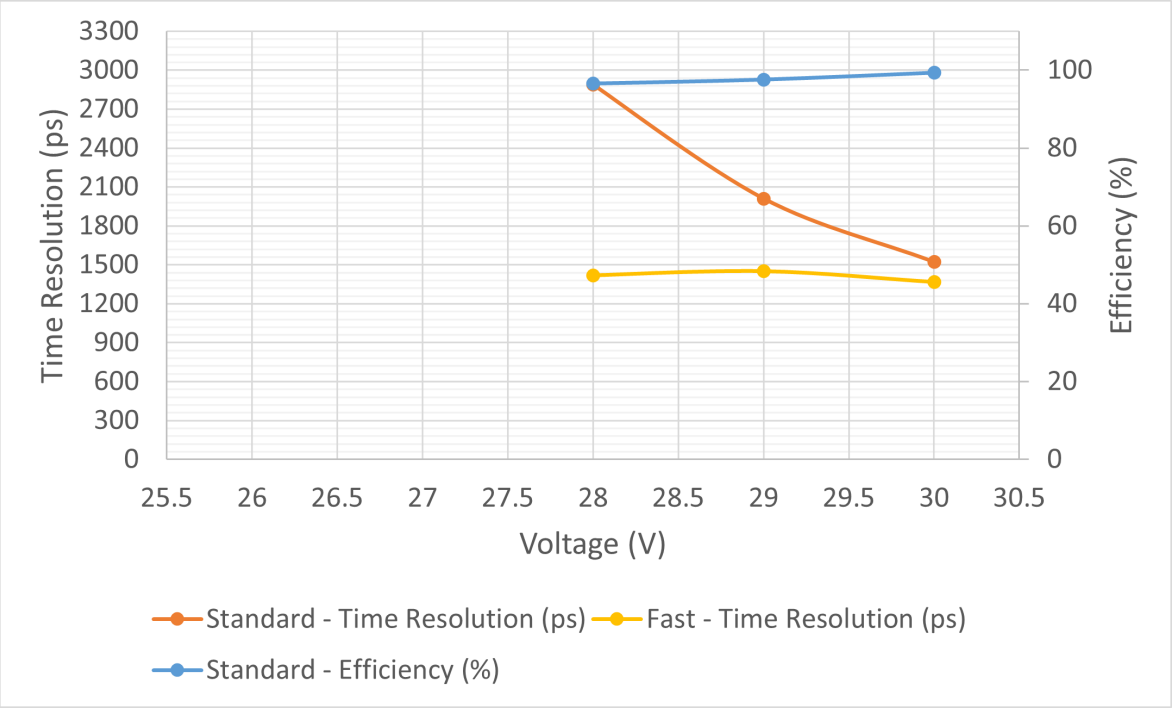

Figure 5.17: Results of the time resolution and efficiency of the detector configuration of BC-404 hexagonal plastic scintillator (new) with 3x3 mm SiPM (new) using the TDC and QDC.

Table 5.18: Gain results of the detector configuration of BC-404 hexagonal plastic scintillator (old) with 6x6 *mm* SiPM (old) using the TDC and QDC.

BC-404 hexagonal plastic scintillator (old) with 6x6 *mm* SiPM (old)	
	Standard Signal
Voltage (V)	MPV (ADC Counts)
26	832
27	891
28	928
29	1290
30	2030

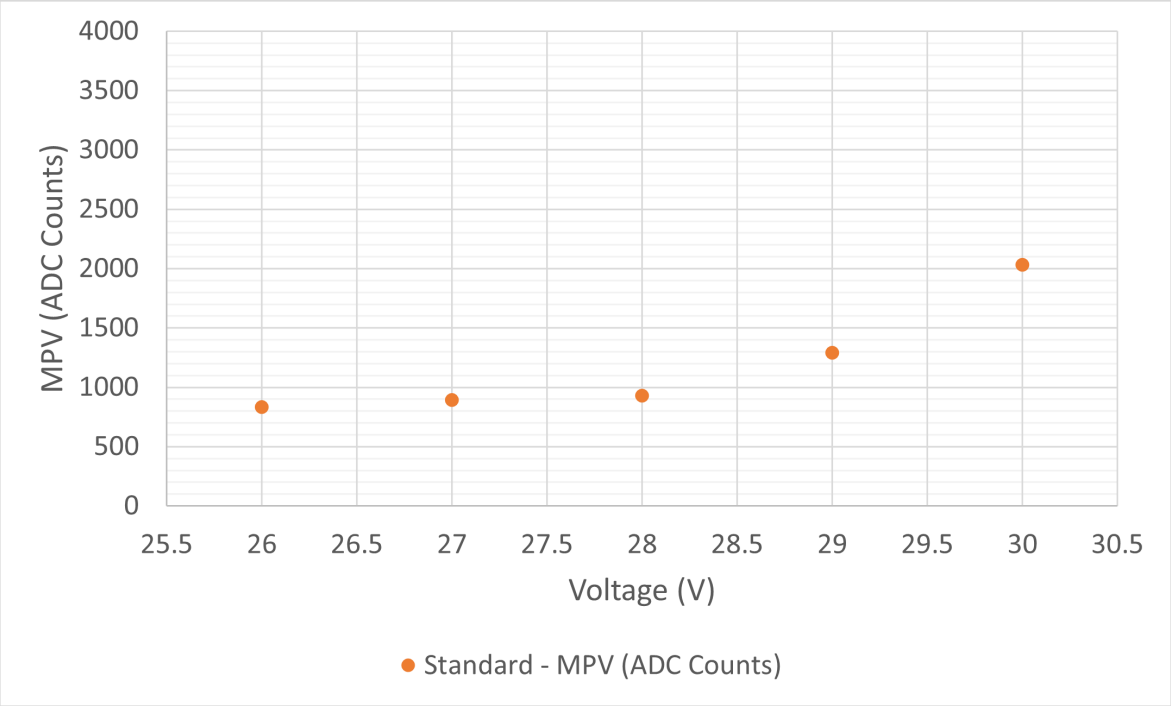

Figure 5.18: Gain results of the detector configuration of BC-404 hexagonal plastic scintillator (old) with 6x6 *mm* SiPM (old) using the TDC and QDC.

Table 5.19: Gain results of the detector configuration of BC-404 hexagonal plastic scintillator (old) with 3x3 *mm* SiPM (new) using the TDC and QDC.

BC-404 hexagonal plastic scintillator (old) with 3x3 *mm* SiPM (new)	
	Standard Signal
Voltage (V)	MPV (ADC Counts)
26	-
27	771
28	981
29	1775
30	3010

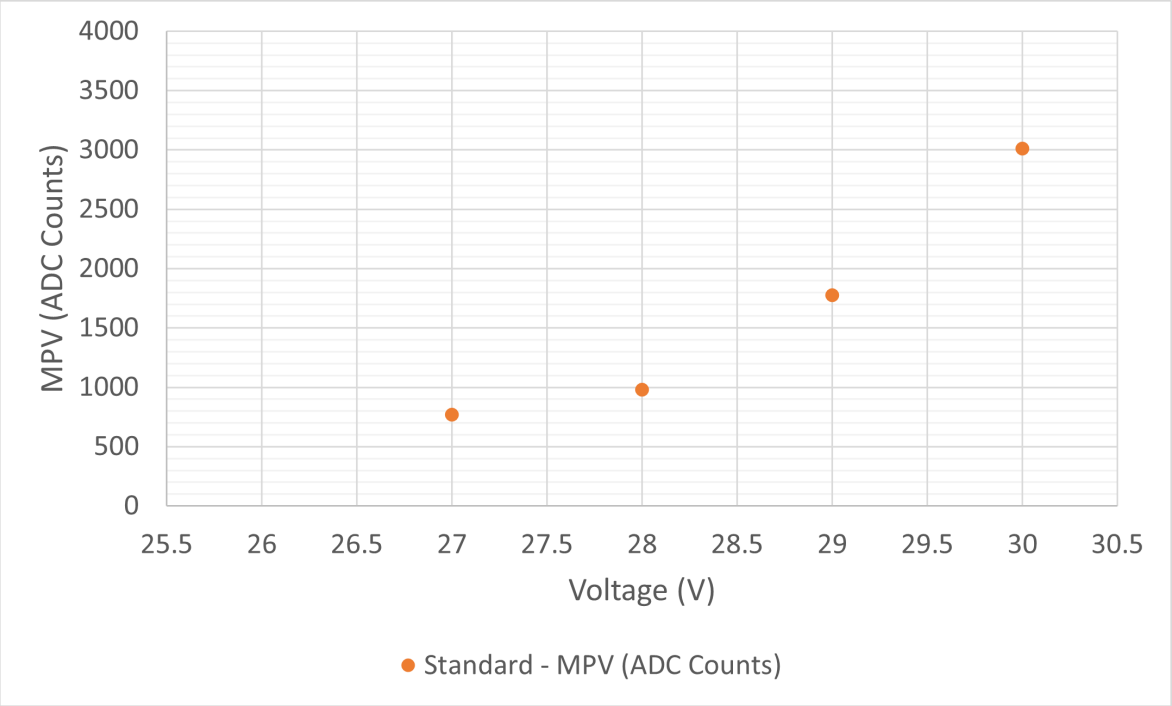

Figure 5.19: Gain results of the detector configuration of BC-404 hexagonal plastic scintillator (old) with 3x3 *mm* SiPM (new) using the TDC and QDC.

Table 5.20: Gain results of the detector configuration of BC-404 hexagonal plastic scintillator (new) with 6x6 *mm* SiPM (old) using the TDC and QDC.

BC-404 hexagonal plastic scintillator (new) with 6x6 *mm* SiPM (old)	
	Standard Signal
Voltage (V)	MPV (ADC Counts)
26	539
27	627
28	1043
29	1800
30	2949

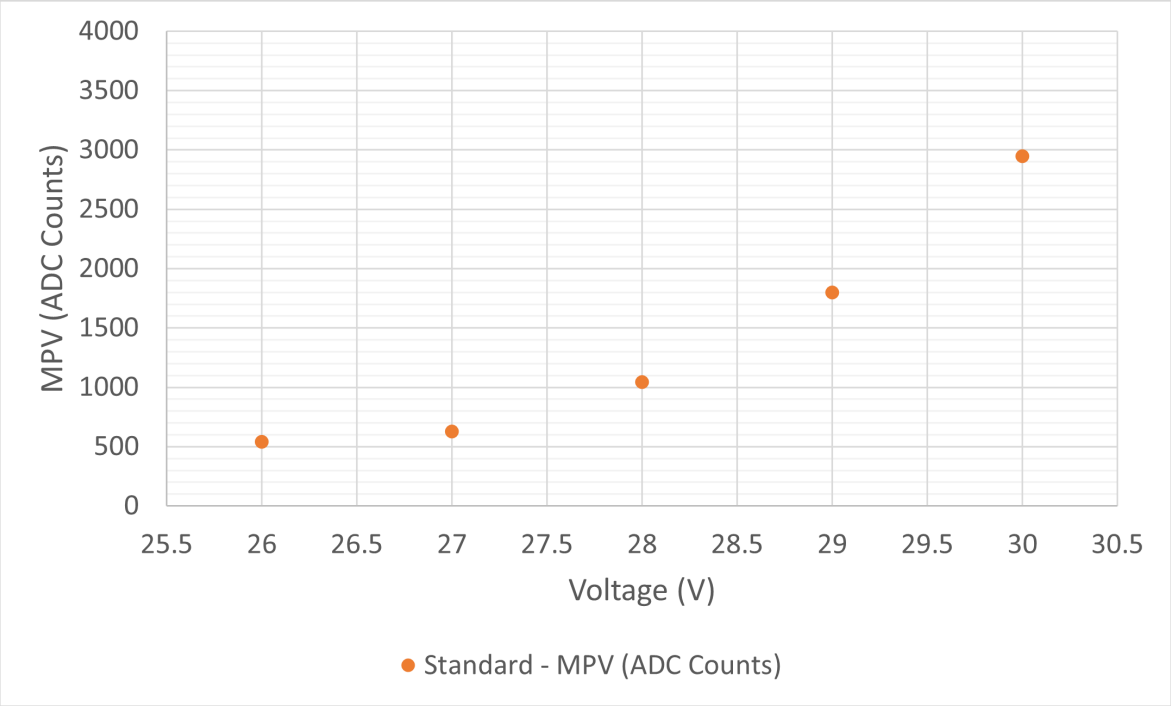

Figure 5.20: Gain results of the detector configuration of BC-404 hexagonal plastic scintillator (new) with 6x6 *mm* SiPM (old) using the TDC and QDC.

Table 5.21: Gain results of the detector configuration of BC-404 hexagonal plastic scintillator (new) with 3x3 *mm* SiPM (new) using the TDC and QDC.

BC-404 hexagonal plastic scintillator (new) with 3x3 *mm* SiPM (new)	
	Standard Signal
Voltage (V)	MPV (ADC Counts)
26	-
27	-
28	480
29	632
30	1417

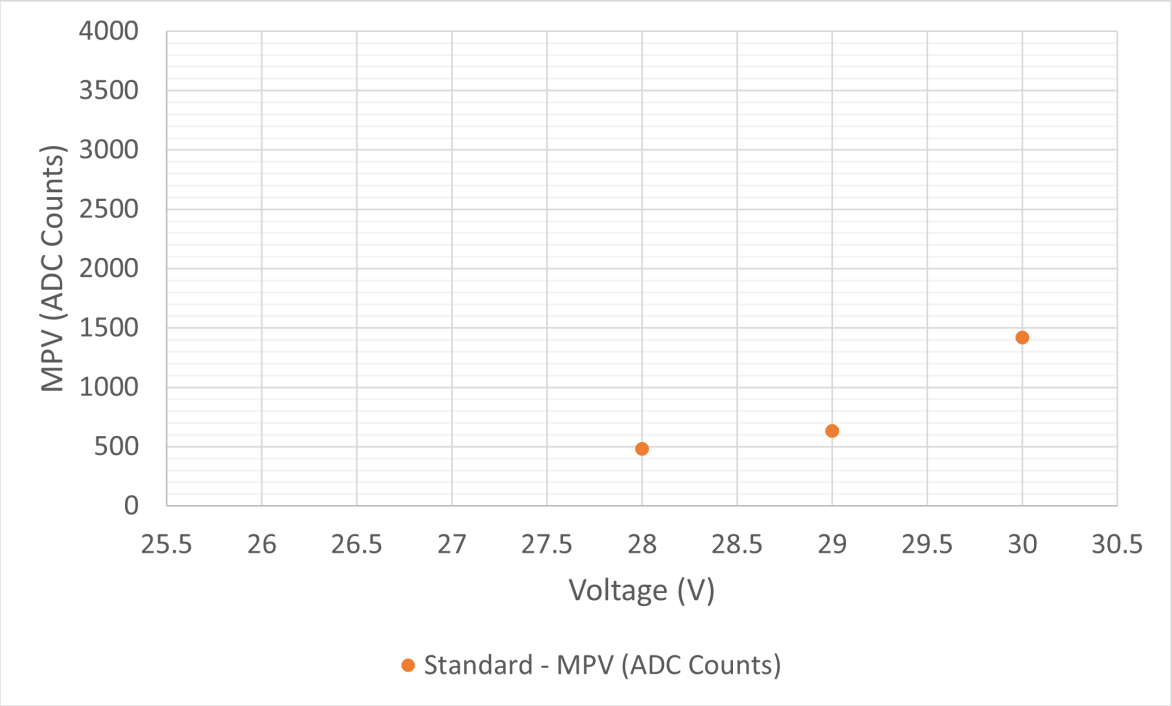

Figure 5.21: Gain results of the detector configuration of BC-404 hexagonal plastic scintillator (new) with 3x3 *mm* SiPM (new) using the TDC and QDC.

5.5 Two SiPMs detector results using the TDC and QDC

Results of time resolution and efficiency of the tests performed with the BC-404 hexagonal plastic scintillator (thick) with a 6x6 *mm* SiPM on each side (Two SiPMs) detector are shown in the next order; Table 5.22 and Figure 5.22 show the time resolution and efficiency results obtained for the standard signal of each SiPM sensor.

As before, the time resolutions obtained were also compared when calculating the time resolution with the minimum time value between the two SiPM detectors and the average between the two SiPM time values. These results are shown in Table 5.23 and Figure 5.23. Additionally, Table 5.24 and Figure 5.24 show the gain obtained with this detector.

Table 5.22: Results of the detector configuration of BC-404 hexagonal plastic scintillator (thick) with a 6x6 *mm* SiPM on each side (TwoSiPMs) using the TDC and QDC.

BC-404 hexagonal plastic scintillator (thick) with a 6x6 *mm* SiPM on each side (TwoSiPMs)				
	Standard Signal 1		Standard Signal 2	
Voltage (V)	Efficiency (%)	Time Resolution (ps)	Efficiency (%)	Time Resolution (ps)
26	47.48	2407 ± 3.4	47.48	1967 ± 4.1
27	75.35	1688 ± 4.8	75.35	1014 ± 8.0
28	98.84	1421 ± 5.7	99.03	952 ± 8.5
29	98.31	1114 ± 7.3	98.17	921 ± 8.8
30	99.00	1048 ± 7.7	98.97	885 ± 9.2

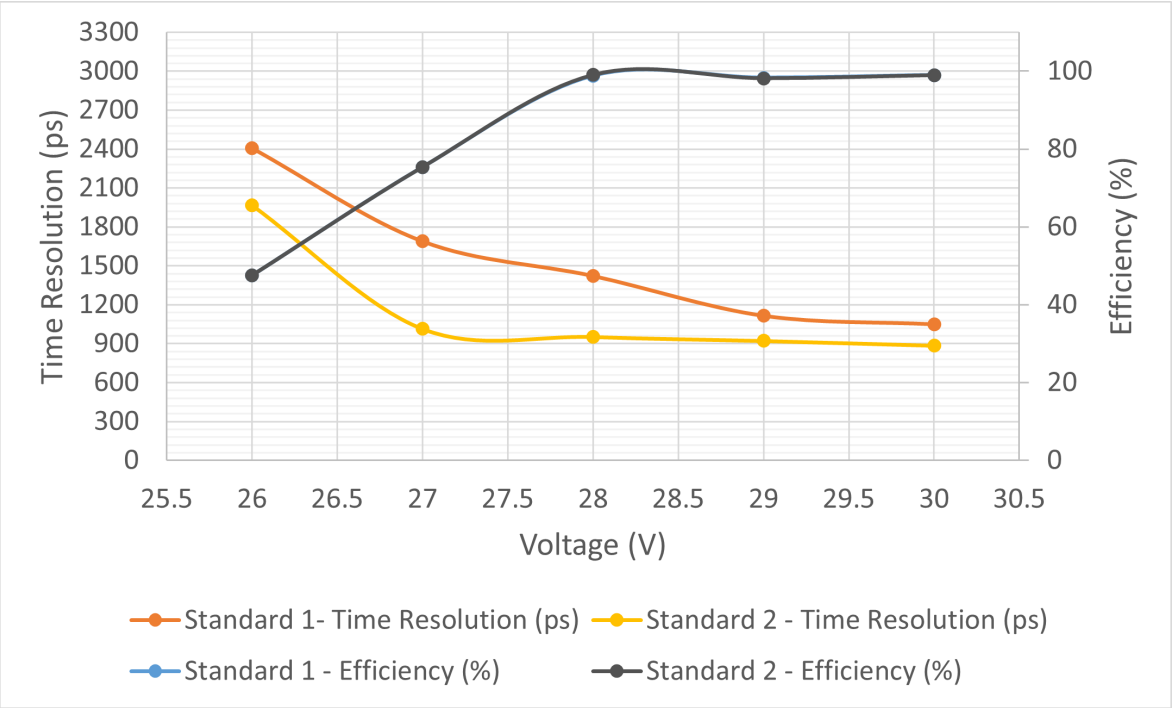

Figure 5.22: Results of the time resolution and efficiency of the detector configuration of BC-404 hexagonal plastic scintillator (thick) with a 6x6 *mm* SiPM on each side (TwoSiPMs) using the TDC and QDC.

Table 5.23: Average and minimum time results of the detector configuration of BC-404 hexagonal plastic scintillator (thick) with a 6x6 *mm* SiPM on each side (TwoSiPMs) using the TDC and QDC.

BC-404 hexagonal plastic scintillator (thick) with a 6x6 *mm* SiPM on each side (TwoSiPMs)		
	Average Time	Minimum Time
Voltage (V)	Time Resolution (ps)	Time Resolution (ps)
26	2196 ± 3.8	2034 ± 4.0
27	1403 ± 5.8	1044 ± 7.7
28	1281 ± 6.3	962 ± 8.4
29	1230 ± 6.6	948 ± 8.5
30	1207 ± 6.7	915 ± 8.9

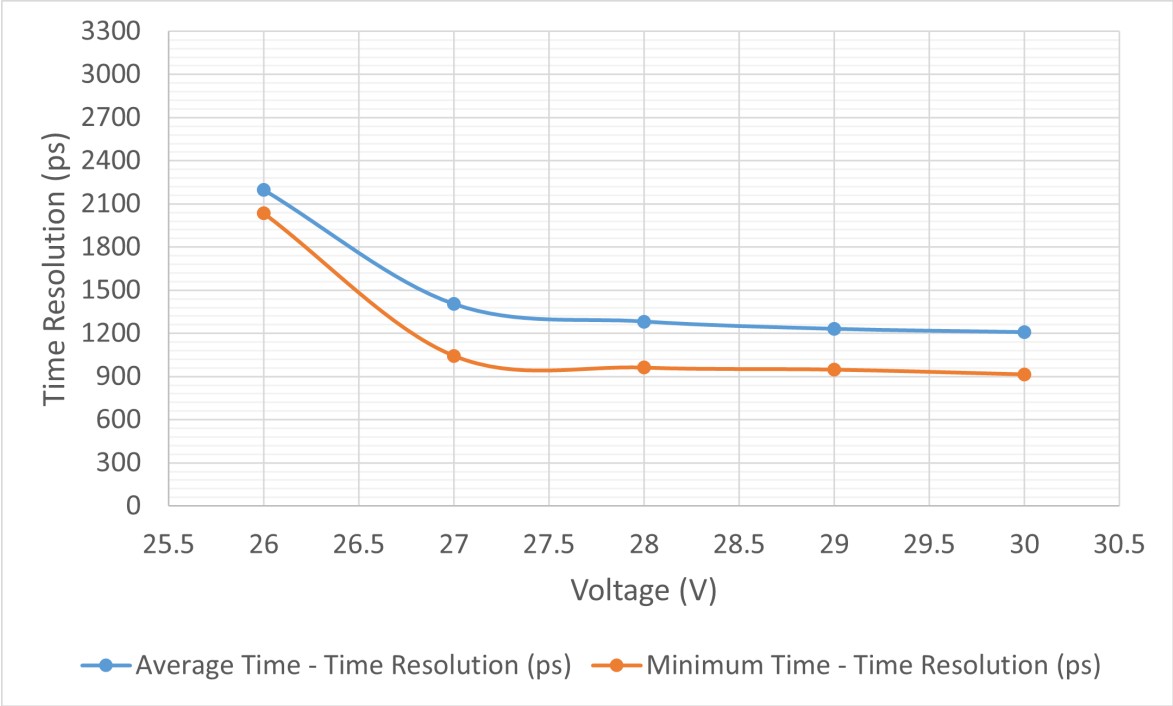

Figure 5.23: Results of the time resolution obtained using the minimum and average values of the detector configuration of BC-404 hexagonal plastic scintillator (thick) with a 6x6 *mm* SiPM on each side (TwoSiPMs) using the digitizer.

Table 5.24: Gain results of the detector configuration of BC-404 hexagonal plastic scintillator (thick) with a 6x6 *mm* SiPM on each side (TwoSiPMs) using the TDC and QDC.

BC-404 hexagonal plastic scintillator (thick) with a 6x6 *mm* SiPM on each side (TwoSiPMs)		
	Standard Signal 1	Standard Signal 2
Voltage (V)	MPV (ADC Counts)	MPV (ADC Counts)
26	-	-
27	515	235
28	1191	606
29	1955	1525
30	3135	2510

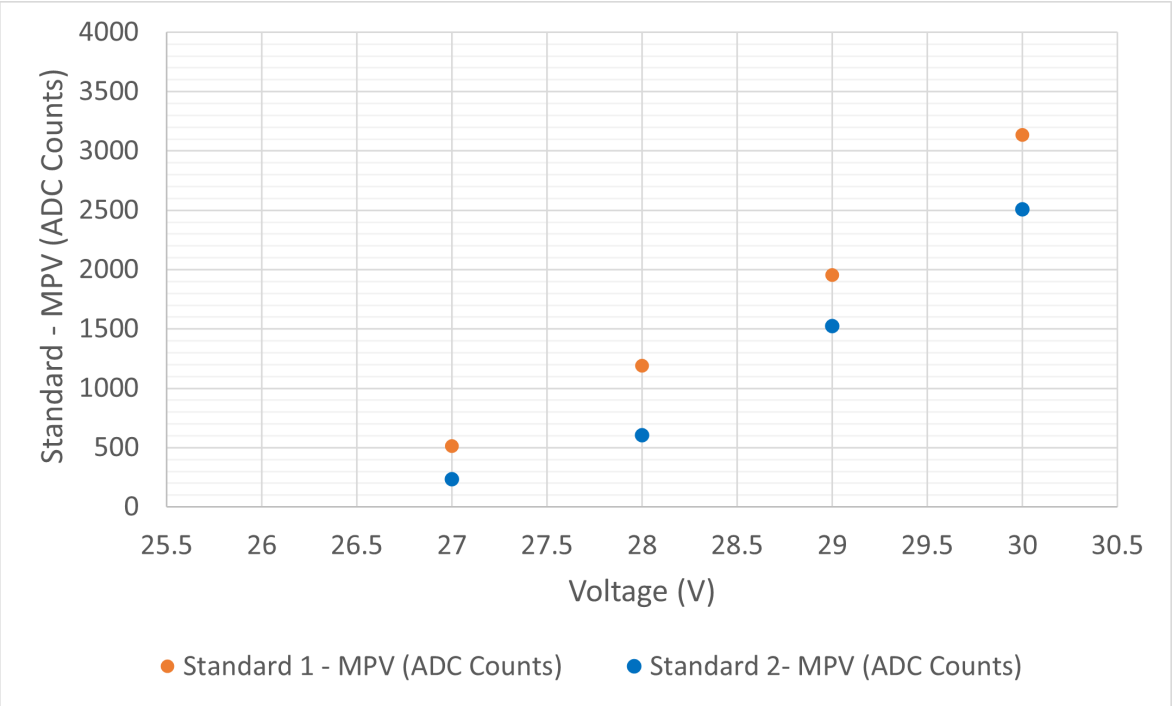

Figure 5.24: Gain results of the detector configuration of BC-404 hexagonal plastic scintillator (thick) with a 6x6 *mm* SiPM on each side (TwoSiPMs) using the TDC and QDC.

Time resolution results obtained for the detector configuration of BC-404 hexagonal plastic scintillator (thick) with a SiPM on each side (Two SiPMs) and using the TDC and QDC instrumentation were worse than those using the digitizer. For this detector, the best time resolution was obtained with the SiPM 2 sensor of 885 $\pm$ 9.2 *ps* for its standard signal. The fast signal from this detector could not be analyzed in parallel with the TDC instrument due to a lack of channels in the instruments used.

5.6 BC-422Q plastic scintillator detector results using the TDC and QDC

Table 5.25 and Figure 5.25 show the time resolution and efficiency graphs of the tests performed with the BC-422Q square plastic scintillator detector with the 6x6 *mm* SiPM (old). Also, Table 5.26 and Figure 5.26 show the gain obtained with this detector.

Table 5.25: Results of the time resolution and efficiency of the detector configuration of BC-422Q square plastic scintillator with 6x6 *mm* SiPM (old) using the TDC and QDC.

BC-422Q square plastic scintillator with 6x6 *mm* SiPM (old)			
	Standard Signal		Fast Signal
Voltage (V)	Efficiency (%)	Time Resolution (ps)	Time Resolution (ps)
26	63.90	1254 ± 6.4	956 ± 8.5
27	78.51	846 ± 9.6	627 ± 13.0
28	95.55	832 ± 9.8	446 ± 18.5
29	98.96	753 ± 10.8	281 ± 30.3
30	98.30	657 ± 12.4	257 ± 33.6

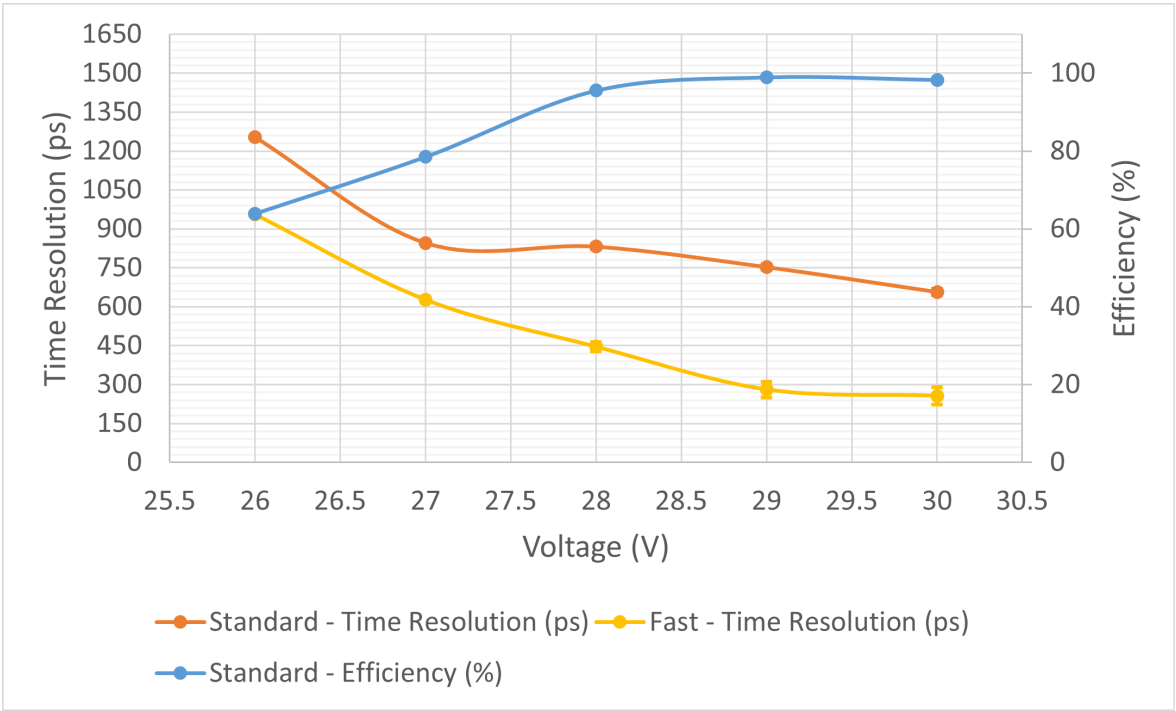

Figure 5.25: Gain results of the detector configuration of BC-422Q square plastic scintillator with 6x6 *mm* SiPM (old) using the TDC and QDC.

Table 5.26: Gain results of the detector configuration of BC-422Q square plastic scintillator with 6x6 *mm* SiPM (old) using the TDC and QDC.

BC-422Q square plastic scintillator with 6x6 *mm* SiPM (old)	
	Standard Signal
Voltage (V)	MPV (ADC Counts)
26	282
27	729
28	1114
29	1958
30	3118

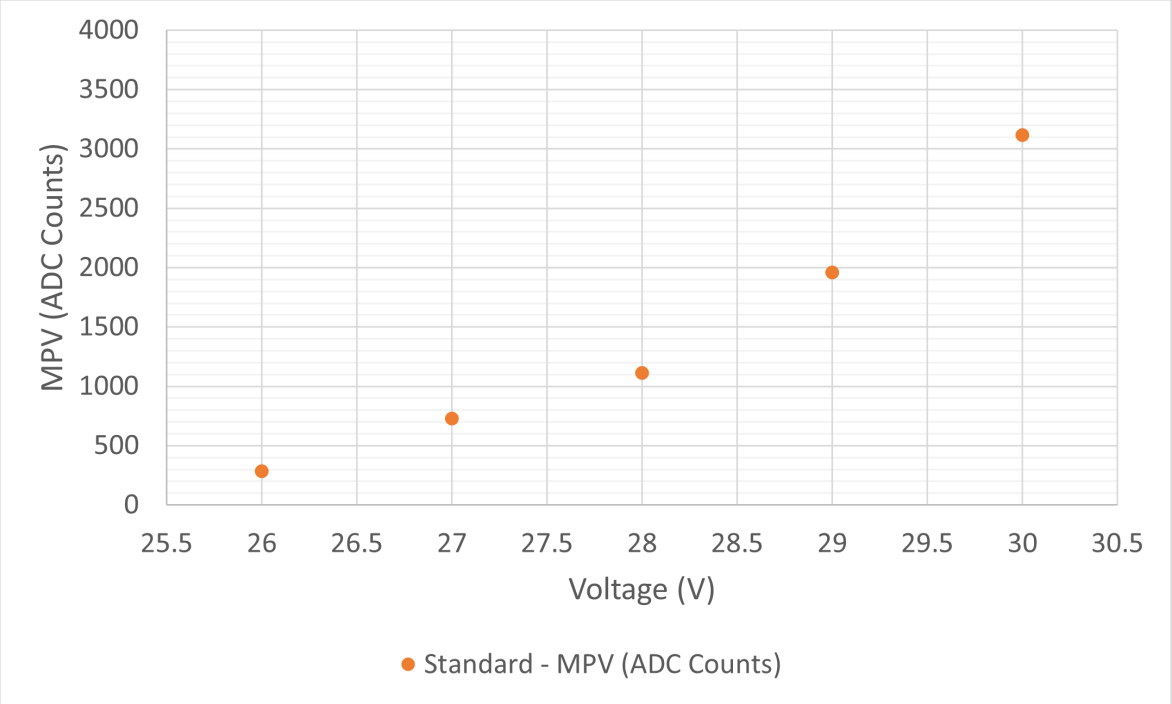

Figure 5.26: Gain results of the detector configuration of BC-422Q square plastic scintillator with 6x6 *mm* SiPM (old) using the TDC and QDC.

From these results, it can be highlighted that the best time resolution obtained is 657 ± 12.4 *ps* for the standard signal and 257 ± 33.6 *ps* for the fast signal. Comparing the results with those of the BC-404 hexagonal plastic scintillator (old) with 6x6 *mm* SiPM (old) detector, it can be confirmed that the fastest detector is the BC-404 hexagonal plastic scintillator (old) with 6x6 *mm* SiPM (old).

5.7 SiPM standard signal charge reconstruction using the digitizer

An additional analysis that was performed with the digitizer data recollected is the reconstruction of the charge of the SiPM standard (slow) signal using the charge of the SiPM fast signal. To perform this analysis, firstly, a linear relationship is obtained between the charge of the fast signal and the charge of the slow signal. Secondly, a reconstruction of the slow signal charge is obtained by applying the linear relationship to the charge of the fast signal. Finally, the Kolmogorov test is used to compare the actual charge of the slow signal and its reconstruction based on their histograms [19]. The procedure described above was performed for the detector configuration of BC-404 hexagonal plastic scintillator (old) with 6x6 *mm* SiPM (old). Figure 5.27 shows the linear relationship obtained from the slow and fast signal charges, while Figure 5.28 shows the comparison between the charge reconstruction of the slow signal and the actual charge of the slow signal. The best result of the Kolmogorov test is obtained with a supply voltage of 29 V and it is 97% similar.

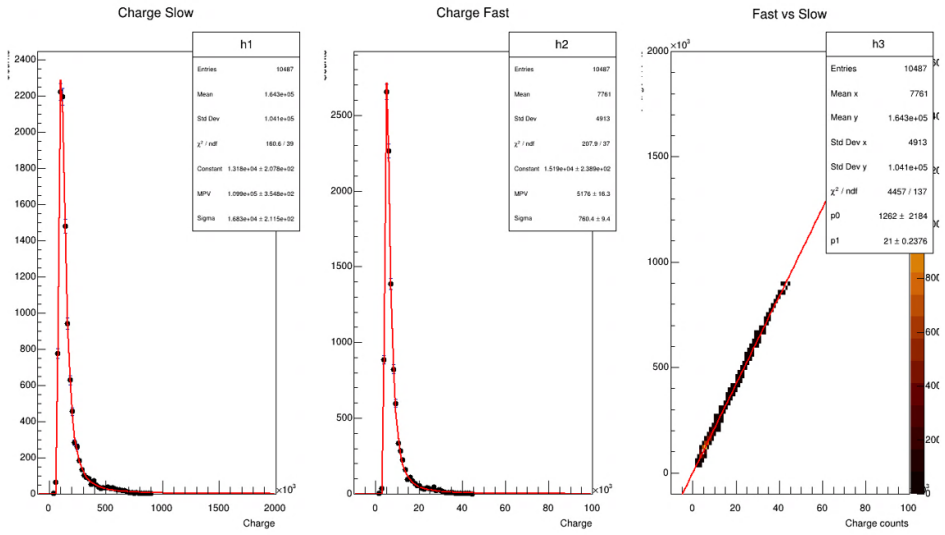

Figure 5.27: Linear relationship between the slow and fast signal charges of the detector configuration of BC-404 hexagonal plastic scintillator (old) with 6x6 *mm* SiPM (old).

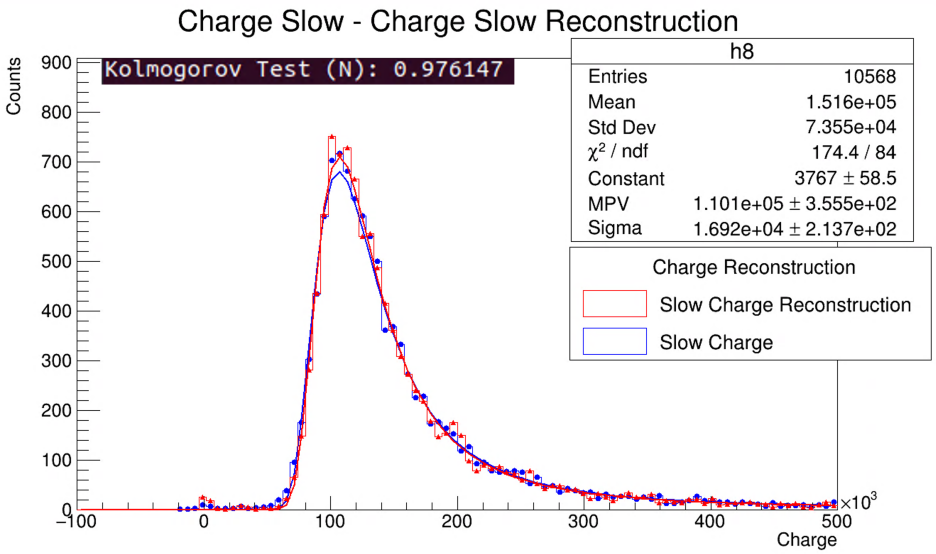

Figure 5.28: Result of the normalized Kolmogorov test of the slow signal charge reconstruction of the detector configuration of BC-404 hexagonal plastic scintillator (old) with 6x6 *mm* SiPM (old).

This analysis was also performed for the BC-404 hexagonal plastic scintillator (new) with 6x6 *mm* SiPM (old) detector. Figure 5.29 shows the linear relationship obtained from the slow and fast signal charges, while Figure 5.30 shows the comparison between the charge reconstruction of the slow signal and the actual charge of the slow signal. The best result of the Kolmogorov test is obtained with a supply voltage of 30 V and it is 87% similar.

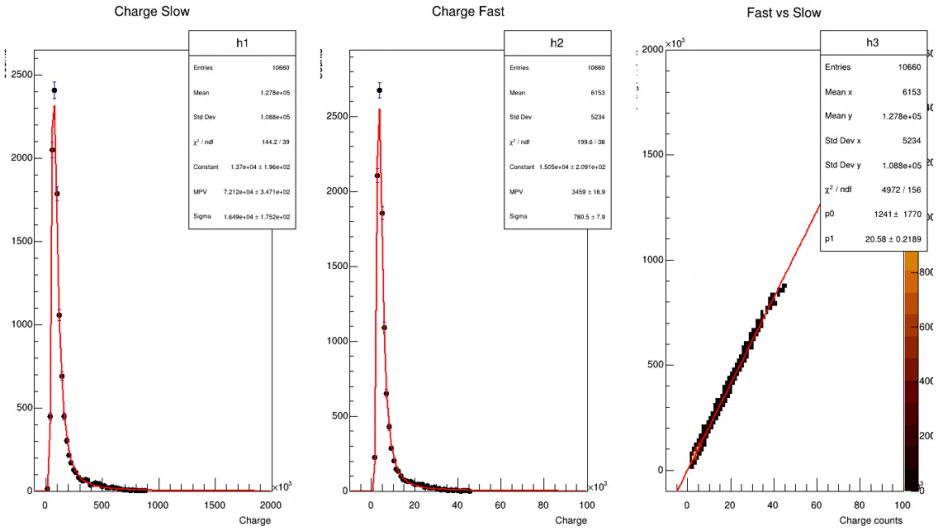

Figure 5.29: Linear relationship between the slow and fast signal charges of the detector configuration of BC-404 hexagonal plastic scintillator (new) with 6x6 *mm* SiPM (old).

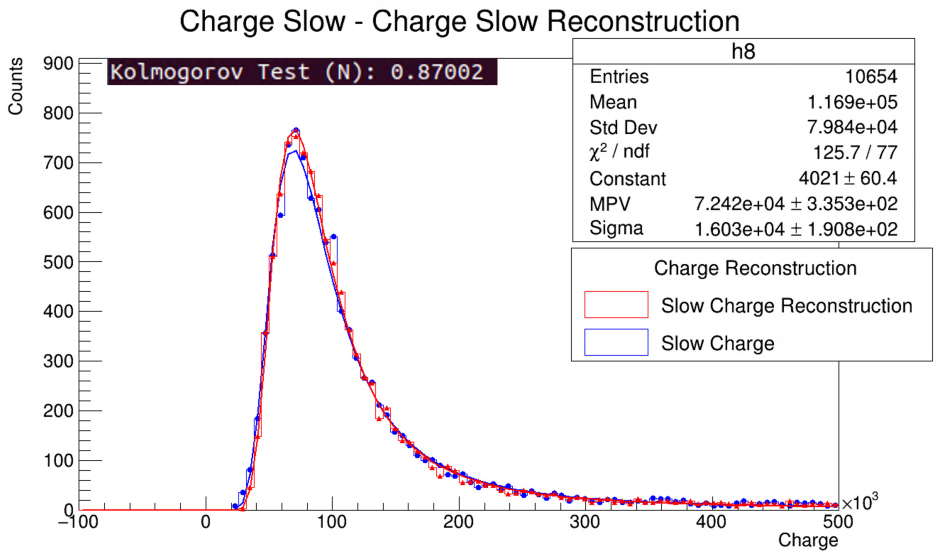

Figure 5.30: Result of the normalized Kolmogorov test of the slow signal charge reconstruction of the detector configuration of BC-404 hexagonal plastic scintillator (new) with 6x6 *mm* SiPM (old).

Reconstruction was also performed for the BC-404 hexagonal plastic scintillator (thick) with a 6x6 *mm* SiPM on each side (Two SiPMs) detector. Figure 5.31 shows the linear relationship obtained from the charges of the slow and fast signals, while Figure 5.32 shows the comparison between the charge reconstruction of the slow signal and the actual charge of the slow signal. The best result of the Kolmogorov test is obtained with a supply voltage of 30 V and it is 98% similar.

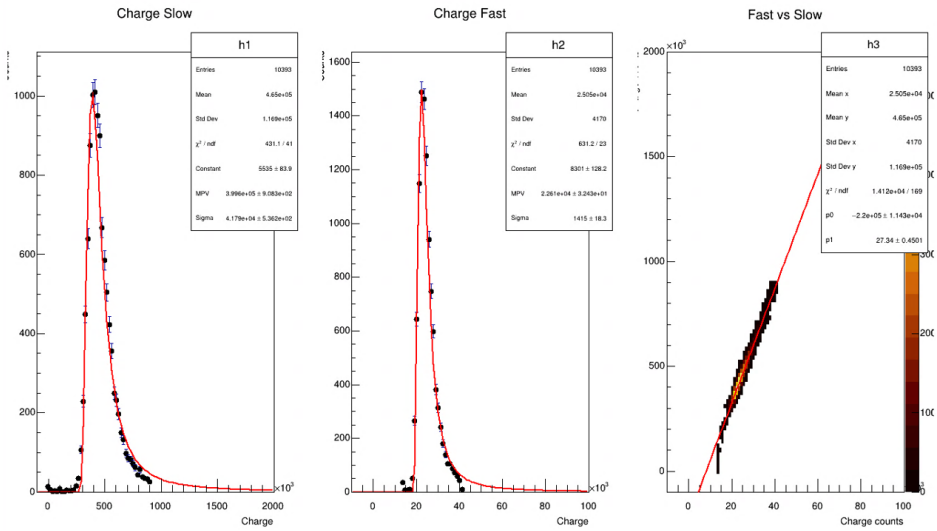

Figure 5.31: Linear relationship between the slow and fast signal charges of the detector configuration of BC-404 hexagonal plastic scintillator (thick) with a 6x6 *mm* SiPM on each side (Two SiPMs).

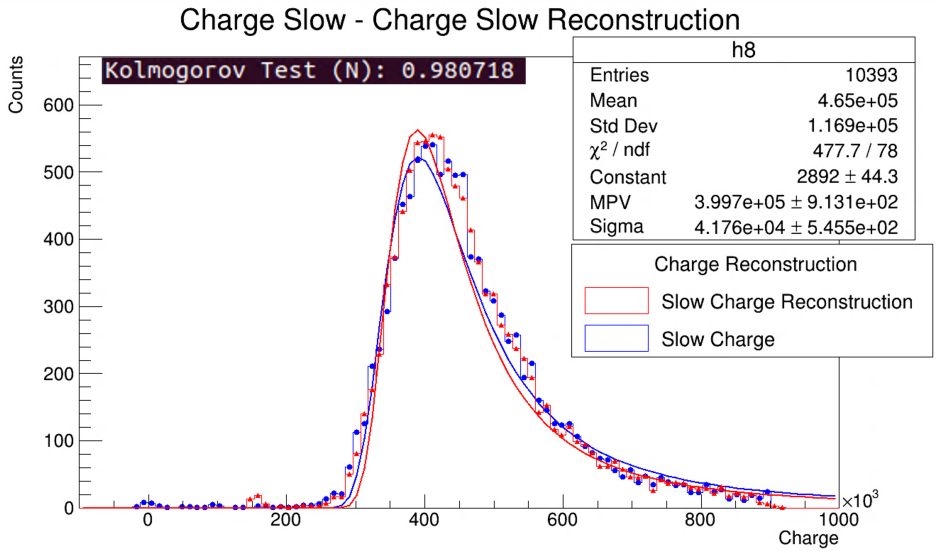

Figure 5.32: Result of the normalized Kolmogorov test of the slow signal charge reconstruction of the detector configuration of BC-404 hexagonal plastic scintillator (thick) with a 6x6 *mm* SiPM on each side (Two SiPMs).

Finally, the procedure was also performed for the detector configuration of BC-422Q square plastic scintillator with 6x6 *mm* SiPM (old). Figure 5.33 shows the linear relationship obtained from the charges of the slow and fast signals, while Figure 5.34 shows the comparison between the charge reconstruction of the slow signal and the actual charge of the slow signal. The best result of the Kolmogorov test is obtained with a supply voltage of 30 *V* and it is 95% similar.

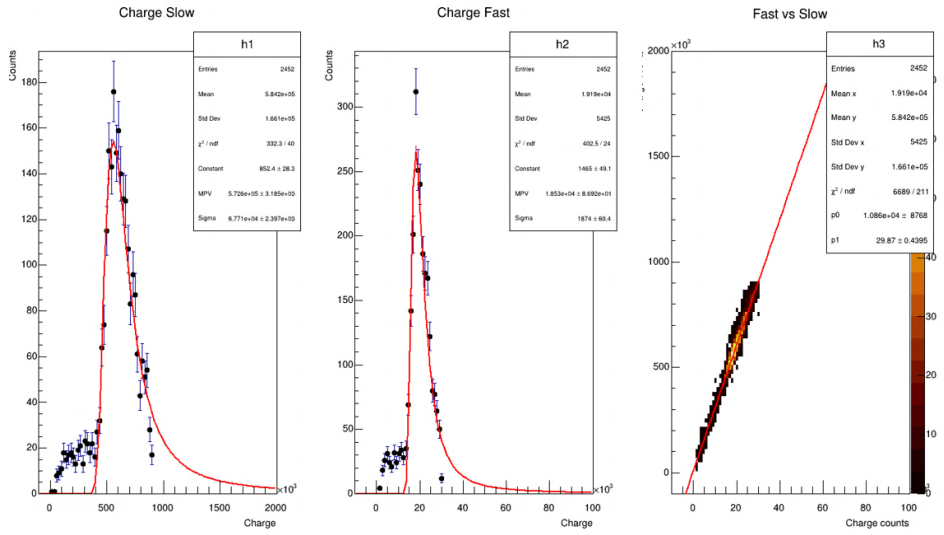

Figure 5.33: Linear relationship between the slow and fast signal charges of the detector configuration of BC-422Q square plastic scintillator with 6x6 *mm* SiPM (old).

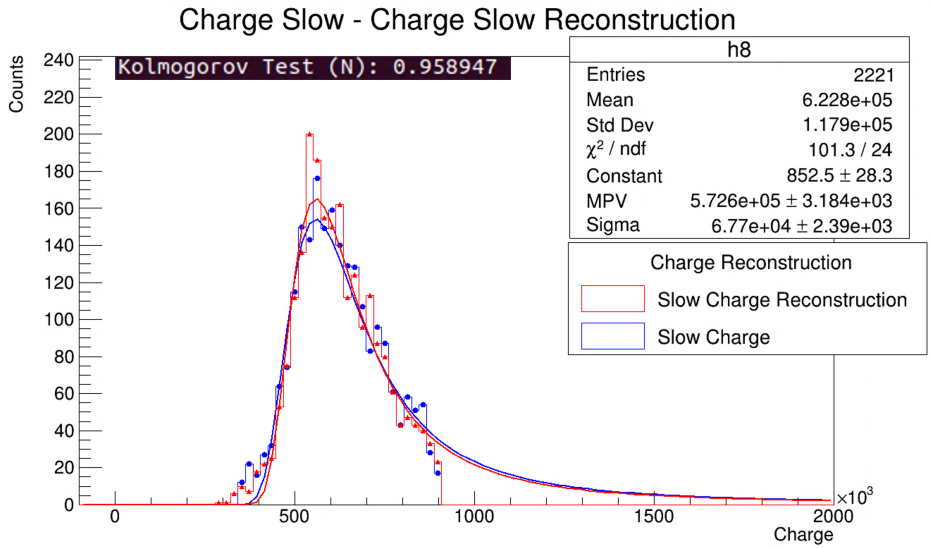

Figure 5.34: Result of the normalized Kolmogorov test of the slow signal charge reconstruction of the detector configuration of BC-422Q square plastic scintillator with 6x6 *mm* SiPM (old).

Table 5.27 shows the summary of the best Kolmogorov test result obtained for each of the detector configurations.

Table 5.27: Summary of the best Kolmogorov test results.

Detector configuration	Best Kolmogorov Test Result (%)
Old Hex - Old SiPM	97
New Hex - Old SiPM	87
Thick Hex - Two SiPMs	98
Square - Old SiPM	95

5.8 Comparison of the best results obtained.

Table 5.28 shows the summary of the best time resolution and efficiency results obtained for each of the detector configurations.

Table 5.28: Summary of the best time resolution and efficiency results.

Detector configuration	Instrumentation	Standard Signal		Fast Signal	
		Efficiency (%)	Time Resolution (ps)	Efficiency (%)	Time Resolution (ps)
Old Hex - Old SiPM	Digitizer	99.61	306 ± 118.7	99.58	366 ± 91.4
Old Hex - New SiPM	Digitizer	85.96	607 ± 50.3	67.94	560 ± 55.0
New Hex - Old SiPM	Digitizer	99.99	482 ± 65.1	99.97	502 ± 62.2
New Hex - New SiPM	Digitizer	99.64	485 ± 64.7	64.53	597 ± 51.2
Thick Hex - Two SiPMs	Digitizer	99.54	308 ± 117.5	99.53	461 ± 68.6
Square - Old SiPM	Digitizer	92.57	304 ± 120.0	92.74	294 ± 127.0
Old Hex - Old SiPM	TDC & QDC	99.24	611 ± 13.3	–	159 ± 63.3
Old Hex - New SiPM	TDC & QDC	99.64	466 ± 17.6	–	917 ± 8.8
New Hex - Old SiPM	TDC & QDC	99.31	597 ± 13.7	–	199 ± 45.8
New Hex - New SiPM	TDC & QDC	99.30	1521 ± 5.3	–	1367 ± 5.9
Thick Hex - Two SiPMs	TDC & QDC	98.97	885 ± 9.2	–	–
Square - Old SiPM	TDC & QDC	98.30	657 ± 12.4	–	257 ± 33.6

Chapter 6

Conclusions

From the digitizer results, it can be highlighted that the best time resolution and the best efficiency were obtained using the detector configuration of BC-404 hexagonal plastic scintillator (old) with the 6x6 mm SiPM sensor (old). The value of the best time resolution obtained is 306 $\pm$ 118.7 ps for the standard signal and 366 $\pm$ 91.4 ps for the fast signal under the application of a 30 V supply voltage.

Comparing with the TDC and QDC results, it is confirmed that the best detector configuration is the BC-404 hexagonal plastic scintillator (old) with 6x6 mm SiPM sensor (old). With this instrumentation, the value of the best time resolution obtained is 611 $\pm$ 13.3 ps for the standard signal and 159 $\pm$ 63.3 ps for the fast signal under the application of a 30 V supply voltage to this SiPM detector. Additionally, good behavior of the detector gain is observed for the detector configuration of BC-404 hexagonal plastic scintillator (old) with the 6x6 mm SiPM sensor (old) using either the digitizer or the TDC and QDC.

Results when using the 3x3 mm SiPM (new) have higher time resolution and non-exponential gain behavior. The board that was made for the 3x3 mm SiPM (new) had some manufacturing imperfections that greatly impaired the features expected from this device. Furthermore, by analyzing the digitizer results and comparing to the TDC and QDC results, it is possible to observe that the BC-404 hexagonal plastic

scintillator (new) is slightly slower than the BC-404 hexagonal plastic scintillator (old).

Using the detector configuration of BC-404 hexagonal plastic scintillator (thick) with a SiPM on each side (Two SiPMs), the best time resolution was obtained using the digitizer instrumentation. Furthermore, this time resolution was calculated using the average between the two SiPM standard signals' time values. The value obtained was 308 ± 117.5 ps under the application of a 30 V supply voltage. Also, good behavior of the detector gain was observed with both signals. An unexpected result of importance was that the time resolution obtained using the TDC and QDC was worse than the time resolution obtained using the digitizer.

Analyzing the detector configuration of BC-422Q square plastic scintillator with 6x6 mm SiPM (old) with the digitizer, the best time resolutions obtained are 304 ± 120 ps for the standard signal and 297 ± 124.8 ps for the fast signal, both under the application of a 30 V supply voltage to this SiPM detector. But comparing with the TDC and QDC results, the best time resolutions obtained are 657 ± 12.4 ps for the standard signal and 257 ± 33.6 ps for the fast signal. Also, the gain behaves exponentially in both cases indicating the good functioning of the detector. In conclusion, a better time resolution is obtained when using the TDC and QDC instrumentation, but the fastest detector is the BC-404 hexagonal plastic scintillator (old) with 6x6 mm SiPM (old).

It is important to mention that the time resolution of 25 ps of the TDC helps to have greater reliability of the obtained results. It is thanks to the resolution of the TDC that the systematic error is much lower when using the TDC than the digitizer.

Also, it is important to remember that the possibility of reconstructing the standard pulse using the fast pulse allows estimating the charge deposited by the particle in the detector based only on the fast signal from the SiPM sensor. In this way, the number of channels required in data acquisition can be reduced, as well as the instrumentation

and cables to be needed. This option is very useful, especially when there are not enough instruments for the different stages of amplification, discrimination, and signal conversion, among others.

Finally, the best time resolution result of the AD detector [1] reported is $0.74 \pm 0.04\ ns$, being for the case of pions with a momentum of 1 GeV/c. In the case of the VZERO detector [5], the reported time resolution is in the range of 1.1 to 1.3 ns using cosmic rays.

Comparing the detectors built for this project with the detectors of the ALICE experiment, it can be highlighted that the detectors of this project achieved better time resolutions than those reported by the ALICE detectors during Run 2.

Bibliography

[1] E. Abbas et al. Performance of the ALICE VZERO system. *JINST*, 8:P10016, 2013.

[2] K. Aamodt et al. The ALICE experiment at the CERN LHC. *JINST*, 3(08):S08002–S08002, Aug 2008.

[3] Ramón Acevedo Kado et al. The conceptual design of the miniBeBe detector proposed for NICA-MPD. *JINST*, 16(02):P02002, 2021.

[4] Mauricio Alvarado et al. A beam–beam monitoring detector for the MPD experiment at NICA. *Nucl. Instrum. Meth. A*, 953:163150, 2020.

[5] M. Broz et al. Performance of ALICE AD modules in the CERN PS test beam. *JINST*, 16(01):P01017, 2021.

[6] Y. Ayyad. Conceptos básicos sobre interacción de la radiación con la materia. `http://www.usc.es/genp/docencia/Inter_Rad_Mat_2011_Ayyad.pdf`, 2011. Accessed: 2022-09-12.

[7] M. González. Cálculos de dosimetría interna para emisores de partículas beta-gamma utilizando el método del kernel puntual y técnicas de imagen molecular. `http://catarina.udlap.mx/u_dl_a/tales/documentos/lfa/gonzalez_t_mj/`, 2011. Accessed: 2022-09-12.

[8] Sergei Dolinsky, Geng Fu, and Adrian Ivan. Timing resolution performance comparison for fast and standard outputs of sensl sipm. In *2013 IEEE Nuclear Science Symposium and Medical Imaging Conference (2013 NSS/MIC)*, pages 1–6, 2013.

[9] Saint-Gobain Crystals. Organic scintillation materials and assemblies. https://www.crystals.saint-gobain.com/sites/hps-mac3-cma-crystals/files/2021-12/Organics-Plastic-Scintillators.pdf, 2021. Accessed: 2022-09-12.

[10] Saint-Gobain Crystals. Bc-422q: Ultra-fast timing plastic scintillators. https://www.crystals.saint-gobain.com/sites/hps-mac3-cma-crystals/files/2021-10/BC422Q-Data-Sheet.pdf, 2018. Accessed: 2022-09-12.

[11] Sense Light (SensL). An introduction to the silicon photomultiplier. https://www.seti.net/cosmic-rays/SETIPixel/CosmicWatch-Desktop-Muon-Detector-v2-master/Datasheets/Intro_to_SiPMs.pdf, 2011. Accessed: 2022-09-12.

[12] Saint-Gobain Crystals. Bc-400,bc-404,bc-408,bc-412,bc-416 premium plastic scintillators. https://www.crystals.saint-gobain.com/sites/hps-mac3-cma-crystals/files/2021-10/BC400-404-408-412-416-Data-Sheet.pdf, 2021. Accessed: 2022-09-12.

[13] Francesca Carnesecchi. Performance of the ALICE Time-Of-Flight detector at the LHC. *JINST*, 14(06):C06023, 2019.

[14] CERN Accelerating Science. How a detector works. https://home.cern/science/experiments/how-detector-works, 2021. Accessed: 2022-09-12.

[15] IAEA. What is cherenkov radiation? https://www.iaea.org/newscenter/news/what-is-cherenkov-radiation, 2022. Accessed: 2022-09-12.

[16] Wei Jiang, Yamn Chalich, and M. Jamal Deen. Sensors for positron emission tomography applications. *Sensors*, 19(22), 2019.

[17] T. Niknejad et al. Validation of a highly integrated SiPM readout system with a TOF-PET demonstrator. *JINST*, 11(12):P12003–P12003, Dec 2016.

[18] Onsemi. *Silicon Photomultipliers (SiPM), Low-Noise, Blue-Sensitive*, 2018.

[19] C.H. Zepeda-Fernández, L.F. Rebolledo-Herrera, M. Rodríguez-Cahuantzi, and E. Moreno-Barbosa. Electric charge estimation using a SensL SiPM. *Journal of Instrumentation*, 15(09):P09008–P09008, sep 2020.

[20] QT-Brightek. *QT-Brightek Chip LED Series*, 2014.

Appendix A

Additional tests performed

A.1 LED test for the characterization of the charge deposited on the SiPM detector

A blue LED model QBLP631-IB [20] was used to perform the characterization of the deposited charge in the BC-404 hexagonal plastic scintillator (old) with 6x6 mm SiPM (old) detector configuration.

A signal generator was used to obtain the LED supply signal. The pulse signal properties were as follows: pulse width of 20 ns and frequency of 50 KHz. The pulse amplitude (V) was increased in steps of 0.05 V. The connection diagram used can be seen in Figure A.1.

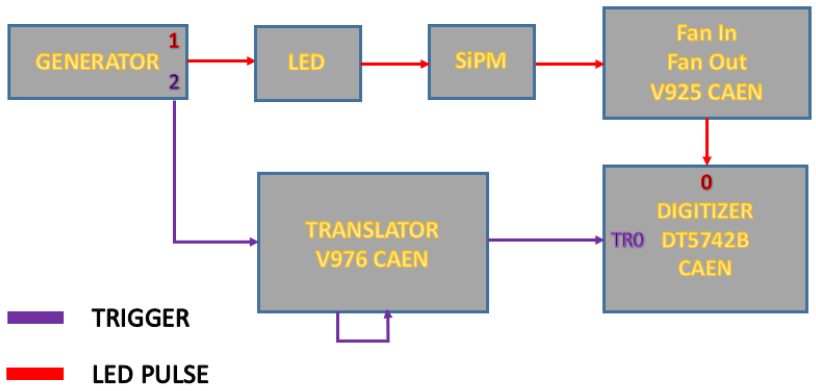

Figure A.1: Connection diagram for the characterization with the LED of the detector configuration of BC-404 hexagonal plastic scintillator (old) with 6x6 mm SiPM (old).

This test allows obtaining a behavior curve of the charge deposited on the detector by applying a controlled supply signal to the LED. In addition, it allows obtaining a reference of the behavior of the detector to know the changes due to the aging of the detector in future tests.

Table A.1 and Figure A.2 show the data and plot, respectively, of the results obtained from the charge deposited on the detector and the electric current supplied to the LED using the detector configuration of BC-404 hexagonal plastic scintillator (old) with 6x6 mm SiPM (old).

Table A.1: Results with the LED of the detector configuration of BC-404 hexagonal plastic scintillator (old) with 6x6 mm SiPM (old) using the digitizer.

LED test of BC-404 hexagonal plastic scintillator (old) with 6x6 mm SiPM (old) detector		
Pulse Amplitude (V)	Pulse Current (mA)	SiPM Charge (ADC Counts)
2.75	15.27	9536
2.80	15.55	20528
2.85	15.83	38831
2.90	16.11	63889
2.95	16.39	97999
3.00	16.67	137815
3.05	16.94	180892
3.10	17.22	296680
3.15	17.50	394191
3.20	17.78	513055
3.25	18.05	584865
3.30	18.33	656890
3.35	18.61	723241
3.40	18.89	783254

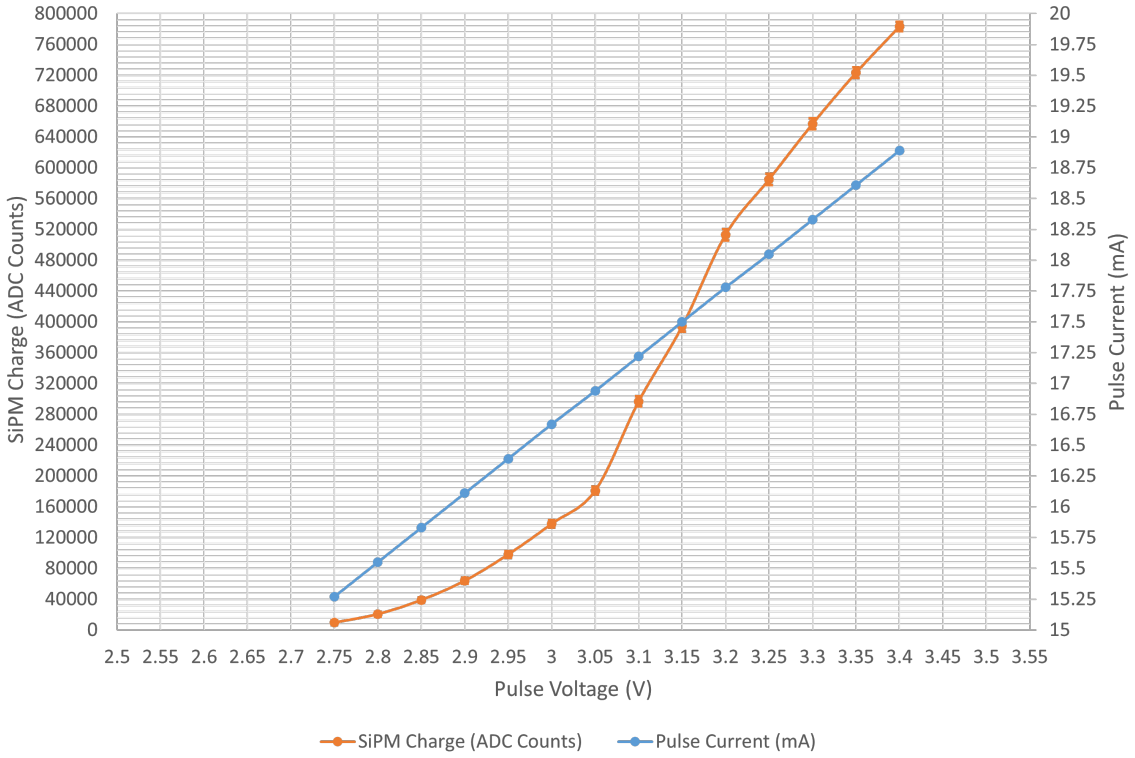

Figure A.2: Results with the LED of the detector configuration of BC-404 hexagonal plastic scintillator (old) with 6x6 mm SiPM (old) using the digitizer.

An example of the SiPM signal obtained on the digitizer screen by applying a pulse with an amplitude of 3.25 V to the LED can be seen in the Figure A.3.

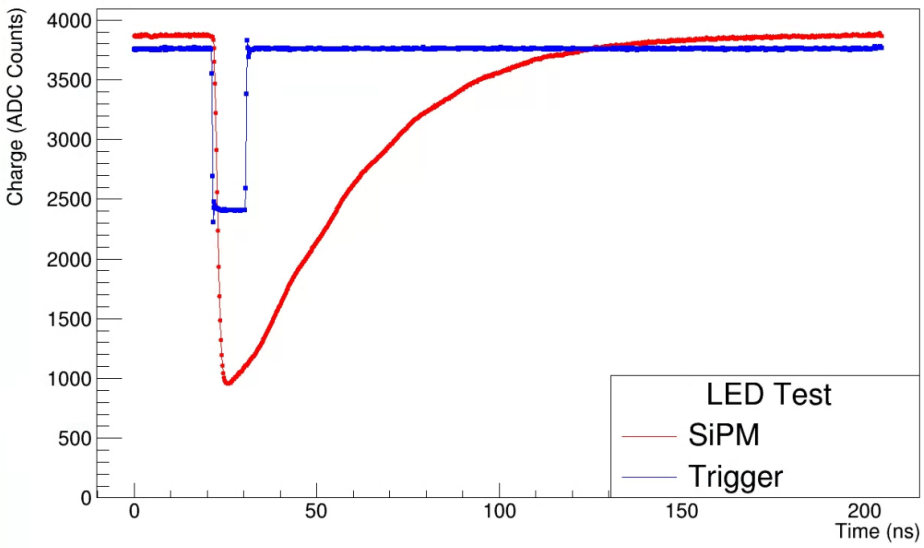

Figure A.3: SiPM signal obtained by applying a pulse with an amplitude of 3.25 V to the LED with the detector configuration of BC-404 hexagonal plastic scintillator (old) with 6x6 mm SiPM (old).

A.2 RPC characterization of time resolution and efficiency

The characterization of an RPC detector was performed using the instrumentation shown in the diagram of the Figure A.4.The experimental setup used can be seen in Figure A.5. The placement of the PMT detectors at the top and bottom of the RPC detector can be seen in Figure A.6.

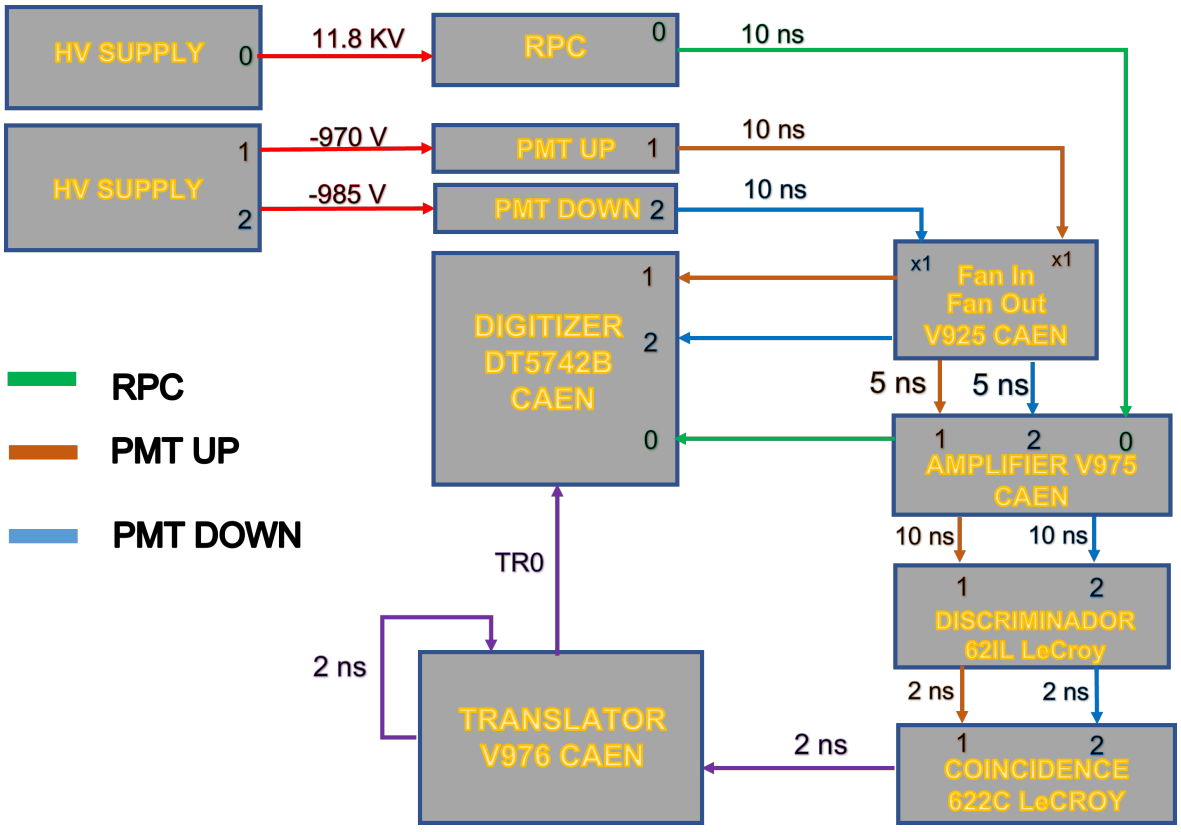

Figure A.4: Connection diagram of the RPC characterization.

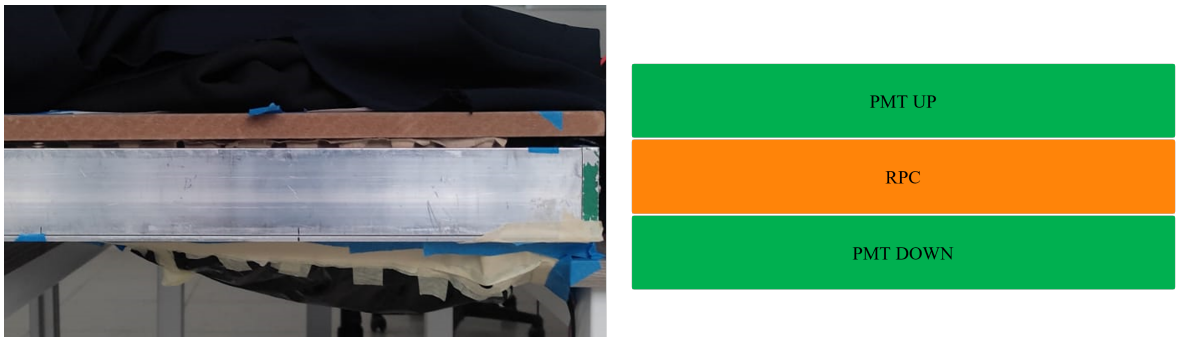

Figure A.5: Experimental setup of the RPC characterization.

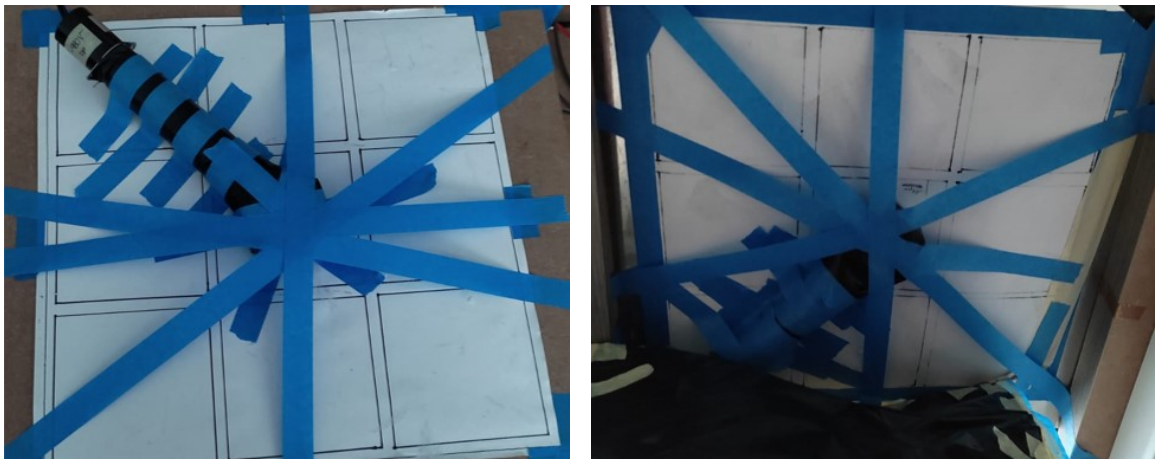

(a) PMT Up (b) PMT Down

Figure A.6: Placement of the PMT detectors.

The data were analyzed with the root framework to obtain the results of time resolution and efficiency with a supply voltage of 11.8 KV. The selection criteria of valid events for this test are described by the two points below:

1. The pulse area of the RPC signal must be more than 50,000 ADC counts. Lower values are considered noise. In Figure A.7, the pulse of the RPC detector can be seen.

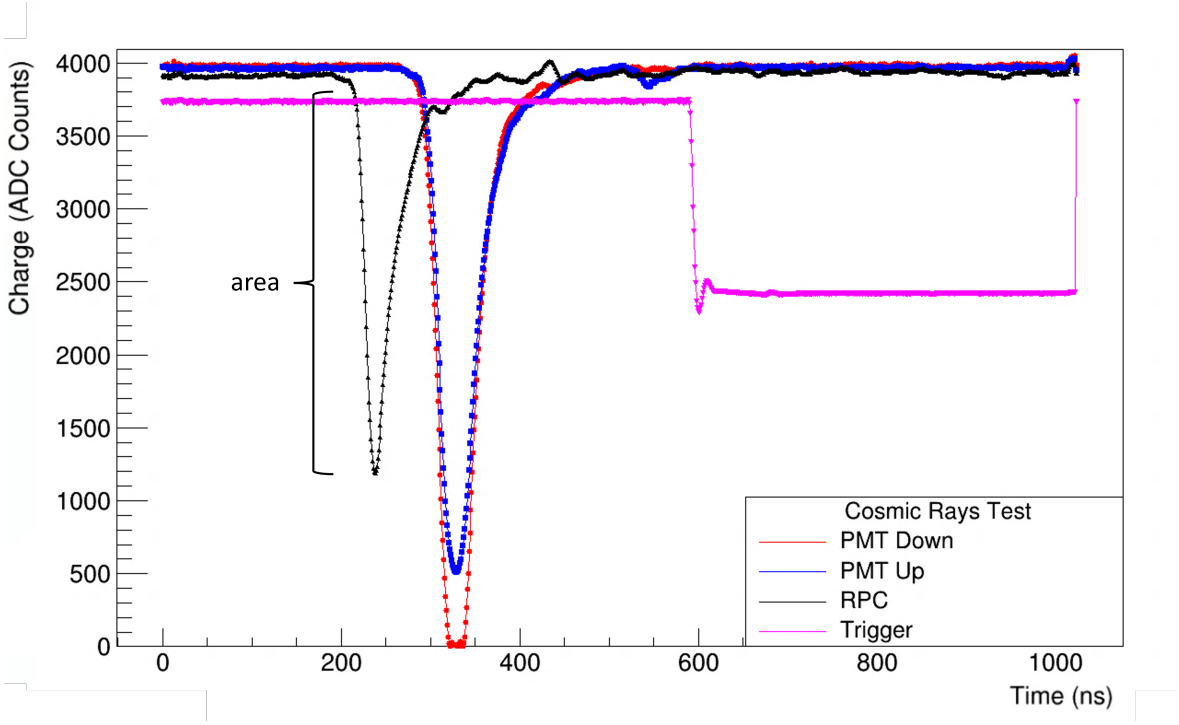

Figure A.7: First selection criterion of the RPC characterization.

2. The events of greatest interest are within the average of the PMT charges, giving a radius around the average of 10,000 ADC counts. In Figure A.8, the graph of the PMT Up charge against the PMT Down charge can be seen and it is possible to visualize a pattern with a circle where the greatest number of events are found. Within the red circle, the events of interest will be considered for the analysis of the time resolution and the efficiency of the RPC detector.

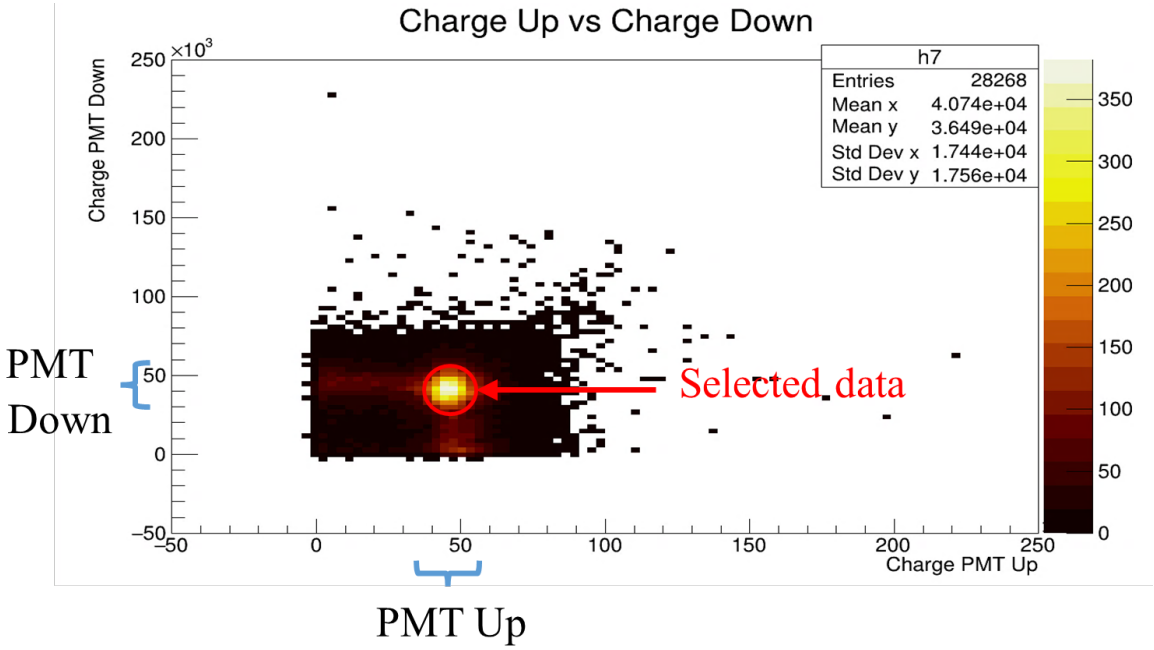

Figure A.8: Second selection criterion of the RPC characterization.

The equation used to calculate the efficiency is

$$P(RPC|PMTUp \wedge PMTDown) = \frac{N_{RPC}}{N_{PMT}} = \frac{N(RPC \wedge PMTUp \wedge PMTDown)}{N(PMTUp \wedge PMTDown)}, \tag{A.1}$$

where N_{RPC} is the number of events that fulfilled the 3-fold coincidence condition, defined by the logic AND between PMT Up, PMT Down, and the RPC detector, while N_{PMT} is the total number of events given by the 2-fold coincidence between the PMT Up and PMT Down.

The equation used to calculate the time resolution is

$$\sigma_3^2 = \sqrt{\frac{\sigma_{13}^2 + \sigma_{23}^2 - \sigma_{12}^2}{2}}. \tag{A.2}$$

where the RPC time resolution is denoted by σ_3, the variance of the difference between the starting time of the PMT Up and PMT Down events is denoted by σ_{12}, the variance of the difference between the starting time of the PMT Up and RPC events is denoted by σ_{13}, and the variance of the difference between starting time of the PMT Down and RPC events is denoted by σ_{23}.

The time resolution of the RPC was obtained by applying the equation before to the time differences between the RPC and the PMTs shown in Figure A.9. The value of σ_{12} is the sigma from the first plot, the value of σ_{13} is the sigma from the second plot, and the value of σ_{23} is the sigma from the third plot. The value of the time resolution obtained was 4.09 $ns\pm$ 0.16 ns with an efficiency of 8.08 %.

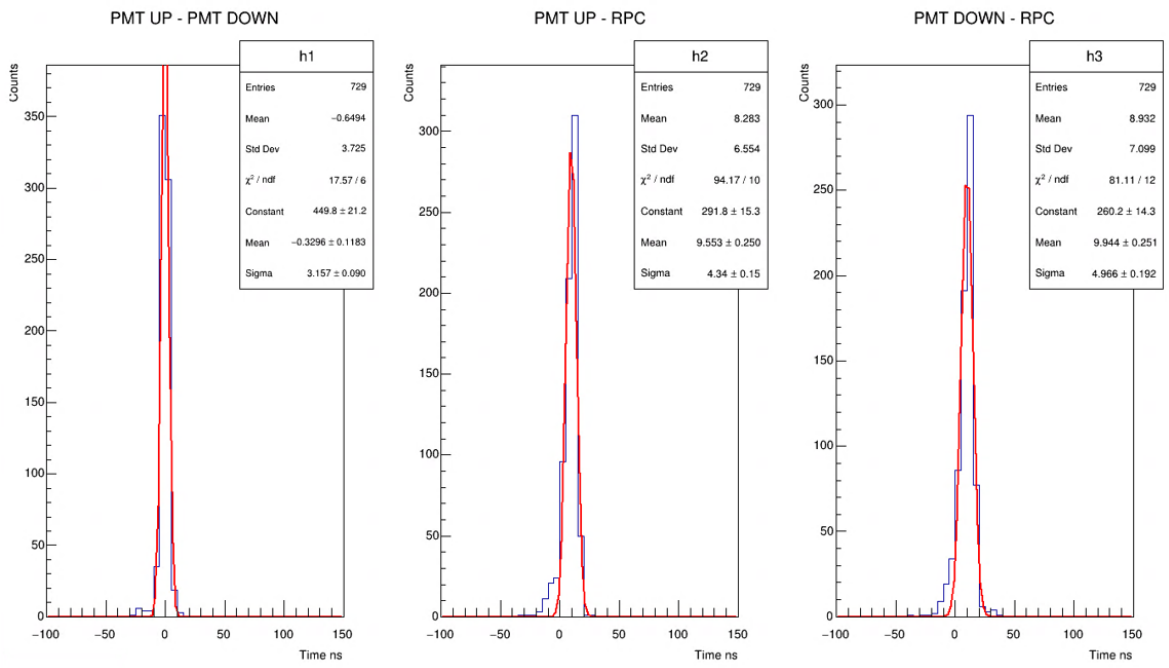

Figure A.9: RPC time resolution result.

A.3 SiPM characterization with an adjustable support base

An adjustable support base was designed to separate the PMT detectors from the SiPM detector so that the cosmic rays pass perpendicularly through all three detectors. The separation distance between the detectors for this characterization was 10 *cm*. The detector configuration of BC-404 hexagonal plastic scintillator (old) with 6x6 *mm* SiPM (old) was used. Figure A.10 shows the experimental setup and the designed support base. The connection diagram used was the same as the one used in the tests with the TDC and QDC instrumentation. This diagram can be seen in the Figure 4.16.

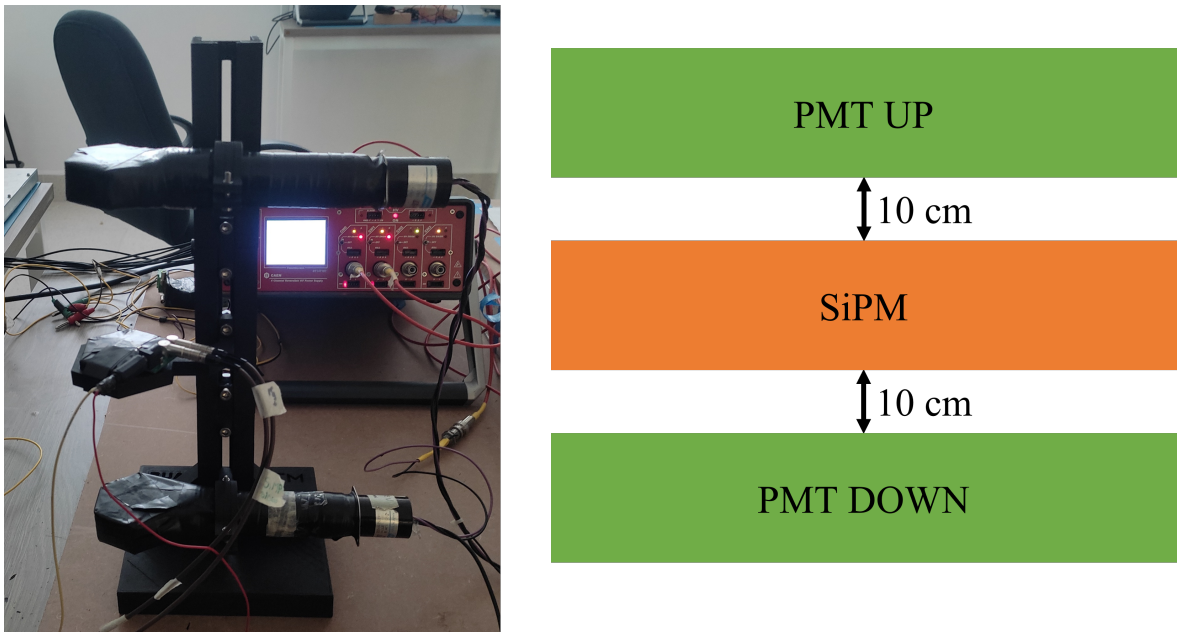

Figure A.10: Experimental setup for the characterization of the SiPM detector with the adjustable support base.

By separating the detectors, the number of events decreased greatly, so the number of statistics that were obtained for the results that will be presented below was much less than in the tests performed without the base. In addition, a component of the SiPM board had to be soldered again due to problems caused by handling the board, which affected the behavior this detector had shown in the previous tests.

Table A.2 and Figure A.11 show the time resolution and efficiency data and plot, respectively, of the tests performed with the BC-404 hexagonal plastic scintillator (old) with 6x6 *mm* SiPM (old) detector using the adjustable support base. In addition, Table A.3 and Figure A.12 show the gain results obtained from these tests.

Table A.2: Results of the detector configuration of BC-404 hexagonal plastic scintillator (old) with 6x6 *mm* SiPM (old) using the support base.

BC-404 hexagonal plastic scintillator (old) with 6x6 *mm* SiPM (old)			
	Standard Signal		Fast Signal
Voltage (V)	Efficiency (%)	Time Resolution (ps)	Time Resolution (ps)
26	18.55	2055 ± 4.0	1409 ± 5.9
27	39.87	1876 ± 4.4	1190 ± 7.0
28	91.39	1678 ± 4.9	1222 ± 6.8
29	89.78	843 ± 9.9	1241 ± 6.7
30	92.33	747 ± 11.1	1263 ± 6.6

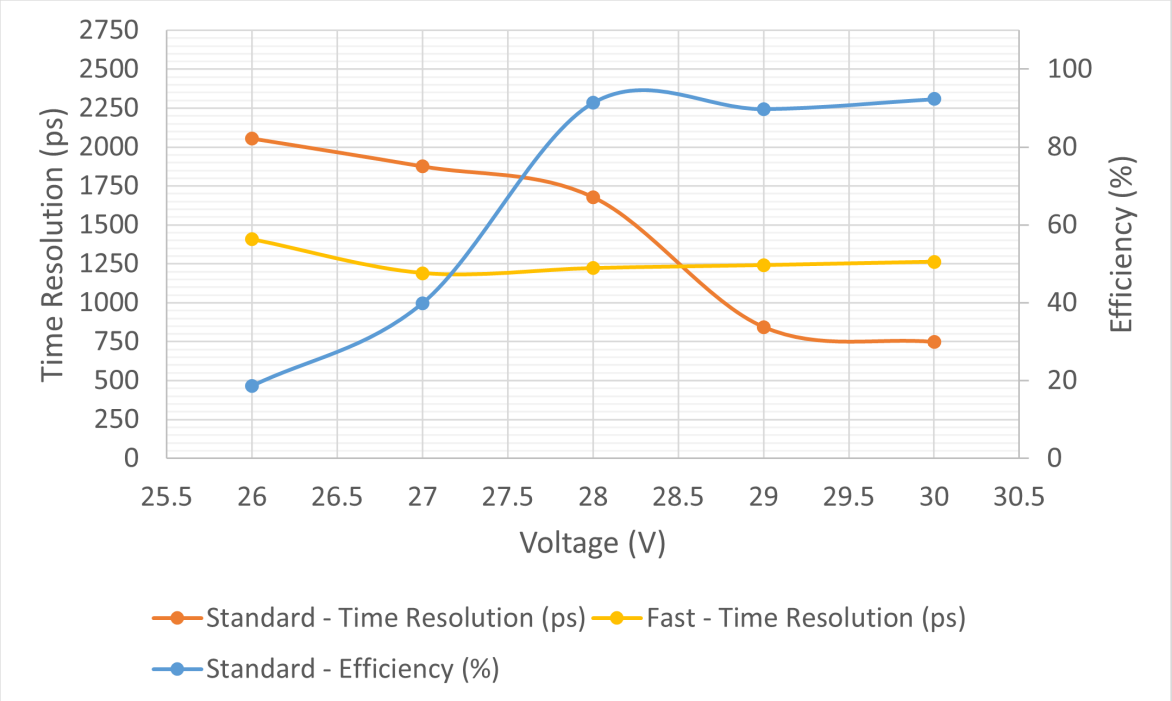

Figure A.11: Results of the time resolution and efficiency of the detector configuration of BC-404 hexagonal plastic scintillator (old) with 6x6 *mm* SiPM (old) using the support base.

Table A.3: Gain results of the detector configuration of BC-404 hexagonal plastic scintillator (old) with 6x6 *mm* SiPM (old) using the support base.

BC-404 hexagonal plastic scintillator (old) with 6x6 *mm* SiPM (old)	
	Standard Signal
Voltage (V)	MPV (ADC Counts)
26	685
27	900
28	1053
29	1650
30	2595

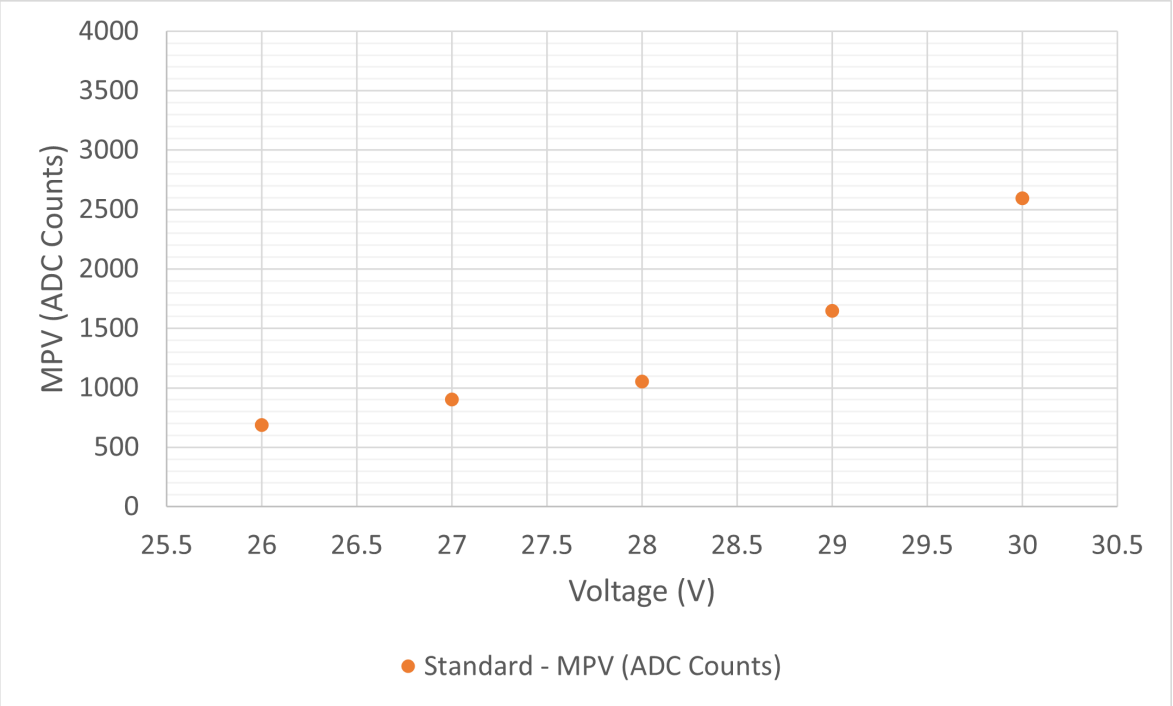

Figure A.12: Gain results of the detector configuration of BC-404 hexagonal plastic scintillator (old) with 6x6 *mm* SiPM (old) using the support base.